Top quark effects on multijet production and electroweak parameters

J.B. Tausk

03 SEP. 1993

RIJKSUNIVERSITEIT TE LEIDEN
BIBLIOTHEEK INSTITUUT-LORENTZ
Postbus 9506 - 2300 RA Leiden
Nederland

Kast dissertaties

Top quark effects on multijet production and electroweak parameters

Top quark effects on multijet production and electroweak parameters

Proefschrift

ter verkrijging van de graad van Doctor
aan de Rijksuniversiteit te Leiden,
op gezag van de Rector Magnificus Dr. L. Leertouwer,
hoogleraar in de faculteit der Godgeleerdheid,
volgens besluit van het college van dekanen
te verdedigen op woensdag 22 september 1993
te klokke 16.15 uur

door

Jan Boudewijn Tausk

geboren te Keulen, Bondsrepubliek Duitsland in 1965

Promotiecommissie:

Promotor:	Prof. dr. F.A. Berends
Referent:	Dr. W.L.G.A.M. van Neerven
Overige leden:	Prof. dr. P.J. van Baal
	Prof. dr. K.J.F. Gaemers
	Prof. dr. H.J. Habing

This investigation is part of the research program of the "Stichting voor Fundamenteel Onderzoek der Materie (FOM)" which is financially supported by the "Nederlandse Organisatie voor Wetenschappelijk Onderzoek (NWO)".

Contents

1 Introduction 1
1.1 The standard model 1
1.2 The top quark 3

References to chapter 1 4

2 On the production of a W and jets at hadron colliders 6
2.1 Introduction 6
2.2 Matrix elements with one quark pair 9
2.3 Matrix elements with two quark pairs 12
2.4 Matrix elements with three quark pairs 22
2.5 Results 26

Appendix 30
2A The colour matrix for the four quark processes 31

References to chapter 2 32

3 Recognizing the top quark in multijet events 34
3.1 Introduction 34
3.2 The production cross section and backgrounds 35
3.3 Determination of the top mass 43
3.4 Conclusion 48

References to chapter 3 51

4 Two-loop self-energy diagrams with massless fermions 52
4.1 Introduction 52
4.2 Definitions 52
4.3 The dispersion method 55
4.4 Massive phase space integrals 57
4.5 An example 60
4.6 Results 63
4.7 Conclusion 72

References to chapter 4 72

5 Series expansions of two-loop self-energy diagrams 74
5.1 Introduction 74
5.2 The expansion for small k^2 76
5.2.1 Reduction to vacuum integrals 76
5.2.2 Vacuum integrals with two different masses 78
5.2.3 Vacuum integrals with three different masses 82
5.2.4 Recurrence relations for two-loop vacuum integrals 86
5.2.5 Numerical results 88
5.3 The expansion for large k^2 92
5.3.1 Constructing the asymptotic expansion 93
5.3.2 Analytical results 95
5.3.3 Numerical results 98
5.4 Conclusion 102

Appendices 103
5A Massless two-point integrals 103
5B Massive vacuum integrals 104

References to chapter 5 106

6 Numerical integration of two-loop self-energy diagrams 109
6.1 Introduction 109
6.2 Kreimer's method 110
6.3 Results 113

References to chapter 6 114

Samenvatting 115

Curriculum vitae 117

List of publications 118

Chapter 1

Introduction

1.1 The standard model

According to the standard model, all matter is composed of leptons and quarks. There should be six kinds of quarks, but the sixth one, called truth or top quark, has not been observed yet. This thesis is about how the top quark could be found by experiments currently being performed at Fermi National Accelerator Laboratory (FNAL) in Batavia, Illinois, and how the top quark influences the properties of other particles. To introduce these subjects, let us make a short tour of the standard model.

In this model, there are three families of fermions, shown in Table 1.1. They all have spin 1/2. The behaviour of these elementary particles is determined by three forces: the electromagnetic force, the weak force and the strong force. The force of gravity, which is much weaker, is not included in the standard model. The forces are carried by particles called gauge bosons, of which there are four kinds. They have spin 1 and are therefore also called vector bosons. The first is the photon, which is responsible for the electromagnetic force. Then there is the gluon for the strong force. Both these particles are massless. The weak force is carried by two massive gauge bosons, called W and Z bosons. In order to allow the W and Z to have masses, the theory requires the existence of one more particle, which is called the Higgs boson and has spin 0.

leptons	ν_e	~ 0	ν_μ	~ 0	ν_τ	~ 0
	e	0.511 MeV	μ	105.66 MeV	τ	1784 MeV
quarks	u	0.041 GeV	c	1.5 GeV	t	not yet seen
	d	0.041 GeV	s	0.15 GeV	b	4.5 GeV

Table 1.1. The fermions in the standard model and their masses

Until now, the theory has been in agreement with all experimental data [1, 2, 3]. However, two particles have not yet been observed in experiments. One is the top quark, as already mentioned, and the other one is the Higgs particle. Both of them

photon	0
gluon	0
Z	91 GeV
W	80 GeV
Higgs	not yet seen

Table 1.2. The bosons in the standard model and their masses

are needed to ensure the renormalizability of the theory.

The model depends on a number of free parameters. For example, once the masses of the particles, the fine structure constant, α, and the strong coupling constant, α_S, are given, one can, in principle, calculate the cross section for any reaction between elementary particles one wishes.

In practice, most calculations are done using perturbation theory. To obtain accurate predictions, two things are needed. Firstly, the input parameters must be accurately known, and secondly, higher order terms in the perturbation expansion must be included.

As for the input parameters, the masses of the electron, the muon and the tau have been measured directly. The masses of the up, down, charm, strange and bottom quarks have been obtained indirectly from experimentally measured quantities [4]. The neutrino masses are known to be small in comparison with the other particles. The value of α_S depends on a renormalization scale μ. If we choose $\mu = M_Z$, α_S is approximately 0.12.

In electroweak interactions, three parameters are especially important, namely α, M_Z and M_W. The first is known to 1 part in 10^7,

$$\alpha = \frac{e^2}{4\pi} = \frac{1}{137.03599}\,. \tag{1.1.1}$$

The mass of the Z boson, M_Z, has been measured to 0.01% accuracy by the recent LEP experiments [5], but the mass of the W has not been measured as accurately. Therefore, it is better not to use the experimentally measured value of M_W as input, but instead to calculate it from the Fermi constant G_μ. This constant is directly related to the muon lifetime, which has been measured to 0.002% accuracy. The relationship between M_W and G_μ can be written as [6]

$$M_W^2\left(1 - \frac{M_W^2}{M_Z^2}\right) = \frac{\pi\alpha}{\sqrt{2}G_\mu(1-\Delta r)}\,, \tag{1.1.2}$$

where the quantity Δr represents radiative corrections to the muon decay rate. It is a function of α, α_S and all the masses, in particular the unknown masses of the top quark, m_t, and the Higgs boson M_H. By numerically solving eq. (1.1.2), a value for M_W is found which depends on m_t and M_H. As a consequence, *any* prediction

about weak interactions derived from the model will depend on m_t and M_H, unless, as sometimes happens, this dependence is cancelled by other effects.

By comparing the predictions with experimental results, the following bounds on m_t and M_H can be derived [7]:

$$m_t = 124^{+26}_{-28}\text{GeV}\,, \tag{1.1.3}$$

$$m_H = 25^{+275}_{-19}\text{GeV}\,. \tag{1.1.4}$$

The bounds on M_H are less tight than those on m_t, because, in general, one-loop corrections depend only logarithmically on M_H, whereas some of the m_t-dependent contributions to Δr are proportional to m_t^2. From direct searches we know that $m_t > 91$ GeV [8] and $m_H > 60$ GeV [3].

1.2 The top quark

The particle that is most likely to be discovered first is the top quark. If it is found, an important test of the standard model would be to see whether its mass is within the bounds (1.1.3). Knowing m_t would allow a direct test of the relation (1.1.2) when M_W is measured more accurately in the future. It would also make it possible to tighten the bounds on M_H (1.1.4).

Experiments to find the top quark are being performed at FNAL. Protons and antiprotons are accelerated in opposite directions around a ring two kilometres in diameter and then made to collide with each other at a centre of mass energy of 1.8 TeV. In these collisions, top quarks should be produced in pairs. They will not be observed directly, because they will decay before they have had time to reach the detectors. Therefore, their existence must be deduced from the observed decay products. For this, it is necessary to know the rates of any other reactions, not involving top quarks, that can occur in proton antiproton collisions and produce the same decay products. In chapter 2, the cross section is calculated for one of these background reactions, the production of a W and four jets of hadrons. In chapter 3, different ways to distinguish the top signal from the background are investigated.

Another way to test the model is by performing all kinds of even more precise measurements. To match the experimental precision, it is then necessary to include two-loop electroweak corrections in the theoretical predictions of the measured quantities. An example is the quantity Δr in eq. (1.1.2), which can be obtained experimentally by measuring M_W, M_Z, G_μ and α.

The theoretical predictions for Δr and the other measured quantities all depend on the unknown values of m_t and M_H. It may happen, that no values for m_t and M_H exist, such that all measurements are consistent with their one-loop theoretical predictions, but that if one uses more precise two-loop theoretical predictions, one does find agreement with all measurements for some values of m_t and M_H.

Let us now discuss a few of the two-loop calculations that have been done in the literature. First of all, there is the calculation of the vacuum polarization in

quantum electrodynamics by Källén and Sabry [9]. Later, order $\alpha\alpha_S$ corrections to the W and Z propagators were calculated [10], but second order results for the electroweak sector have only been obtained in certain limits. The limit $M_H \to \infty$ was considered in ref. [11]. The effect of a very heavy fermion doublet was studied in ref. [12]. These results were used to find the leading two-loop contributions to Δr in the limit $m_t \to \infty$, which are of order $\alpha^2 m_t^4$ [13]. In this approximation, all masses except m_t are neglected. In a more recent calculation [14], the leading terms in the limit $m_t \to \infty$ were obtained without neglecting M_H, but the vector boson masses were still neglected.

Considering that m_t may be something like 140 GeV, which is larger than M_W and M_Z, but still of the same order of magnitude, it is not clear that the above approximations are justified. In order to find out, full two-loop calculations would be needed.

Such calculations would involve vast numbers of Feynman diagrams. For instance, there are several thousand two-loop diagrams that contribute to the reaction

$$e^+e^- \to \mu^+\mu^- . \tag{1.2.1}$$

Note that in many diagrams, the internal particles are massive, e.g. W and Z bosons, Higgs particles or top quarks, which makes the corresponding Feynman integrals much more complicated than integrals that involve only massless particles. These difficulties must be overcome before a full two-loop calculation can be done.

In chapters 4, 5 and 6 of this thesis, some steps in this direction are made. We consider the calculation of self-energy diagrams, which will be an essential ingredient in any complete two-loop calculation. These self-energy diagrams can all be expressed in terms of a set of basic scalar integrals.

In chapter 4, we calculate a subclass of the scalar integrals analytically in terms of polylogarithms. These results can be used in cases where some of the internal particles are still massless. When more of the internal particles are massive, it is no longer possible to express the integrals in terms of polylogarithms, so we must then turn to other methods to calculate them. Two such methods are discussed in this thesis.

In chapter 5, we study two series expansions of scalar self-energy diagrams, one for small and one for large external momenta. In both cases, the coefficients of the series are calculated analytically for arbitrary values of the internal masses. By truncating these series, we obtain accurate approximations to the full integrals.

In general, however, there will be an intermediate range of external momenta where neither series converges. Therefore we discuss, in chapter 6, a numerical method that works for arbitrary internal masses and arbitrary external momenta. It is based on a two dimensional integral representation discovered by Kreimer [15]. His method works very well, but it can only be used for diagrams with one particular topology, the so-called master diagram, which has no ultraviolet divergence. Using some of the results of chapter 4, we extend Kreimer's algorithm so that it can also be applied to divergent diagrams.

References

[1] The LEP collaborations: ALEPH, DELPHI, L3 and OPAL, *Phys. Lett.* B276 (1992) 247.

[2] L. Rolandi, CERN–PPE–92–175, Precision tests of the electroweak interaction, talk at ICHEP 92 conference, Dallas (August 1992);
G. Altarelli, CERN–TH.6525/92, Precision electroweak data and constraints on new physics, talk at XXVIIth Rencontres de Moriond, Les Arcs (March 1992);
P. Renton, *Z. Phys.* C56 (1992) 355.

[3] G. Quast, *Mod. Phys. Lett.* A8 (1993) 675.

[4] F.A. Berends et al. in "Z physics at LEP 1", CERN 89-08, p.89, eds. G. Altarelli, R. Kleiss and C. Verzegnassi.

[5] The Working Group on LEP Energy and the LEP collaborations, *Phys. Lett.* B307 (1993) 187.

[6] A. Sirlin, *Phys. Rev.* D22 (1980) 971;
F. Halzen and B.A. Kniehl, *Nucl.Phys.* B353 (1991) 567;
F. Halzen, B.A. Kniehl and M.L. Stong, *Z. Phys.* C58 (1993) 119.

[7] J. Ellis, G.L. Fogli and E. Lisi, *Phys. Lett.* B292 (1992) 427.

[8] F. Abe et al., *Phys. Rev. Lett.* 68 (1992) 447.

[9] G. Källén and A. Sabry, *Dan.Mat.Fys.Medd.* 29 (1955) No.17.

[10] D.J. Broadhurst, *Phys.Lett.* B101 (1981) 423;
T.H. Chang, K.J.F. Gaemers and W.L. van Neerven, *Nucl.Phys.* B202 (1982) 407;
A. Djouadi, *Nuovo Cim.* 100A (1988) 357;
B.A. Kniehl, *Nucl.Phys.* B347 (1990) 86.

[11] J.J. van der Bij and M. Veltman, *Nucl.Phys.* B231 (1984) 205;
J.J. van der Bij, *Nucl.Phys.* B248 (1984) 141.

[12] J. van der Bij and F. Hoogeveen, *Nucl. Phys.* B283 (1987) 477.

[13] M. Consoli, W. Hollik and F. Jegerlehner, *Phys. Lett.* B227 (1989) 167.

[14] R. Barbieri, M. Beccaria, P. Ciafaloni, G. Curci and A. Viceré, *Phys. Lett.* B288 (1992) 95;
R. Barbieri, M. Beccaria, P. Ciafaloni, G. Curci and A. Viceré, CERN preprint CERN-TH.6713/92.

[15] D. Kreimer, Phys.Lett. B273 (1991) 277.

Chapter 2

On the production of a W and jets at hadron colliders

2.1 Introduction

In ref. [1], analytic expressions were given for processes involving a vector boson V and l partons. The number l was restricted to $l \leq 5$. An evaluation which was more numerically oriented has also been published [2]. Both approaches agree numerically [3].

In other words the decay

$$V \to l \text{ partons} \tag{2.1.1}$$

could be described in terms of the given expressions. By suitable crossing one obtains descriptions of

$$e^+ + e^- \to l \text{ jets}, \tag{2.1.2}$$

$$e^- + P \to \begin{pmatrix} e^- \\ \nu_e \end{pmatrix} + X + (l-1) \text{ jets}, \tag{2.1.3}$$

$$P + \begin{pmatrix} \bar{P} \\ P \end{pmatrix} \to X + V + (l-2) \text{ jets}, \tag{2.1.4}$$

where X represents unobserved hadrons originating from the partons which are not involved in the main reaction. It turns out that for a number of reasons the process (2.1.4) with $l = 6$ is of particular interest. This has to do with its role as background to interesting physics signals.

The first signal is that of $t\bar{t}$ production in a hadron collider, where one looks at the semileptonic t decay and at the quark decay of $\bar{t}$:

$$P + \begin{pmatrix} \bar{P} \\ P \end{pmatrix} \to X + t + \bar{t}$$

$$t \hookrightarrow W^+ + b \qquad \bar{t} \hookrightarrow W^- + \bar{b}$$

$$W^+ \hookrightarrow e^+ + \nu_e \qquad W^- \hookrightarrow q_1 + \bar{q}_2$$

If b, $\bar{b}$, q_1 and $\bar{q}_2$ are all sufficiently energetic to develop into jets, one will observe an e^+ and four jets:

$$P + \begin{pmatrix} \bar{P} \\ P \end{pmatrix} \rightarrow X + e^+ + 4 \text{ jets.} \tag{2.1.5}$$

The signal e^- and four jets arises in a similar way. Obviously the QCD process (2.1.4) can be a serious background. For the top quark search at hadron colliders one shall be interested in the signal (2.1.5) besides the cleaner dilepton signal plus two jets arising from both W's decaying leptonically.

The second signal of interest is that of heavy Higgs boson production by means of W^+W^--fusion, when one applies jet tagging [4].

$$\begin{array}{ccccccccc} P + P & \rightarrow & X & + & H & + & q_1 & + & \bar{q}_2 \\ & & & & \hookrightarrow W^+ & & + & & W^- \\ & & & & & \hookrightarrow e^+ + \nu_e & & \hookrightarrow q_3 + \bar{q}_4 & \end{array} \tag{2.1.6}$$

Again the result is an e^+ (or e^-) and four jets, so the process (2.1.4) will constitute a background. Although q_1 and $\bar{q}_2$ develop into jets relatively close to the beam direction one hopes to detect these jets. Of course signals other than (2.1.6) may give easier evidence for the Higgs boson (see e.g. [5]), but it would be worthwhile to study (2.1.6) as well.

For top masses below approximately 160 GeV the top quark could be found at the Tevatron in the near future and the knowledge of reaction (2.1.4) becomes important. When the top quark remains elusive at the Tevatron the signal and background question comes back again when LHC or SSC studies are made. For those accelerators also signal (2.1.6) and its background will have to be known.

Therefore we shall extend in this chapter the previous calculations to $l = 6$. Although the formalism is set up in such a way that both W and Z could be considered, we shall focus on the W case, since that seems to be the most relevant case in view of the above signals.

The complexity of the process (2.1.1) rapidly increases with growing l. This is illustrated in Table 2.1. In this table a typical parton combination is given and the number of subprocesses related to it using different flavour choices. Also the number of diagrams for the matrix element is listed. Let us take a specific case in order to indicate the meaning of the entries.

For the $l = 4$ case in reaction (2.1.4) one has the following incoming parton combinations related to the generic $u\bar{d}gg$ case:

$$u\bar{d} \rightarrow W^+gg, \tag{2.1.7}$$
$$ug \rightarrow W^+dg, \tag{2.1.8}$$
$$\bar{d}g \rightarrow W^+\bar{u}g, \tag{2.1.9}$$
$$gg \rightarrow W^+\bar{u}d. \tag{2.1.10}$$

l	Process type	# diagrams	# subprocesses
2	$u\bar{d}$	1	4
3	$u\bar{d}g$	2	12
4	$u\bar{d}gg$	8	14
	$u\bar{d}c\bar{c}$	2	52
	$u\bar{d}u\bar{u}$	4	14
	$u\bar{d}d\bar{d}$	4	14
5	$u\bar{d}ggg$	50	14
	$u\bar{d}c\bar{c}g$	12	92
	$u\bar{d}u\bar{u}g$	24	26
	$u\bar{d}d\bar{d}g$	24	26
6	$u\bar{d}gggg$	428	14
	$u\bar{d}c\bar{c}gg$	98	98
	$u\bar{d}u\bar{u}gg$	196	28
	$u\bar{d}d\bar{d}gg$	196	28
	$u\bar{d}c\bar{c}s\bar{s}$	16	108
	$u\bar{d}c\bar{c}c\bar{c}$	32	60
	$u\bar{d}u\bar{u}c\bar{c}$	32	98
	$u\bar{d}d\bar{d}c\bar{c}$	32	98
	$u\bar{d}u\bar{u}d\bar{d}$	64	28
	$u\bar{d}d\bar{d}d\bar{d}$	96	16
	$u\bar{d}u\bar{u}u\bar{u}$	96	16

Table 2.1. The numbers of subprocesses in which a W^+ and $l-2$ jets are produced in hadron-hadron collisions, and the number of diagrams per subprocess, assuming that there is no mixing and that there are no b quarks in the initial state.

Since the incoming hadrons contain four flavours, the cases (2.1.7)–(2.1.10) represent the following number of subprocesses: 4,4,4,2. Here we distinguish for example the $u\bar{d}$ incoming state from $\bar{d}u$. The number of subprocesses is not the number of times a parton cross section has to be evaluated. This number is generally lower because different flavours can possess the same cross sections.

From the table it is clear that the $l = 6$ case is considerably more complex than the $l = 5$ case. Space limitations prevent us from listing explicitly analytic answers for helicity amplitudes as in the $l = 5$ case. Nevertheless we shall give a description of the various kinds of amplitudes, i.e. 2, 4 and 6 quark matrix elements. The 2 quark matrix elements will be evaluated numerically with recursive techniques. The four quark matrix element calculation is similar to the $l = 4$ and 5 cases as far as the quark structure is concerned. The 6 quark case occurs here for the first time and is a generalization of the 4 quark case.

Besides a description of the calculation this chapter also presents some numerical results for reaction (2.1.4), hereby extending the previous numbers [6] to the four jet case. The results are for Tevatron, LHC and SSC situations. A more extensive phenomenological study for the Tevatron is given in chapter 3.

The outline of this chapter is as follows. Sections 2.2, 2.3 and 2.4 describe the 2, 4 and 6 quark amplitudes. In section 2.5, we present our numerical results and discuss their implications.

2.2 Matrix elements with one quark pair

In this section we deal with the calculation of the matrix elements involving a $q\bar{q}$ pair, a vector boson and an arbitrary number of gluons. We choose for this case a different calculational technique than for the two and three quark pair cases. The reason is that when more gluons participate in a process, the number of diagrams increases rapidly. Therefore the calculation of helicity amplitudes by using Feynman diagrams becomes too complex, even when we use Weyl-van der Waerden spinor calculus. A technique recursive in the number of gluons has been introduced [7] for these situations. It pays off to use this technique when we have three or more gluons in a process, so for the one quark pair case we favour this approach.

After briefly summarizing those parts of the recursive calculation methods [7] required for the vector boson processes we look at the production of a W and at some numerical implications. We will show that for the process under consideration both the matrix element and the sum over the parton processes can be systematically dealt with for any number of gluons.

For the sake of presentation we consider the process with outgoing partons created from the vacuum

$$\emptyset \to V + q(Q;i) + \bar{q}(P;j) + g(K_1;a_1) + \ldots + g(K_n;a_n). \tag{2.2.1}$$

The momenta and the colour indices are explicitly given. It is not of importance that process (2.2.1) is not a physical process. Later on we will cross two momenta

from the final to the initial state. The matrix element for process (2.2.1) is given by a vector current $\hat{S}_\mu(Q;1\ldots n;P)$ contracted with the polarization vector V^μ of the boson. For the sake of clarity we frequently omit colour and momentum indices in $\hat{S}_\mu$, they are implicitly understood. In [1] process (2.2.1) is discussed in great detail. Here we only present the main elements of the method to obtain $\hat{S}_\mu$.

The vector boson couples to the quark line breaking the Feynman diagram into two parts, one spinor current with the $q(Q)$ and gluons 1 through m and one spinor current with $\bar{q}(P)$ and the rest of the gluons, $m+1$ through n. These two spinor currents can be decomposed in a colour base of fundamental representation matrices T^a of the SU(N) colour gauge group. The spinor currents are given by

$$\hat{J}_k(Q;1\ldots m) = g^m \sum_{P(1\ldots m)} (T^{a_1}\ldots T^{a_m})_{ik} J(Q;1\ldots m) \tag{2.2.2}$$

and

$$\hat{J}_k(m+1\ldots n;P) = g^{n-m} \sum_{P(m+1\ldots n)} (T^{a_{m+1}}\ldots T^{a_n})_{kj} J(m+1\ldots n;P), \tag{2.2.3}$$

where the sum is over all gluon permutations. The quark currents $J(Q;1\ldots m)$ and $J(m+1\ldots n;P)$ are calculated using recursion in the number of gluons [7]. For the no gluon case they are: $J(Q) = \bar{u}(Q)$ and $J(P) = v(P)$. Using eqs. (2.2.2) and (2.2.3) $\hat{S}_\mu$ can be written as

$$\hat{S}_\mu(Q;1\ldots n;P) = ieg^n \sum_{P(1\ldots n)} (T^{a_1}\ldots T^{a_n})_{ij} S_\mu(Q;1\ldots n;P) \tag{2.2.4}$$

with

$$S_\mu(Q;1\ldots n;P) = \sum_{m=0}^{n} J(Q;1\ldots m)\Gamma_\mu^{V,f_1,f_2} J(m+1\ldots n;P). \tag{2.2.5}$$

Eqs. (2.2.4) and (2.2.5) reflect the coupling of the vector boson at all possible positions on the quark line with the gluons randomly distributed over both sides. The vertex Γ_μ^{V,f_1f_2} depends on the nature of the vector boson and on the quark flavours. Throughout this chapter we set the KM matrix equal to unity. This has very little influence on the results [6]. All the S_μ's are conserved quantities,

$$S_\mu(Q;1\ldots n;P)\,(Q+K_1+\ldots+K_n+P)^\mu = 0. \tag{2.2.6}$$

They are also gauge invariant in the sense that replacing a gluon polarization vector $J(i)$ by the momentum K_i gives zero. The matrix element is given by

$$\mathcal{M}(Q;1,2,\ldots,n;P) = V^\mu \hat{S}_\mu. \tag{2.2.7}$$

The computation of the matrix element squared $|V^\mu \hat{S}_\mu|^2$ is done as follows. First determine all the S_μ's using eq. (2.2.5). The fact that we let the vector boson decay

has two consequences. The first is that we have to include a propagator for it. Thus one has

$$V^{\mu} = \frac{-ig^{\mu\nu}}{s - M_V^2 + iM_V\Gamma_V} L_{\nu}. \tag{2.2.8}$$

In this formula, s, M_V and Γ_V are the momentum squared, the mass and the width of the vector boson, respectively, and L_{ν} is a lepton current, which is given by

$$L_{\nu} = ie\bar{u}(l_1)\Gamma_{\nu}^{V,l_1 l_2} v(l_2). \tag{2.2.9}$$

Secondly, we need to sum over the polarization states of the decay products. Finally the square $|V^{\mu}\hat{S}_{\mu}|^2$ contains a colour matrix which originates from the product of the colour parts. We work out those products with

$$(T^a)_{ij}(T^a)_{kl} = \tfrac{1}{2}\left[\delta_{il}\delta_{kj} - \delta_{ij}\delta_{kl}/N\right] \tag{2.2.10}$$

resulting in a rational function in N. This procedure has to be repeated for all helicity configurations of the quarks, gluons and the decay products of the vector boson. The method sketched above is valid for any number of gluons. Only the colour matrix has to be determined separately for each value of n.

Nr. Gluons	W/Z old	W/Z new
0	0.00226	0.00223
1	0.00404	0.00386
2	0.01168	0.01233
3	0.1046	0.0807
4	—	0.8908
5	—	14.580

Table 2.2. CPU-time in seconds of the W/Z matrix elements with a quark pair and n gluons. Old entry stands for the routines based on [1]. New entry is the general method with recursion. Timing on a VAX 3500.

Specifying that the vector boson is a W leads to a reduction in the number of helicity amplitudes that has to be evaluated because the W only couples left-handedly. When implemented numerically the general recursive method can very well compete with analytical results as far as numerical evaluation speed is concerned. In Table 2.2 we made a comparison between two programs, one based on the analytical results of [1] and one based on the numerical recursion method. One can see that there is not much difference in the CPU-times needed. Together with the fact that for $n \geq 3$ the analytical results are very hard to obtain it shows that the recursive approach is the best method to use.

In the physical situation where we consider $P\bar{P} \rightarrow V+$ jets, two of the QCD particles in process (2.2.1) have to be crossed from the final to the initial state.

There are four possible ways :

$$q(P)\bar{q}(Q) \to V + g(K_1) + \ldots + g(K_n) \qquad n \geq 0 \quad (2.2.11)$$
$$q(P)g(K_1) \to V + q(Q) + g(K_2) + \ldots + g(K_n) \qquad n \geq 1 \quad (2.2.12)$$
$$\bar{q}(Q)g(K_1) \to V + \bar{q}(P) + g(K_2) + \ldots + g(K_n) \qquad n \geq 1 \quad (2.2.13)$$
$$g(K_1)g(K_2) \to V + q(Q) + \bar{q}(P) + g(K_3) + \ldots + g(K_n) \qquad n \geq 2 \quad (2.2.14)$$

In the case $n \geq 2$ four different matrix elements have to be evaluated. The fact that for more final state particles the extra gluon always ends up in the final state of the four processes mentioned above enables us to write down a general algorithm for the sum over physical subprocesses.

2.3 Matrix elements with two quark pairs

Here we discuss the calculation of the tree level matrix elements for the creation of a vector boson, two quarks, two antiquarks and two gluons, followed by the decay of the vectorboson into a lepton pair:

$$\emptyset \to V q_1 \bar{q}_2 q_3 \bar{q}_4 g_1 g_2, \qquad V \to l_1 \bar{l}_2. \tag{2.3.1}$$

Again we get the matrix elements for physical processes that occur in collision experiments by crossing two particles to the initial state. In contrast to the previous section we use explicit Feynman diagrams which will be grouped in gauge invariant sets. Helicity amplitudes will eventually be obtained from them with help of Weyl-van der Waerden spinor calculus.

The matrix element $\mathcal{M}$ is given by

$$\mathcal{M} = V^\mu \hat{T}_\mu, \tag{2.3.2}$$

where V^μ is given by eq. (2.2.8). From now on, we focus on the calculation of the four quark, two gluon coloured current $\hat{T}_\mu$. All quarks are assumed to be massless.

For the (anti-)quarks we will use the symbol Q_i, which stands for $(Q_i, \lambda_{q_i}, c_i, f_i)$, with Q_i = momentum, λ_{q_i} = helicity, c_i = colour and f_i = flavour. We denote the gluons by 1 and 2, which stand for $(K_i, \lambda_{g_i}, a_i)$, $(i = 1, 2)$, with K_i = momentum, λ_{g_i} = helicity and a_i = colour.

The calculation of the current $\hat{T}_\mu$ is in many ways similar to that of the $q\bar{q}q\bar{q}$ and $q\bar{q}q\bar{q}g$ currents presented in [1]. We will use several definitions, and also some results given there.

First, we write $\hat{T}_\mu$ as the sum of four parts $\hat{A}_\mu$:

$$\begin{aligned} \hat{T}_\mu(Q_1Q_2Q_3Q_4; 12) &= \hat{A}_\mu(Q_1Q_2Q_3Q_4; 12) - \hat{A}_\mu(Q_3Q_2Q_1Q_4; 12) \\ &- \hat{A}_\mu(Q_1Q_4Q_3Q_2; 12) + \hat{A}_\mu(Q_3Q_4Q_1Q_2; 12). \end{aligned} \tag{2.3.3}$$

$\hat{A}_\mu(Q_1Q_2Q_3Q_4; 12)$ is the sum of all Feynman diagrams that can be constructed by attaching two gluons g_1 and g_2 to the two basic diagrams in Fig. 2.1. We will refer to

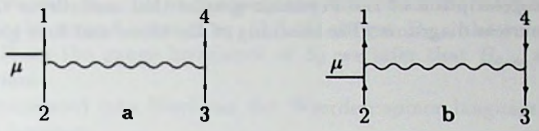

Fig. 2.1. The two basic diagrams for the four quark current $\hat{A}_\mu$.

the diagrams constructed using the left diagram as a-type diagrams and to the ones using the right diagram as b-type diagrams.

By combining the colour matrices associated with the vertices of a particular diagram using eq. (2.2.10), we can write it as the product of a colour factor and a colour independent factor. Doing this for all diagrams we find that the following factors occur:

$$\gamma_1(c_1c_2c_3c_4;a_1a_2) = \delta_{c_1c_4}(T^{a_1}T^{a_2})_{c_3c_2} \tag{2.3.4}$$

$$\gamma_2(c_1c_2c_3c_4;a_1a_2) = (T^{a_1})_{c_1c_4}(T^{a_2})_{c_3c_2} \tag{2.3.5}$$

$$\gamma_3(c_1c_2c_3c_4;a_1a_2) = (T^{a_1}T^{a_2})_{c_1c_4}\delta_{c_3c_2} \tag{2.3.6}$$

$$\gamma_4(c_1c_2c_3c_4;a_1a_2) = -\frac{1}{N}\delta_{c_1c_2}(T^{a_1}T^{a_2})_{c_3c_4} \tag{2.3.7}$$

$$\gamma_5(c_1c_2c_3c_4;a_1a_2) = -\frac{1}{N}(T^{a_1})_{c_1c_2}(T^{a_2})_{c_3c_4} \tag{2.3.8}$$

$$\gamma_6(c_1c_2c_3c_4;a_1a_2) = -\frac{1}{N}(T^{a_1}T^{a_2})_{c_1c_2}\delta_{c_3c_4} \tag{2.3.9}$$

$$\gamma_{i+6}(c_1c_2c_3c_4;a_1a_2) = \gamma_i(c_1c_2c_3c_4;a_2a_1) \text{ for } i=1,\ldots,6. \tag{2.3.10}$$

Splitting off the colour factors, and using the invariance of $\hat{A}_\mu$ when g_1 and g_2 are interchanged, we obtain:

$$\hat{A}_\mu(Q_1Q_2Q_3Q_4;12) = ieg^4\delta^{f_3f_4}\sum_{P(12)}\sum_{i=1}^{6}\gamma_i(c_1c_2c_3c_4;a_1a_2)B_{i\mu}^{f_1f_2}(Q_1Q_2Q_3Q_4;12). \tag{2.3.11}$$

The sum is over the two possible orders of the gluons. A common factor $ieg^4\delta^{f_3f_4}$ has also been extracted.

Before proceeding to describe the calculation of the functions $B_{i\mu}^{f_1f_2}$, we note that $\hat{A}_\mu$ is gauge invariant, i.e. it vanishes when a gluon polarization vector J_μ is replaced by its momentum K_μ. Because the colour factors γ_i are independent, this means that the $B_{i\mu}^{f_1f_2}$'s are also gauge invariant. Our strategy is to divide the $B_{i\mu}^{f_1f_2}$'s into as many gauge invariant pieces as possible and then to calculate all those pieces separately, choosing the most convenient gauge for the gluon polarization vectors in each piece.

We will give a description of the Feynman graphs that contribute to the $B_{i\mu}$'s. They are now colourless diagrams. The meaning of the three and four gluon vertices is as follows:

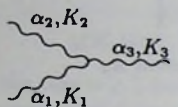

$$igV^{\alpha_1\alpha_2\alpha_3}(K_1,K_2,K_3) = ig\,[(K_1-K_2)^{\alpha_3}g^{\alpha_1\alpha_2} + (K_2-K_3)^{\alpha_1}g^{\alpha_2\alpha_3} + (K_3-K_1)^{\alpha_2}g^{\alpha_3\alpha_1}]\,, \tag{2.3.12}$$

where all the momenta K_i are defined as outgoing, and

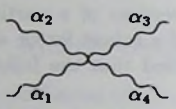

$$ig^2\,[2g^{\alpha_1\alpha_3}g^{\alpha_2\alpha_4} - g^{\alpha_1\alpha_2}g^{\alpha_3\alpha_4} - g^{\alpha_1\alpha_4}g^{\alpha_2\alpha_3}]\,. \tag{2.3.13}$$

These vertices are not symmetric under permutations of the gluons, so to have an unambiguous correspondence between the diagrams and the formulae, we adopt the convention that the gluons with labels $(1,2,3)$ in eq. (2.3.12) must be arranged in ascending order when one goes around the diagram clockwise. Similarly, for the four gluon vertex, the gluons labeled $(1,2,3,4)$ in (2.3.13) must be arranged clockwise around the diagram.

Let us begin with $B_{4\mu}$, $B_{5\mu}$ and $B_{6\mu}$, since they are somewhat simpler than $B_{1\mu}$, $B_{2\mu}$ and $B_{3\mu}$. We shall derive some expressions for them consisting of parts which we already know from [1] and new quantities. For the latter we don't give the explicit results but we indicate which types of diagram contribute. Also the occurrence of gauge invariant subsets is noticed for the reason mentioned above.

The diagrams for $B_{4\mu}$ are obtained by attaching g_1 and g_2 to the quark line that connects Q_3 with Q_4 in diagram a or diagram b. Gluon 1 must be attached below gluon 2. In other words, if we follow the quark line from Q_3 up towards Q_4, we should reach g_1 before we reach g_2. $B_{4\mu}$ also contains the diagrams where g_1 and g_2 are connected to each other by a three gluon vertex which is connected to the Q_3-Q_4 quark line. By adding all the diagrams we obtain:

$$B_{4\mu}^{f_1f_2}(Q_1Q_2Q_3Q_4;12) = \frac{1}{2}S_{\mu\alpha}^{V,f_1f_2}(Q_1;Q_2)\frac{g^{\alpha\beta}}{(Q_3+Q_4+K_1+K_2)^2}S_\beta(Q_3;12;Q_4), \tag{2.3.14}$$

with

$$\begin{aligned} S_{\mu\alpha}^{V,f_1f_2}(Q_1;Q_2) &= J(Q_1)\Gamma_\mu^{V,f_1f_2}[\not{Q}_2+\not{Q}_3+\not{Q}_4+\not{K}_1+\not{K}_2]^{-1}\gamma_\alpha J(Q_2) \\ &- J(Q_1)\gamma_\alpha[\not{Q}_1+\not{Q}_3+\not{Q}_4+\not{K}_1+\not{K}_2]^{-1}\Gamma_\mu^{V,f_1f_2}J(Q_2) \end{aligned} \tag{2.3.15}$$

and $S_\beta(Q_3;12;Q_4)$ as in eq. (2.2.5), but now with Γ_μ^{V,f_1f_2} replaced by γ_β. By inserting only the first term of eq. (2.3.15) in eq. (2.3.14) instead of the whole $S_{\mu\alpha}^{V,f_1f_2}$, we obtain

a quantity we call $B_{4\mu a}$. It is precisely the sum of all the a-type diagrams in $B_{4\mu}$. Taking only the second term of eq. (2.3.15) we get $B_{4\mu b}$, the sum of all the b-type diagrams. From the gauge invariance of S_β we infer that $B_{4\mu a}$ and $B_{4\mu b}$ are both gauge invariant.

When translated into Weyl-van der Waerden spinor language, eq. (2.3.14) and eq. (2.3.15) become:

$$B_{4\mu}^{f_1 f_2}(Q_1^+ Q_2^- Q_3 Q_4; 12) = \frac{(\sqrt{2})^2 R^{V,f_1 f_2} \sigma_\mu^{\dot{A}B} S^V_{\dot{A}B\dot{C}D}(Q_1^+ Q_2^-) S^{\dot{C}D}(Q_3; 12; Q_4)}{(Q_3 + Q_4 + K_1 + K_2)^2} \tag{2.3.16}$$

$$B_{4\mu}^{f_1 f_2}(Q_1^- Q_2^+ Q_3 Q_4; 12) = \frac{(\sqrt{2})^2 L^{V,f_1 f_2} \sigma_\mu^{\dot{A}B} S^V_{\dot{A}B\dot{C}D}(Q_1^- Q_2^+) S^{\dot{C}D}(Q_3; 12; Q_4)}{(Q_3 + Q_4 + K_1 + K_2)^2} \tag{2.3.17}$$

with

$$\begin{aligned} S^V_{\dot{A}B\dot{C}D}(Q_1^+ Q_2^-) &= \frac{q_{1\dot{A}}(Q_2 + Q_3 + Q_4 + K_1 + K_2)_{\dot{C}B} q_{2D}}{(Q_2 + Q_3 + Q_4 + K_1 + K_2)^2} \\ &- \frac{q_{1\dot{C}}(Q_1 + Q_3 + Q_4 + K_1 + K_2)_{\dot{A}D} q_{2B}}{(Q_1 + Q_3 + Q_4 + K_1 + K_2)^2} \end{aligned} \tag{2.3.18}$$

and

$$S^V_{\dot{A}B\dot{C}D}(Q_1^- Q_2^+) = -S^V_{\dot{A}B\dot{C}D}(Q_2^+ Q_1^-). \tag{2.3.19}$$

The quantities $L^{V,f_1 f_2}$ and $R^{V,f_1 f_2}$ are the coupling constants in

$$\Gamma_\mu^{V,f_1 f_2} = L^{V,f_1 f_2} \gamma_\mu \left(\frac{1-\gamma_5}{2}\right) + R^{V,f_1 f_2} \gamma_\mu \left(\frac{1+\gamma_5}{2}\right). \tag{2.3.20}$$

$S_{\dot{A}B}(Q_3; 12; Q_4)$ is defined by

$$S_\beta(Q_3; 12; Q_4) = (\sqrt{2})^2 \sigma_\beta^{\dot{A}B} S_{\dot{A}B}(Q_3; 12; Q_4). \tag{2.3.21}$$

Expressions for $S_{\dot{A}B}(Q_3; 12; Q_4)$ are listed in [1].[1]

The diagrams for $B_{5\mu}$ have g_1 attached to the left quark line and g_2 attached to the right quark line. Their sum can be expressed as a product in a way similar to $B_{4\mu}$:

$$\begin{aligned} &B_{5\mu}^{f_1 f_2}(Q_1 Q_2 Q_3 Q_4; 12) = \\ &\frac{1}{2} S^{V,f_1 f_2}_{\mu\alpha}(Q_1; 1; Q_2) \frac{g^{\alpha\beta}}{(Q_3 + Q_4 + K_2)^2} S_\beta(Q_3; 2; Q_4). \end{aligned} \tag{2.3.22}$$

[1]There is a misprint in the expression for $S(+;-,+;-)_{\dot{A}B}$. The second term should read

$$-\frac{(qk_2)^{*2}(Q + K_2)_{\dot{A}D} k_1^D p_B}{(qk_1)^*(K_1 + K_2)^2 (Q + K_1 + K_2)^2}.$$

$S^{V,f_1f_2}_{\mu\alpha}$ is the sum of six diagrams:

$$
\begin{aligned}
S^{V,f_1f_2}_{\mu\alpha}(Q_1;1;Q_2) = \\
&+J(Q_1;1)\Gamma^{V,f_1f_2}_{\mu}[\not{a}]^{-1}\gamma_\alpha J(Q_2) \\
&+J(Q_1)\Gamma^{V,f_1f_2}_{\mu}[\not{a}+\not{K}_1]^{-1}\not{P}(1)[\not{a}]^{-1}\gamma_\alpha J(Q_2) \\
&+J(Q_1)\Gamma^{V,f_1f_2}_{\mu}[\not{a}+\not{K}_1]^{-1}\gamma_\alpha J(1;Q_2) \\
&-J(Q_1;1)\gamma_\alpha[\not{b}+\not{K}_1]^{-1}\Gamma^{V,f_1f_2}_{\mu}J(Q_2) \\
&+J(Q_1)\gamma_\alpha[\not{b}]^{-1}\not{P}(1)[\not{b}+\not{K}_1]^{-1}\Gamma^{V,f_1f_2}_{\mu}J(Q_2) \\
&-J(Q_1)\gamma_\alpha[\not{b}]^{-1}\Gamma^{V,f_1f_2}_{\mu}J(1;Q_2),
\end{aligned}
\tag{2.3.23}
$$

where the abbreviations $a = Q_2 + Q_3 + Q_4 + K_2$ and $b = Q_1 + Q_3 + Q_4 + K_2$ have been used. $B_{5\mu}$ is the sum of two gauge invariant parts, $B_{5\mu a}$ and $B_{5\mu b}$, which consist of all the a-type and b-type diagrams, respectively. This corresponds to separating the first three terms and the last three terms in eq. (2.3.23). Translating eq. (2.3.22) into spinor language using

$$
S^{V,f_1f_2}_{\mu\alpha}(Q_1^+;1;Q_2^-) = \sqrt{2}\sigma_\mu^{\dot{A}B}\sigma_\alpha^{\dot{C}D}R^{V,f_1f_2}S^V_{\dot{A}B\dot{C}D}(Q_1^+;1;Q_2^-), \tag{2.3.24}
$$

$$
S^{V,f_1f_2}_{\mu\alpha}(Q_1^-;1;Q_2^+) = \sqrt{2}\sigma_\mu^{\dot{A}B}\sigma_\alpha^{\dot{C}D}L^{V,f_1f_2}S^V_{\dot{A}B\dot{C}D}(Q_1^-;1;Q_2^+), \tag{2.3.25}
$$

and

$$
S_\beta(Q_3;2;Q_4) = \sqrt{2}\sigma_\beta^{\dot{A}B}S_{\dot{A}B}(Q_3;2;Q_4) \tag{2.3.26}
$$

we find

$$
B^{f_1f_2}_{5\mu}(Q_1^+Q_2^-Q_3Q_4;12) = \frac{(\sqrt{2})^2R^{V,f_1f_2}\sigma_\mu^{\dot{A}B}S^V_{\dot{A}B\dot{C}D}(Q_1^+;1;Q_2^-)S^{\dot{C}D}(Q_3;2;Q_4)}{(Q_3+Q_4+K_2)^2} \tag{2.3.27}
$$

$$
B^{f_1f_2}_{5\mu}(Q_1^-Q_2^+Q_3Q_4;12) = \frac{(\sqrt{2})^2L^{V,f_1f_2}\sigma_\mu^{\dot{A}B}S^V_{\dot{A}B\dot{C}D}(Q_1^-;1;Q_2^+)S^{\dot{C}D}(Q_3;2;Q_4)}{(Q_3+Q_4+K_2)^2}. \tag{2.3.28}
$$

Expressions for $S_{\dot{A}B}(Q_3;2;Q_4)$ can be found in [1]. $S^V_{\dot{A}B\dot{C}D}$ must be calculated for each helicity combination. Although eq. (2.3.23) contains six terms, the number of terms in $S^V_{\dot{A}B\dot{C}D}$ can be reduced to four by using an appropriate gauge.

The next function, $B_{6\mu}$, is treated in the same way. The diagrams for $B_{6\mu}$ have g_1 and g_2 both attached to the left quark line of diagram a or diagram b, with g_1 nearest to Q_1 and g_2 nearest to Q_2

$$
\begin{aligned}
B^{f_1f_2}_{6\mu}(Q_1Q_2Q_3Q_4;12) = \\
&\frac{1}{2}S^{V,f_1f_2}_{\mu\alpha}(Q_1;12;Q_2)\frac{g^{\alpha\beta}}{(Q_3+Q_4)^2}S_\beta(Q_3;Q_4).
\end{aligned}
\tag{2.3.29}
$$

Here $S^{V,f_1f_2}_{\mu\alpha}(Q_1;12;Q_2)$ is defined analogously to $S^{V,f_1f_2}_{\mu\alpha}(Q_1;1;Q_2)$ and $S^{V,f_1f_2}_{\mu\alpha}(Q_1;Q_2)$. It contains contributions from 18 diagrams and it has to be calculated for every

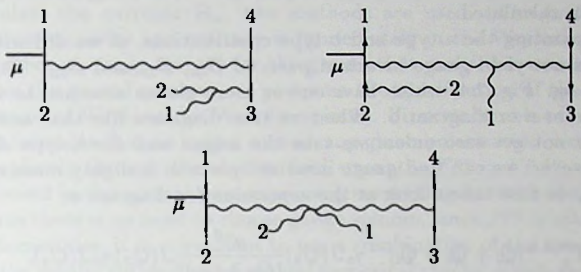

Fig. 2.2. Examples of diagrams for $B_{1\mu}$. The first one also contributes to $B_{4\mu}$.

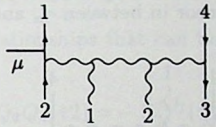

Fig. 2.3. This diagram does not contribute to $B_{1\mu}$.

helicity combination. Once again, the **a**-type part $B_{6\mu a}$ and the **b**-type part $B_{6\mu b}$ are separately gauge invariant.

The other B–functions, $B_{1\mu}$, $B_{2\mu}$ and $B_{3\mu}$, will now be discussed. The diagrams for $B_{1\mu}$ are obtained by adding g_1 and g_2 on to the bottom of diagram **a** or diagram **b**, i.e. they must be connected to the diagram somewhere along the line which starts at Q_3 and goes to Q_2. Someone travelling along that line should meet g_1 before he meets g_2. There are 25 diagrams of this kind. Some examples are shown in Fig. 2.2. The quarks and gluons, starting from Q_1 and going clockwise, are arranged in the order $Q_1Q_4Q_312Q_2$. Note that the colour labels in the colour factor (2.3.4) occur in the same order, i.e. $c_1c_4c_3a_1a_2c_2$ (reading the labels of a string $(T^aT^b\ldots T^k)_{xy}$ in the order $xab\ldots ky$). On the other hand the diagram in Fig. 2.3 has g_1 and g_2 in the wrong order and should not be included in $B_{1\mu}$.

The connection between diagrams and their colour factors is a general feature of all colour structures. For $B_{2\mu}$ there are 28 diagrams. They have g_1 attached to the top of the diagram, somewhere between Q_1 and Q_4, and g_2 attached to the bottom, like for example Fig. 2.4. The diagrams for $B_{3\mu}$ have both g_1 and g_2 attached on the top, with g_1 to the left of g_2. The number of diagrams is again 25 and there is, in fact, a one to one correspondence between the diagrams of $B_{1\mu}$ and those of $B_{3\mu}$. This is an instance of a more general symmetry of $\hat{A}_\mu$, which follows from CP invariance,

that we will discuss later on. It can be exploited to derive $B_{3\mu}$ from $B_{1\mu}$, once the latter has been calculated.

Simply separating the a-type and b-type contributions, as we did with $B_{4\mu}$, $B_{5\mu}$ and $B_{6\mu}$, does not yield gauge invariant parts of $B_{1\mu}$, $B_{2\mu}$ and $B_{3\mu}$. This is due to diagrams like eg. Fig. 2.4, which have one or more gluons attached to the internal gluon of diagram a or diagram b. When we take diagrams like that and replace J_μ by K_μ, we do not get zero unless we take the a-type and the b-type diagrams all together. However, we can find gauge invariant parts in a slighty more complicated way. For this, we first take a look at the expression for diagram a:

$$\frac{1}{2}J(Q_1)\Gamma_\mu^{V,f_1f_2}[\not{Q}_2+\not{Q}_3+\not{Q}_4]^{-1}\gamma_\alpha J(Q_2)\frac{g^{\alpha\beta}}{(Q_3+Q_4)^2}J(Q_3)\gamma_\beta J(Q_4). \tag{2.3.30}$$

It contains a γ_α on the left quark line and a γ_β on the right quark line, connected by the metric tensor $g^{\alpha\beta}$. All the diagrams for $B_{4\mu}$, $B_{5\mu}$ and $B_{6\mu}$ contain this factor, but in diagrams where gluons are attached to the internal gluon of diagram a or diagram b, there is a more complicated tensor in between γ_α and γ_β.

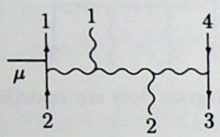

Fig. 2.4. A contribution to $B_{2\mu}$.

For example in Fig. 2.4 it is:

$$\begin{aligned} &J(1)_\nu V^{\alpha\nu\kappa}(-(Q_3+Q_4+K_1+K_2),K_1,Q_3+Q_4+K_2)\\ &\times g_{\kappa\lambda}V^{\lambda\beta\rho}(-(Q_3+Q_4+K_2),Q_3+Q_4,K_2)J(2)_\rho. \end{aligned} \tag{2.3.31}$$

When we substitute eq. (2.3.12) in eq. (2.3.31) and contract all the dummy indices we find, among many other terms, one that is proportional to $g^{\alpha\beta}$. This happens in all the other diagrams as well. The quantity containing all contributions to $B_{1\mu}$ that are proportional to $g^{\alpha\beta}$, is gauge invariant. Let us call it "$B_{1\mu}(g^{\alpha\beta})$" for the moment. Of course, the rest of $B_{1\mu}$, "$B_{1\mu}(\text{no } g^{\alpha\beta})$", is also gauge invariant. Within $B_{1\mu}(g^{\alpha\beta})$ we can still separate the a-type and the b-type contributions, but in $B_{1\mu}(\text{no } g^{\alpha\beta})$ we cannot. So, our final decomposition of $B_{1\mu}$ is:

$$\begin{aligned} B_{1\mu} &= B_{1\mu a}+B_{1\mu b}+B_{1\mu c} \text{ with}\\ B_{1\mu a} &= \text{sum of a-type contributions proportional to } g^{\alpha\beta},\\ B_{1\mu b} &= \text{sum of b-type contributions proportional to } g^{\alpha\beta},\\ B_{1\mu c} &= \text{everything else.} \end{aligned} \tag{2.3.32}$$

The quantities $B_{2\mu}$ and $B_{3\mu}$ are decomposed in exactly the same way.

To calculate the currents $B_{i\mu}$, two methods are used. The first is to take a gauge invariant quantity and evaluate it immediately in the Weyl-van der Waerden formalism, choosing gauge spinors for the gluons that make this as easy as possible. When we use the second method, we postpone the specification of the helicities and the introduction of Weyl-van der Waerden spinors. First we combine terms so that we end up with formulae that no longer contain any gluon polarization vectors explicitly, but only implicitly through the abelian field strengths $F^{\mu\nu} = K^\mu J^\nu - K^\nu J^\mu$. After that, we proceed in the normal way, expressing everything in terms of spinors, except that this time there is no need to choose gauge spinors, since $F^{\mu\nu}$ is manifestly gauge invariant. Sometimes, it is convenient to use a combination of the two methods.

To test the results we performed several numerical checks, which are based on the following properties of the $B-$functions.

The first is current conservation:

$$(Q_1 + Q_2 + Q_3 + Q_4 + K_1 + K_2)^\mu B_{i\mu} = 0. \tag{2.3.33}$$

Then there is a set of relationships that can be proved using charge conjugation invariance.

$$\begin{aligned}
B_{1\mu}^{f_1 f_2}(Q_1Q_2Q_3Q_4;12) &= -\tilde{B}_{3\mu}^{f_2 f_1}(Q_2Q_1Q_4Q_3;21)\\
B_{2\mu}^{f_1 f_2}(Q_1Q_2Q_3Q_4;12) &= -\tilde{B}_{2\mu}^{f_2 f_1}(Q_2Q_1Q_4Q_3;21)\\
B_{4\mu}^{f_1 f_2}(Q_1Q_2Q_3Q_4;12) &= -\tilde{B}_{4\mu}^{f_2 f_1}(Q_2Q_1Q_4Q_3;21)\\
B_{5\mu}^{f_1 f_2}(Q_1Q_2Q_3Q_4;12) &= -\tilde{B}_{5\mu}^{f_2 f_1}(Q_2Q_1Q_4Q_3;12)\\
B_{6\mu}^{f_1 f_2}(Q_1Q_2Q_3Q_4;12) &= -\tilde{B}_{6\mu}^{f_2 f_1}(Q_2Q_1Q_4Q_3;21)
\end{aligned} \tag{2.3.34}$$

The wiggle above the $B-$functions on the right hand side means that they must be calculated with the vector boson vertex (2.3.20) replaced by

$$\tilde{\Gamma}_\mu^{V,f_1 f_2} = R^{V,f_1 f_2}\gamma_\mu(\frac{1-\gamma_5}{2}) + L^{V,f_1 f_2}\gamma_\mu(\frac{1+\gamma_5}{2}). \tag{2.3.35}$$

In certain regions of phase space the $B-$functions diverge because they contain diagrams with denominators that vanish. This happens when the energy of one of the gluons goes to zero, and also, because we are neglecting quark masses, when particles are collinear. In these limits, our tree level calculation is certainly not a good approximation to the exact S-matrix element. Nevertheless, it is useful to evaluate the $B-$functions numerically in the soft and collinear limits, because asymptotically, they can be related to currents B_μ and S_μ that have been calculated and checked before [1].

The soft limits that were tested are the limit when g_1 becomes soft:

$$B_{1\mu}^{f_1 f_2}(Q_1Q_2Q_3Q_4;g_1g_2) \;\rightarrow\; S_{Q_3\underline{K_1}K_2}B_{1\mu}^{f_1 f_2}(Q_1Q_2Q_3Q_4;g_2), \tag{2.3.36}$$

$$B_{2\mu}^{f_1 f_2}(Q_1Q_2Q_3Q_4;g_1g_2) \;\rightarrow\; S_{Q_1\underline{K_1}Q_4}B_{1\mu}^{f_1 f_2}(Q_1Q_2Q_3Q_4;g_2), \tag{2.3.37}$$

$$B_{3\mu}^{f_1 f_2}(Q_1Q_2Q_3Q_4;g_1g_2) \rightarrow S_{Q_1\underline{K_1}K_2}B_{2\mu}^{f_1 f_2}(Q_1Q_2Q_3Q_4;g_2), \tag{2.3.38}$$
$$B_{4\mu}^{f_1 f_2}(Q_1Q_2Q_3Q_4;g_1g_2) \rightarrow S_{Q_3\underline{K_1}K_2}B_{3\mu}^{f_1 f_2}(Q_1Q_2Q_3Q_4;g_2), \tag{2.3.39}$$
$$B_{5\mu}^{f_1 f_2}(Q_1Q_2Q_3Q_4;g_1g_2) \rightarrow S_{Q_1\underline{K_1}Q_2}B_{3\mu}^{f_1 f_2}(Q_1Q_2Q_3Q_4;g_2), \tag{2.3.40}$$
$$B_{6\mu}^{f_1 f_2}(Q_1Q_2Q_3Q_4;g_1g_2) \rightarrow S_{Q_1\underline{K_1}K_2}B_{4\mu}^{f_1 f_2}(Q_1Q_2Q_3Q_4;g_2); \tag{2.3.41}$$

the limit when g_2 becomes soft:

$$B_{1\mu}^{f_1 f_2}(Q_1Q_2Q_3Q_4;g_1g_2) \rightarrow S_{K_1\underline{K_2}Q_2}B_{1\mu}^{f_1 f_2}(Q_1Q_2Q_3Q_4;g_1), \tag{2.3.42}$$
$$B_{2\mu}^{f_1 f_2}(Q_1Q_2Q_3Q_4;g_1g_2) \rightarrow S_{Q_3\underline{K_2}Q_2}B_{2\mu}^{f_1 f_2}(Q_1Q_2Q_3Q_4;g_1), \tag{2.3.43}$$
$$B_{3\mu}^{f_1 f_2}(Q_1Q_2Q_3Q_4;g_1g_2) \rightarrow S_{K_1\underline{K_2}Q_4}B_{2\mu}^{f_1 f_2}(Q_1Q_2Q_3Q_4;g_1), \tag{2.3.44}$$
$$B_{4\mu}^{f_1 f_2}(Q_1Q_2Q_3Q_4;g_1g_2) \rightarrow S_{K_1\underline{K_2}Q_4}B_{3\mu}^{f_1 f_2}(Q_1Q_2Q_3Q_4;g_1), \tag{2.3.45}$$
$$B_{5\mu}^{f_1 f_2}(Q_1Q_2Q_3Q_4;g_1g_2) \rightarrow S_{Q_3\underline{K_2}Q_4}B_{4\mu}^{f_1 f_2}(Q_1Q_2Q_3Q_4;g_1), \tag{2.3.46}$$
$$B_{6\mu}^{f_1 f_2}(Q_1Q_2Q_3Q_4;g_1g_2) \rightarrow S_{K_1\underline{K_2}Q_2}B_{4\mu}^{f_1 f_2}(Q_1Q_2Q_3Q_4;g_1); \tag{2.3.47}$$

and the limit when g_1 and g_2 both become soft:

$$B_{1\mu}^{f_1 f_2}(Q_1Q_2Q_3Q_4;g_1g_2) \rightarrow S_{Q_3\underline{K_1K_2}Q_2}B_{\mu}^{f_1 f_2}(Q_1Q_2Q_3Q_4), \tag{2.3.48}$$
$$B_{2\mu}^{f_1 f_2}(Q_1Q_2Q_3Q_4;g_1g_2) \rightarrow S_{Q_1\underline{K_1}Q_4}S_{Q_3\underline{K_2}Q_2}B_{\mu}^{f_1 f_2}(Q_1Q_2Q_3Q_4), \tag{2.3.49}$$
$$B_{3\mu}^{f_1 f_2}(Q_1Q_2Q_3Q_4;g_1g_2) \rightarrow S_{Q_1\underline{K_1K_2}Q_4}B_{\mu}^{f_1 f_2}(Q_1Q_2Q_3Q_4), \tag{2.3.50}$$
$$B_{4\mu}^{f_1 f_2}(Q_1Q_2Q_3Q_4;g_1g_2) \rightarrow S_{Q_3\underline{K_1K_2}Q_4}B_{\mu}^{f_1 f_2}(Q_1Q_2Q_3Q_4), \tag{2.3.51}$$
$$B_{5\mu}^{f_1 f_2}(Q_1Q_2Q_3Q_4;g_1g_2) \rightarrow S_{Q_1\underline{K_1}Q_2}S_{Q_3\underline{K_2}Q_4}B_{\mu}^{f_1 f_2}(Q_1Q_2Q_3Q_4), \tag{2.3.52}$$
$$B_{6\mu}^{f_1 f_2}(Q_1Q_2Q_3Q_4;g_1g_2) \rightarrow S_{Q_1\underline{K_1K_2}Q_2}B_{\mu}^{f_1 f_2}(Q_1Q_2Q_3Q_4). \tag{2.3.53}$$

The soft factors are given by [8]:

$$S_{Q\underline{K}P} = \frac{Q\cdot F\cdot P}{Q\cdot KK\cdot P} \tag{2.3.54}$$

$$\begin{aligned} S_{Q\underline{K_1K_2}P} &= \frac{Q\cdot F_1\cdot F_2\cdot P}{Q\cdot K_1K_1\cdot K_2K_2\cdot P} - \frac{Q\cdot F_1\cdot F_2\cdot Q}{Q\cdot K_1K_1\cdot K_2(K_1+K_2)\cdot Q} \\ &- \frac{P\cdot F_1\cdot F_2\cdot P}{P\cdot (K_1+K_2)K_1\cdot K_2K_2\cdot P}. \end{aligned} \tag{2.3.55}$$

The following collinear limit was tested: when $Q_3 \rightarrow zK$, $Q_4 \rightarrow (1-z)K$ with K an arbitrary lightlike momentum and $0 < z < 1$:

$$B_{1\mu}^{f_1 f_2} \rightarrow \frac{1}{2}\sum_{\lambda=\pm 1} h_\lambda(\lambda_{q_3}\lambda_{\bar{q}_4})S_\mu^{f_1 f_2}(Q_1;K\lambda,1,2;Q_2) \tag{2.3.56}$$
$$B_{2\mu}^{f_1 f_2} \rightarrow \frac{1}{2}\sum_{\lambda=\pm 1} h_\lambda(\lambda_{q_3}\lambda_{\bar{q}_4})S_\mu^{f_1 f_2}(Q_1;1,K\lambda,2;Q_2) \tag{2.3.57}$$

$$B_{3\mu}^{f_1 f_2} \rightarrow \frac{1}{2}\sum_{\lambda=\pm 1} h_\lambda(\lambda_{q_3}\lambda_{\bar{q}_4}) S_\mu^{f_1 f_2}(Q_1;1,2,K\lambda;Q_2) \tag{2.3.58}$$

$$B_{4\mu}^{f_1 f_2} \rightarrow 0 \tag{2.3.59}$$

$$B_{5\mu}^{f_1 f_2} \rightarrow 0 \tag{2.3.60}$$

$$\begin{aligned} B_{6\mu}^{f_1 f_2} \rightarrow & \frac{1}{2}\sum_{\lambda=\pm 1} h_\lambda(\lambda_{q_3}\lambda_{\bar{q}_4})\{S_\mu^{f_1 f_2}(Q_1;K\lambda,1,2;Q_2) \\ & + S_\mu^{f_1 f_2}(Q_1;1,2,K\lambda;Q_2) + S_\mu^{f_1 f_2}(Q_1;1,2,K\lambda;Q_2)\} \end{aligned} \tag{2.3.61}$$

The collinearity factors are given by:

$$\begin{aligned} h_+(+-) &= \frac{-\sqrt{2}z}{\langle q_3 q_4\rangle^*} \qquad h_-(+-) = \frac{\sqrt{2}(1-z)}{\langle q_3 q_4\rangle} \\ h_+(-+) &= \frac{\sqrt{2}(1-z)}{\langle q_3 q_4\rangle^*} \qquad h_-(-+) = \frac{-\sqrt{2}z}{\langle q_3 q_4\rangle}. \end{aligned} \tag{2.3.62}$$

As a final point of this section we discuss the matrix element squared. To do the colour summation, we write

$$\hat{T}_\mu = \sum_{i=1}^{48} \gamma_i A_{i\mu} \tag{2.3.63}$$

with, for $i = 1,\ldots,6$:

$$\gamma_i = \gamma_i(c_1c_2c_3c_4;a_1a_2) \text{ as in eqs. (2.3.4)–(2.3.9)} \tag{2.3.64}$$

and

$$A_{i\mu} = ieg^4\delta^{f_3 f_4} B_{i\mu}^{f_1 f_2}(Q_1Q_2Q_3Q_4;12). \tag{2.3.65}$$

For $i = 7,\ldots,48$, γ_i and $A_{i\mu}$ are given by:

$$\begin{aligned} \gamma_{i+6} &= \gamma_i(a_1 \leftrightarrow a_2), & A_{i+6\mu} &= A_{i\mu}(g_1 \leftrightarrow g_2) & i &= 1,\ldots,6 \\ \gamma_{i+12} &= -\gamma_i(c_1 \leftrightarrow c_3), & A_{i+12\mu} &= A_{i\mu}(Q_1 \leftrightarrow Q_3) & i &= 1,\ldots,12 \\ \gamma_{i+24} &= \gamma_i(c_1 \leftrightarrow c_3, c_2 \leftrightarrow c_4), & A_{i+24\mu} &= A_{i\mu}(Q_1 \leftrightarrow Q_3, Q_2 \leftrightarrow Q_4) & i &= 1,\ldots,12 \\ \gamma_{i+36} &= -\gamma_i(c_2 \leftrightarrow c_4), & A_{i+36\mu} &= A_{i\mu}(Q_2 \leftrightarrow Q_4) & i &= 1,\ldots,12. \end{aligned} \tag{2.3.66}$$

Using this notation, the colour summed matrix element squared can be written as:

$$\sum_{colours} |\mathcal{M}|^2 = \sum_{i=1}^{48}\sum_{j=1}^{48} c_{ij}(V^\mu A_{i\mu})^*(V^\nu A_{j\nu}) \tag{2.3.67}$$

with

$$c_{ij} = \sum_{c_1c_2c_3c_4a_1a_2} \gamma_i^*(c_1c_2c_3c_4a_1a_2)\gamma_j(c_1c_2c_3c_4a_1a_2). \tag{2.3.68}$$

The matrix c_{ij} can be expressed as a rational function of N using eq. (2.2.10). For completeness it is given explicitly in appendix 2A. Then eq. (2.3.67) must be summed over all helicity combinations.

2.4 Matrix elements with three quark pairs

The matrix element for subprocesses involving six quarks and a vector boson, which decays into a lepton pair, is given by:

$$\mathcal{M} = V^{\mu}\hat{U}_{\mu}, \tag{2.4.1}$$

where $\hat{U}_{\mu}$ is the six quark current. Again all the quarks and antiquarks are outgoing particles. We denote the quarks by q_1, q_3 and q_5 and the antiquarks by $\bar{q}_2$, $\bar{q}_4$ and $\bar{q}_6$. Each of these particles has a momentum Q_i, a helicity λ_i, a colour c_i and a flavour f_i.

$\hat{U}_{\mu}$ is the sum of nine basic Feynman diagrams and all those which arise by permuting the quarks and the antiquarks. We write

$$\hat{U}_{\mu}(123456) = \sum_{P(135),P'(246)} (-1)^{P}(-1)^{P'}\left\{\tfrac{1}{2}\hat{m}_{1\mu} + \hat{m}_{2\mu} + \hat{m}_{3\mu} + \hat{m}_{4\mu}\right\}. \tag{2.4.2}$$

We sum over all quark permutations P and antiquark permutations P'. The quantities $\hat{m}_{i\mu}$ represent the following diagrams:

$\hat{m}_1 =$ 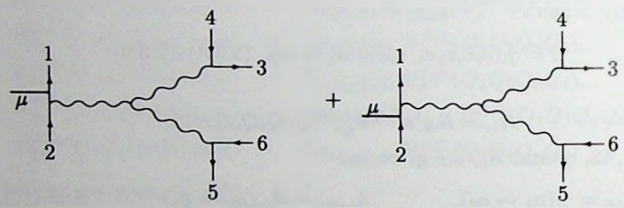

(2.4.3)

$\hat{m}_2 =$ 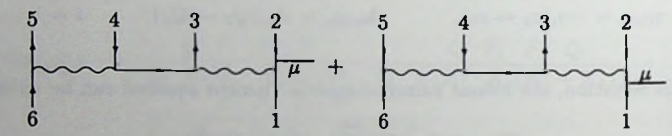

(2.4.4)

$\hat{m}_3 =$ 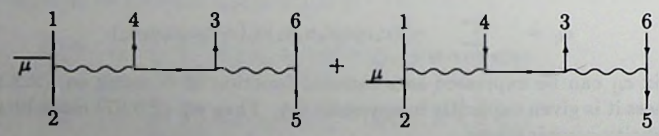

(2.4.5)

$\hat{m}_4 =$ 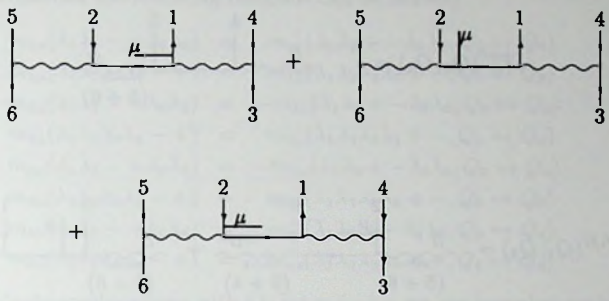

(2.4.6)

The quantity $\hat{m}_{1\mu}$ has a factor of $\frac{1}{2}$ because the diagrams of $\hat{m}_{1\mu}$ do not change when $(3 \leftrightarrow 5)$ and $(4 \leftrightarrow 6)$ are interchanged at the same time. This means that they occur twice in the sum over all the permutations. Extracting some overall factors and the colour factors, we obtain:

$$\hat{m}_{1\mu}(123456) = \tfrac{1}{4} ieg^4 \{\delta_{c_1c_4}\delta_{c_3c_6}\delta_{c_5c_2} m_{1\mu}(123456) + \delta_{c_1c_6}\delta_{c_3c_2}\delta_{c_5c_4} m_{1\mu}(125634)\} \tag{2.4.7}$$

$$\hat{m}_{2\mu}(123456) = \tfrac{1}{4} ieg^4 \left\{\delta_{c_1c_6}\delta_{c_3c_2}\delta_{c_5c_4} - \frac{1}{N}\delta_{c_1c_2}\delta_{c_3c_6}\delta_{c_5c_4} - \frac{1}{N}\delta_{c_1c_4}\delta_{c_3c_2}\delta_{c_5c_6} + \frac{1}{N^2}\delta_{c_1c_2}\delta_{c_3c_4}\delta_{c_5c_6}\right\} m_{2\mu}(123456) \tag{2.4.8}$$

and similar expressions for $\hat{m}_{3\mu}$ and $\hat{m}_{4\mu}$. Substituting them into the formula for $\hat{U}_\mu$ gives:

$$\hat{U}_\mu = \tfrac{1}{4} ieg^4 \sum_{P(135)} (-1)^P \delta_{c_1c_6}\delta_{c_3c_2}\delta_{c_5c_4}\{B_{1\mu} + \frac{1}{N}B_{2\mu} + \frac{1}{N^2}B_{3\mu}\} \tag{2.4.9}$$

where $B_{1\mu}$, $B_{2\mu}$ and $B_{3\mu}$ are linear combinations of $m_{1\mu}$, $m_{2\mu}$, $m_{3\mu}$ and $m_{4\mu}$ with arguments in various different orders. To calculate the $m_{i\mu}$'s, we will first express them in terms of smaller objects like $S_\alpha(Q_1;Q_2)$.

$$m_{1\mu}(123456) = \delta^{f_3f_4}\delta^{f_5f_6}\frac{S^{V,f_1f_2}_{\mu\alpha}(Q_1;Q_2)\, S_\beta(Q_3;Q_4)\, S_\gamma(Q_5;Q_6)}{(Q_3+Q_4)^2(Q_5+Q_6)^2(Q_3+Q_4+Q_5+Q_6)^2} \times V^{\alpha\beta\gamma}(-(Q_3+Q_4+Q_5+Q_6), Q_3+Q_4, Q_5+Q_6). \tag{2.4.10}$$

For $m_{2\mu}$, $m_{3\mu}$ and $m_{4\mu}$ we need some additional building blocks.

$T_2^{\alpha\beta}(Q_3;Q_4) =$ 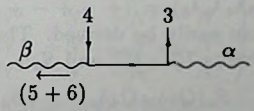

(2.4.11)

$$T_3^{\alpha\beta}(Q_3;Q_4) =$$

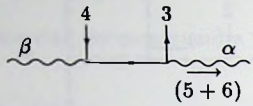

(2.4.12)

$$T_{4\mu}^{\alpha\beta V f_1 f_2}(Q_1;Q_2) =$$

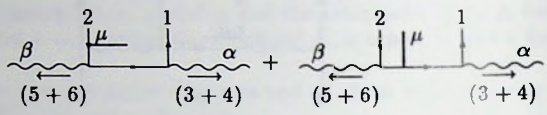

$$+$$

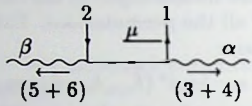

(2.4.13)

or equivalently,

$$T_2^{\alpha\beta}(Q_3;Q_4) = J(Q_3)\gamma^\alpha[\not{Q}_4 + \not{Q}_5 + \not{Q}_6]^{-1}\gamma^\beta J(Q_4) \tag{2.4.14}$$

$$T_3^{\alpha\beta}(Q_3;Q_4) = -J(Q_3)\gamma^\alpha[\not{Q}_3 + \not{Q}_5 + \not{Q}_6]^{-1}\gamma^\beta J(Q_4) \tag{2.4.15}$$

$$\begin{aligned} T_{4\mu}^{\alpha\beta}(Q_1;Q_2) &= J(Q_1)\Gamma_\mu^{V,f_1f_2}[\not{Q}_2+\not{Q}_3+\not{Q}_4+\not{Q}_5+\not{Q}_6]^{-1}\gamma_\alpha[\not{Q}_2+\not{Q}_5+\not{Q}_6]^{-1}\gamma^\beta J(Q_2) \\ &- J(Q_1)\gamma^\alpha[\not{Q}_1+\not{Q}_3+\not{Q}_4]^{-1}\Gamma_\mu^{V,f_1f_2}[\not{Q}_3+\not{Q}_5+\not{Q}_6]^{-1}\gamma^\beta J(Q_2) \\ &+ J(Q_1)\gamma^\alpha[\not{Q}_1+\not{Q}_3+\not{Q}_4]^{-1}\gamma^\beta[\not{Q}_1+\not{Q}_3+\not{Q}_4+\not{Q}_5+\not{Q}_6]^{-1}\Gamma_\mu^{V,f_1f_2}J(Q_2), \end{aligned} \tag{2.4.16}$$

$$m_{2\mu} = \frac{\delta^{f_3f_4}\delta^{f_5f_6}S_{\mu\alpha}^{V,f_1f_2}(Q_1;Q_2)T_2^{\alpha\beta}(Q_3;Q_4)S_\beta(Q_5;Q_6)}{(Q_5+Q_6)^2(Q_3+Q_4+Q_5+Q_6)^2} \tag{2.4.17}$$

$$m_{3\mu} = \frac{\delta^{f_3f_4}\delta^{f_5f_6}S_\alpha(Q_5;Q_6)T_3^{\alpha\beta}(Q_3;Q_4)S_{\mu\beta}^{V,f_1f_2}(Q_1;Q_2)}{(Q_5+Q_6)^2(Q_3+Q_4+Q_5+Q_6)^2} \tag{2.4.18}$$

$$m_{4\mu} = \frac{\delta^{f_3f_4}\delta^{f_5f_6}S_\alpha(Q_3;Q_4)T_{4\mu}^{\alpha\beta}(Q_1;Q_2)S_\beta(Q_5;Q_6)}{(Q_3+Q_4)^2(Q_5+Q_6)^2} \tag{2.4.19}$$

Now we use use Weyl-van der Waerden spinors to calculate the $m_{i\mu}$'s for the helicity combination $(\lambda_1\lambda_2\lambda_3\lambda_4\lambda_5\lambda_6) = (+-+-+-)$. Once they are known, the $m_{i\mu}$'s for other helicities can easily be derived. This is done as follows. First note some properties of the currents $T_2^{\alpha\beta}$, $T_3^{\alpha\beta}$ and S_α:

$$\begin{aligned} S_\alpha(Q_3\lambda_3;Q_4\lambda_4) &= S_\alpha(Q_4\lambda_4;Q_3\lambda_3) \\ T_3^{\alpha\beta}(Q_3\lambda_3;Q_4\lambda_4) &= -T_2^{\beta\alpha}(Q_4\lambda_4;Q_3\lambda_3). \end{aligned} \tag{2.4.20}$$

From these properties the following relations can be derived.

$$
\begin{aligned}
m_{1\mu}(\lambda_1\lambda_2 - +\lambda_5\lambda_6) &= m_{1\mu}(\lambda_1\lambda_2 + -\lambda_5\lambda_6, Q_3 \leftrightarrow Q_4) \\
m_{1\mu}(\lambda_1\lambda_2\lambda_3\lambda_4 - +) &= m_{1\mu}(\lambda_1\lambda_2\lambda_3\lambda_4 + -, Q_5 \leftrightarrow Q_6) \\
m_{2\mu}(\lambda_1\lambda_2 - +\lambda_5\lambda_6) &= -m_{3\mu}(\lambda_1\lambda_2 + -\lambda_5\lambda_6, Q_3 \leftrightarrow Q_4) \\
m_{2\mu}(\lambda_1\lambda_2\lambda_3\lambda_4 - +) &= m_{2\mu}(\lambda_1\lambda_2\lambda_3\lambda_4 + -, Q_5 \leftrightarrow Q_6) \\
m_{3\mu}(\lambda_1\lambda_2 - +\lambda_5\lambda_6) &= -m_{2\mu}(\lambda_1\lambda_2 + -\lambda_5\lambda_6, Q_3 \leftrightarrow Q_4) \\
m_{3\mu}(\lambda_1\lambda_2\lambda_3\lambda_4 - +) &= m_{3\mu}(\lambda_1\lambda_2\lambda_3\lambda_4 + -, Q_5 \leftrightarrow Q_6) \\
m_{4\mu}(\lambda_1\lambda_2 - +\lambda_5\lambda_6) &= m_{4\mu}(\lambda_1\lambda_2 + -\lambda_5\lambda_6, Q_3 \leftrightarrow Q_4) \\
m_{4\mu}(\lambda_1\lambda_2\lambda_3\lambda_4 - +) &= m_{4\mu}(\lambda_1\lambda_2\lambda_3\lambda_4 + -, Q_5 \leftrightarrow Q_6)
\end{aligned}
\tag{2.4.21}
$$

To get the helicity combinations with $(\lambda_1\lambda_2) = (-+)$, we use complex conjugation.

$$
\begin{aligned}
& m_{i\mu}(-,+,\lambda_3,\lambda_4,\lambda_5,\lambda_6) = \\
& \quad [m_{i\mu}(+,-,-\lambda_3,-\lambda_4,-\lambda_5,-\lambda_6, R^{V,f_1f_2} \to L^{V,f_1f_2})]^*
\end{aligned}
\tag{2.4.22}
$$

These relations are sufficient to obtain all other helicity amplitudes.

In order to square the matrix element one introduces an amplitude $X(P)$ depending on a specific permutation P of the quarks.

$$
\mathcal{M} = V^\mu \hat{U}_\mu = \tfrac{1}{4} ieg^4 \sum_{P(135)} (-1)^P X(P) \delta_{c_{P(1)}c_6} \delta_{c_{P(3)}c_2} \delta_{c_{P(5)}c_4}
\tag{2.4.23}
$$

with

$$
\begin{aligned}
X(P) = V^\mu \Big\{ & B_{1\mu}(P(1)2P(3)4P(5)6) \\
& + \frac{1}{N} B_{2\mu}(P(1)2P(3)4P(5)6) + \frac{1}{N^2} B_{3\mu}(P(1)2P(3)4P(5)6) \Big\}
\end{aligned}
\tag{2.4.24}
$$

The six quark orderings (135), (153), (351), (315), (513) and (531) are obtained by permutations P_i $(i = 1, \ldots, 6)$ from the ordering (135). Summing over the colours leads to a 6×6 colour matrix $c_{PP'}$.

$$
\sum_{c_1 \ldots c_6} |\mathcal{M}|^2 = (\frac{eg^4}{4})^2 \sum_P \sum_{P'} c_{PP'} X(P)^* X(P')
\tag{2.4.25}
$$

with

$$
c_{PP'} = \begin{pmatrix}
N^3 & -N^2 & N & -N^2 & N & -N^2 \\
-N^2 & N^3 & -N^2 & N & -N^2 & N \\
N & -N^2 & N^3 & -N^2 & N & -N^2 \\
-N^2 & N & -N^2 & N^3 & -N^2 & N \\
N & -N^2 & N & -N^2 & N^3 & -N^2 \\
-N^2 & N & -N^2 & N & -N^2 & N^3
\end{pmatrix}
\tag{2.4.26}
$$

Finally one has to sum over all the helicities in eq. (2.4.25).

When one restricts the calculations to W production a number of simplifications occur, both in the four and in the six quark cases. Since $R^{W,f_1 f_2} = 0$, all helicity amplitudes with $(\lambda_{q_1}, \lambda_{\bar{q}_2}) = (+-)$ vanish. Knowing the quark flavours, the Kronecker delta in eq. (2.3.11) reduces the number of quark permutations that contribute to $\mathcal{M}$.

In the four quark case at least two quarks must have the same flavour. By rearranging the particles we can label them as q_3 and $\bar{q}_4$. Then q_1 and $\bar{q}_2$ must have different flavours. So we have $f_1 \neq f_2$, $f_3 = f_4$. This leaves three possible situations.

1). $f_1 \neq f_3$, $f_2 \neq f_3$, eg. $u\bar{d}c\bar{c}$. In this case, no quark permutations are allowed:

$$\hat{T}_\mu(Q_1Q_2Q_3Q_4; 12) = \hat{A}_\mu(Q_1Q_2Q_3Q_4; 12). \tag{2.4.27}$$

2). $f_1 = f_3 = f_4 \neq f_2$, eg. $u\bar{d}u\bar{u}$. Now q_1 and q_3 are identical particles, so

$$\hat{T}_\mu(Q_1Q_2Q_3Q_4; 12) = \hat{A}_\mu(Q_1Q_2Q_3Q_4; 12) - \hat{A}_\mu(Q_3Q_2Q_1Q_4; 12). \tag{2.4.28}$$

3). $f_1 \neq f_2 = f_3 = f_4$, eg. $u\bar{d}d\bar{d}$. Here

$$\hat{T}_\mu(Q_1Q_2Q_3Q_4; 12) = \hat{A}_\mu(Q_1Q_2Q_3Q_4; 12) - \hat{A}_\mu(Q_1Q_4Q_3Q_2; 12). \tag{2.4.29}$$

It follows that in case 2), $|\mathcal{M}|^2$ is invariant under $q_1 \leftrightarrow q_3$. In case 3), it is invariant under $\bar{q}_2 \leftrightarrow \bar{q}_4$. In all three cases $|\mathcal{M}|^2$ is invariant under $g_1 \leftrightarrow g_2$. These symmetries were checked numerically.

In the six quark subprocesses there are seven types of flavour combinations. In all seven combinations we have $f_1 \neq f_2$, $f_3 = f_4$ and $f_5 = f_6$.

1). f_1, f_2, f_3, f_5 all different, eg. $u\bar{d}c\bar{c}b\bar{b}$.
2). $f_3 = f_5$, eg. $u\bar{d}c\bar{c}c\bar{c}$.
3). $f_1 = f_3$, eg. $u\bar{d}u\bar{u}c\bar{c}$.
4). $f_2 = f_5$, eg. $u\bar{d}c\bar{c}d\bar{d}$.
5). $f_1 = f_3$, $f_2 = f_5$, eg. $u\bar{d}u\bar{u}d\bar{d}$.
6). $f_1 = f_3 = f_5$ eg. $u\bar{d}u\bar{u}u\bar{u}$.
7). $f_2 = f_3 = f_5$ eg. $u\bar{d}d\bar{d}d\bar{d}$.

Many symmetries exist for these cases. Like in the four quark case we have checked them numerically.

2.5 Results

In this section we present cross sections for the production of $l\,\nu + (2,3,4)$ jets for Fermilab, LHC and SSC energies. Moreover we compare this cross section with the top pair production cross section with the subsequent decay of the top pair $t\bar{t} \to W^+W^-\, b\bar{b} \to l\,\nu + (2,3,4)$ jets. As mentioned in the introduction this is one of the important processes in which the top quark can be found. Therefore the comparison between the signal and the background is crucial for the ability to find the top quark in the lepton plus jets decay channel. For the super colliders both the top signal and the W production are a background to the Higgs search in this decay channel.

Collider	FNAL	LHC	SSC
$\sqrt{s}$ (TeV)	1.8	16	40
Struc. Func.	MRSB	MRSB	MRSB
QCD scale	M_W	M_W	M_W
$E_T^{\min}(jet)$(GeV)	15	50	50
$\lvert\eta^{\max}(jet)\rvert$	2.0	3.0	3.0
$\Delta R^{\min}(jet, jet)$	$\star$	0.4	0.4
$E_T^{\min}(l)$(GeV)	20	50	50
$E_T^{\min}$(mis)(GeV)	20	50	50
$\lvert\eta^{\max}(l)\rvert$	1.0	3.0	3.0
$\Delta R^{\min}(jet, l)$	0.0	0.4	0.4

Table 2.3. Structure functions, QCD scale and cuts used for each collider throughout this section. ($\star$ means defined in text.)

Before presenting and discussing the results we specify the input needed for the numerical calculations. The cuts and parameters used are given in Table 2.3. For each outgoing parton we require a transverse energy

$$E_T \equiv E \sin\theta > E_T^{\min}(jet)\,, \tag{2.5.1}$$

where θ is the angle between the parton's momentum and the beam axis. We also require the pseudorapidity

$$|\eta| \equiv |\ln\tan(\theta/2)| < |\eta^{\max}(jet)|\,. \tag{2.5.2}$$

For each pair of outgoing partons we require

$$\Delta R > \Delta R^{\min}(\text{jet, jet})\,. \tag{2.5.3}$$

The separation ΔR is defined as

$$\Delta R = \sqrt{(\Delta\Phi)^2 + (\Delta\eta)^2}, \tag{2.5.4}$$

where $\Delta\Phi$ is the difference in the azimuthal angle and $\Delta\eta$ the difference in pseudorapidity. For the charged lepton l we impose a minimum transverse energy $E_T^{\min}(l)$ and a maximum pseudorapidity $|\eta^{\max}(l)|$. The minimum required missing energy is $E_T^{\min}$(mis). Finally, we require a minimum separation $\Delta R^{\min}(jet, l)$ between the charged lepton and each outgoing parton.

The cross sections in this chapter are the sum of the (l^+, ν_l) and the $(l^-, \bar{\nu}_l)$ cross sections, for one species of lepton l.

The parton distributions used are the MRSB structure functions [9] ($\Lambda_{\overline{\text{MS}}}$ = 200 MeV) with the QCD scale $Q = M_W$. The Monte Carlo of ref. [10] is used to

generate the top signal cross sections with the QCD scale chosen to be equal to the top mass. In chapter 3, we shall study the scale and structure function dependence of the results. In Table 2.4 we use cuts which more or less typify the CDF-detector.

number of jets	2 quarks	4 quarks	6 quarks	total
0	745	-	-	745
1	130	-	-	130
2	21.5	4.5	-	26.0
3	3.4	1.44	-	4.8
4	0.40	0.30	0.0131	0.71

Table 2.4. The $P\bar{P} \rightarrow W$ + jets cross section (in picobarn) for Fermilab (ΔR$(jet, jet) > 0.7$) divided in subprocesses depending on the number of quarks in the subprocess.

Turning to the results, we first discuss the relative importance of various subprocesses for the measurements at the Tevatron. Table 2.4 gives the total cross section as well as the separate contributions from the subprocesses according to the number of quarks involved in the subprocess. We notice that subprocesses with four quarks become more and more important compared to the two quark subprocesses for an increasing number of jets. For 2, 3 and 4 jets respectively 17%, 30% and 42% of the total cross section comes from the four quark subprocesses. Note further that the six quark subprocess is negligible, the contribution to the total cross section is only 1.8%.

R_n	ΔR$(jet, jet) > 0.4$	ΔR$(jet, jet) > 0.7$	ΔR$(jet, jet) > 1.4$
1	0.17	0.17	0.17
2	0.22	0.20	0.16
3	0.22	0.18	0.11
4	0.22	0.15	0.07

Table 2.5. The ratio R_n for several ΔR(jet, jet) cuts at Fermilab energies.

Next we discuss behaviour of the ratio

$$R_n = \sigma(W + \text{n jets})/\sigma(W + (\text{n -1}) \text{ jets}) . \tag{2.5.5}$$

It was conjectured in ref. [11] and later verified for up to 3 jets [6], that this ratio is approximately constant for reasonable cuts. For loose CDF cuts (see Table 2.3, with ΔR$(jet, jet) > 0.7$) it is roughly equal to 1/5. That there must be a limit on the validity of this rule of thumb is easily understood by considering the available phase space for the extra jet in the ratio. With an increasing number of jets, the available

phase space for adding a jet quickly decreases. Since it eventually becomes impossible to add another jet, the constant ratio rule of thumb breaks down for high numbers of jets. However if we make the jet "small" (e.g. a small jet cone) the breakdown of the constant ratio rule is postponed. This is demonstrated in Table 2.5. We see that for $\Delta R^{min}(jet, jet) = 0.4$ the ratios R_2, R_3 and R_4 are equal within the numerical accuracy. As expected there are increasing deviations as $\Delta R^{min}(jet, jet)$ increases.

m_t (GeV)	$\sigma(l\nu + 2$ jets)	$\sigma(l\nu + 3$ jets)	$\sigma(l\nu + 4$ jets)
90	5.47	2.61	0.23
100	2.74	3.97	1.33
110	0.998	2.60	1.70
120	0.445	1.61	1.44
130	0.235	1.02	1.10
140	0.135	0.669	0.818
150	0.084	0.452	0.601
160	0.053	0.314	0.445
170	0.036	0.222	0.330
180	0.024	0.159	0.245
190	0.017	0.115	0.183
200	0.012	0.085	0.162
background	26.0	4.8	0.71
with b-tagging	0.27	0.087	0.022

Table 2.6. The $P\bar{P} \to t\bar{t} \to l\nu$ + (2,3,4) jet cross sections (in picobarn) for various top masses (in GeV) and the $P\bar{P} \to W$ + jets background with and without b-tagging at Fermilab energies ($\Delta R(jet, jet) > 0.7$).

It is of interest to compare the cross section $P\bar{P} \to l\nu$ + (2,3,4) jets with top pair production where each top quark subsequently decays in a b quark and a W, $P\bar{P} \to b\bar{b}W^+W^-$. One of the possible decay channels is that one W decays hadronically into 2 jets and the other one leptonically to give a charged lepton and a (anti)neutrino. The E_T of the bottom quarks is strongly dependent on the top mass. If the top mass is close to the W mass the bottom quarks will have, in most of the events, a low transverse energy and will not pass the threshold for recognisable jets [12]. When the top mass increases it becomes more likely that one or both of the bottom quarks will pass the $E_T^{min}(j)$ threshold and develop into a jet. For the Tevatron this can be clearly seen in Table 2.6. For $m_t = 90$ GeV most of the events are with two jets, while the fraction of lepton plus four jet events is the smallest. This is in contrast with a heavier top mass. From a mass of 140 GeV onward the situation is reversed and most of the events are with four jets. The important issue is the relative size of the background compared to the top signal. The top search in the lepton plus two jet channel was extensively studied in refs. [12]. Since the top mass is above 89 GeV

[13] the background is too large to observe the top quark in the two jet mode. The top search in the three jet plus lepton channel was studied in refs. [14]. As can seen from Table 2.6 the background remains a problem, though compared to the two jet plus lepton mode the signal to background ratio is improved. For the four jet plus lepton mode the signal is larger than the background over a large mass range of the top. This offers a good possibility of finding the top quark in the four jet plus lepton mode.

m_t (GeV)	$\sigma(l\nu + 2$ jets)	$\sigma(l\nu + 3$ jets)	$\sigma(l\nu + 4$ jets)
100	37.9	7.9	0.48
110	34.0	10.7	1.27
120	29.8	11.4	1.72
130	25.4	11.6	2.10
140	21.5	11.4	2.28
150	18.3	11.2	2.38
160	15.7	10.7	2.46
170	13.4	10.2	2.41
180	11.1	9.82	2.48
190	9.22	9.38	2.49
200	7.51	8.81	2.51
background	52	24	8.7
with b-tagging	0.087	0.24	0.17

Table 2.7. The $PP \to t\bar{t} \to l\nu$ + (2,3,4) jet cross sections (in picobarn) for various top masses (in GeV) and the $PP \to W$ + jets background with and without b-tagging at LHC energies

Table 2.6 also shows the background when we select only those subprocesses containing a $b\bar{b}$ quark pair in the final state. In other words, it is the cross section for $P\bar{P} \to W$ + (2, 3, 4) jets where two of the jets are tagged as b jets. No efficiency for the tagging is folded in.

This b tagging opens the possibility for considerably improving the signal to background ratio for the top search, particularly in the lepton + 4 jets channel. From Table 2.6 we see that the background cross section is reduced by a factor of 30. This means that the W background is no longer a problem. As a simple example assume a top mass of 120 GeV, a tagging efficiency $\epsilon_b = 20\%$ and an integrated luminosity of 25 pb^{-1}. Then we should expect approximately 7 top events and 0.1 background events. If we can be sure no jets are mistakenly tagged as b jets, then any observed $l\nu + 4$ jet events with at least one tagged b are almost certain to be top events.

Finally, we include some results on the processes $PP \to W$+jets and $PP \to t\bar{t} \to l\nu$ + jets at future super collider energies in Tables 2.7 and 2.8.

m_t (GeV)	$\sigma(l\nu + 2$ jets)	$\sigma(l\nu + 3$ jets)	$\sigma(l\nu + 4$ jets)
100	179	39.6	2.3
110	165	54.4	6.5
120	146	59.6	9.4
130	127	62.2	11.9
140	112	62.9	13.2
150	97.6	62.4	14.0
160	84.8	61.6	14.6
170	74.2	59.4	15.1
180	63.6	58.0	15.5
190	54.3	55.9	15.6
200	45.9	53.2	15.8
background	177	107	46
with b-tagging	0.21	1.0	1.0

Table 2.8. The $PP \to t\bar{t} \to l\nu$ + (2,3,4) jet cross sections (in picobarn) for various top masses (in GeV) and the $P\bar{P} \to W$ + jets background with and without b-tagging at SSC energies

Appendix

2A The colour matrix for the four quark processes

The 48×48 colour matrix c defined in (2.3.68) can be written as

$$c = \begin{pmatrix} c_A & c_B & c_C & c_D \\ c_B & c_A & c_D & c_C \\ c_C & c_D & c_A & c_B \\ c_D & c_C & c_B & c_A \end{pmatrix},$$

where

$$c_A = \begin{pmatrix} c_1 & c_2 \\ c_2 & c_1 \end{pmatrix}, c_B = \begin{pmatrix} c_3 & c_4 \\ c_4 & c_3 \end{pmatrix}, c_C = \begin{pmatrix} c_5 & c_6 \\ c_6 & c_5 \end{pmatrix}, c_D = \begin{pmatrix} c_7 & c_8 \\ c_8 & c_7 \end{pmatrix},$$

and

$$c_1 = \begin{pmatrix} \delta_1 & 0 & \delta_2 & -\delta_4 & \delta_3 & -\delta_4 \\ 0 & \delta_1 & 0 & \delta_3 & -\delta_4 & -\delta_4 \\ \delta_2 & 0 & \delta_1 & -\delta_4 & -\delta_4 & -\delta_4 \\ -\delta_4 & \delta_3 & -\delta_4 & \delta_4 & 0 & \delta_3 \\ \delta_3 & -\delta_4 & -\delta_4 & 0 & \delta_4 & 0 \\ -\delta_4 & -\delta_4 & -\delta_4 & \delta_3 & 0 & \delta_4 \end{pmatrix}, c_2 = \begin{pmatrix} -\delta_2 & 0 & \delta_2 & \delta_3 & -\delta_4 & \delta_3 \\ 0 & \delta_2 & 0 & -\delta_4 & -\delta_4 & \delta_3 \\ \delta_2 & 0 & -\delta_2 & \delta_3 & \delta_3 & \delta_3 \\ \delta_3 & -\delta_4 & \delta_3 & -\delta_3 & 0 & \delta_3 \\ -\delta_4 & -\delta_4 & \delta_3 & 0 & \delta_3 & 0 \\ \delta_3 & \delta_3 & \delta_3 & \delta_3 & 0 & -\delta_3 \end{pmatrix},$$

$$c_3=\begin{pmatrix} -\delta_5 & -\delta_5 & -\delta_5 & \delta_6 & 0 & \delta_5 \\ -\delta_5 & -\delta_5 & \delta_6 & 0 & \delta_6 & 0 \\ -\delta_5 & \delta_6 & -\delta_5 & \delta_5 & 0 & \delta_6 \\ \delta_6 & 0 & \delta_5 & -\delta_7 & -\delta_7 & -\delta_7 \\ 0 & \delta_6 & 0 & -\delta_7 & -\delta_7 & \delta_8 \\ \delta_5 & 0 & \delta_6 & -\delta_7 & \delta_8 & -\delta_7 \end{pmatrix}, c_4=\begin{pmatrix} \delta_6 & \delta_6 & \delta_6 & \delta_6 & 0 & -\delta_6 \\ \delta_6 & -\delta_5 & -\delta_5 & 0 & \delta_5 & 0 \\ \delta_6 & -\delta_5 & \delta_6 & -\delta_6 & 0 & \delta_6 \\ \delta_6 & 0 & -\delta_6 & \delta_8 & \delta_8 & \delta_8 \\ 0 & \delta_5 & 0 & \delta_8 & -\delta_7 & -\delta_7 \\ -\delta_6 & 0 & \delta_6 & \delta_8 & -\delta_7 & \delta_8 \end{pmatrix},$$

$$c_5=\begin{pmatrix} \delta_2 & 0 & \delta_1 & -\delta_4 & -\delta_4 & -\delta_4 \\ 0 & \delta_2 & 0 & -\delta_4 & -\delta_4 & \delta_3 \\ \delta_1 & 0 & \delta_2 & -\delta_4 & \delta_3 & -\delta_4 \\ -\delta_4 & -\delta_4 & -\delta_4 & \delta_3 & 0 & \delta_4 \\ -\delta_4 & -\delta_4 & \delta_3 & 0 & \delta_3 & 0 \\ -\delta_4 & \delta_3 & -\delta_4 & \delta_4 & 0 & \delta_3 \end{pmatrix}, c_6=\begin{pmatrix} \delta_2 & 0 & -\delta_2 & \delta_3 & \delta_3 & \delta_3 \\ 0 & \delta_1 & 0 & \delta_3 & -\delta_4 & -\delta_4 \\ -\delta_2 & 0 & \delta_2 & \delta_3 & -\delta_4 & \delta_3 \\ \delta_3 & \delta_3 & \delta_3 & \delta_3 & 0 & -\delta_3 \\ \delta_3 & -\delta_4 & -\delta_4 & 0 & \delta_4 & 0 \\ \delta_3 & -\delta_4 & \delta_3 & -\delta_3 & 0 & \delta_3 \end{pmatrix},$$

$$c_7=\begin{pmatrix} -\delta_5 & \delta_6 & -\delta_5 & \delta_5 & 0 & \delta_6 \\ \delta_6 & -\delta_5 & -\delta_5 & 0 & \delta_5 & 0 \\ -\delta_5 & -\delta_5 & -\delta_5 & \delta_6 & 0 & \delta_5 \\ \delta_5 & 0 & \delta_6 & -\delta_7 & \delta_8 & -\delta_7 \\ 0 & \delta_5 & 0 & \delta_8 & -\delta_7 & -\delta_7 \\ \delta_6 & 0 & \delta_5 & -\delta_7 & -\delta_7 & -\delta_7 \end{pmatrix}, c_8=\begin{pmatrix} \delta_6 & -\delta_5 & \delta_6 & -\delta_6 & 0 & \delta_6 \\ -\delta_5 & -\delta_5 & \delta_6 & 0 & \delta_6 & 0 \\ \delta_6 & \delta_6 & \delta_6 & \delta_6 & 0 & -\delta_6 \\ -\delta_6 & 0 & \delta_6 & \delta_8 & -\delta_7 & \delta_8 \\ 0 & \delta_6 & 0 & -\delta_7 & -\delta_7 & \delta_8 \\ \delta_6 & 0 & -\delta_6 & \delta_8 & \delta_8 & \delta_8 \end{pmatrix}.$$

The constants $\delta_1 \ldots \delta_8$ are given by

$$\delta_i = \frac{N^2-1}{4}(N^2-1,\ 1,\ N^{-2},\ 1-N^{-2},\ N-N^{-1},\ N^{-1},\ N^{-1}-N^{-3},\ N^{-3}).$$

References

[1] F.A. Berends, W.T. Giele and H. Kuijf, *Nucl. Phys.* B321 (1989) 39.

[2] K. Hagiwara and D. Zeppenfeld, *Nucl. Phys.* B313 (1989) 560.

[3] D. Zeppenfeld, *Private communication.*

[4] R. Kleiss and W.J. Stirling, *Phys. Lett.* B200 (1988) 193.

[5] J.F. Gunion, H.E. Haber, G.L. Kane and S. Dawson, Higgs Hunter's Guide, Frontiers in physics lecture note series (Addison Wesley, Reading, MA, 1990).

[6] F.A. Berends, W.T. Giele, R. Kleiss, H. Kuijf and W.J. Stirling, *Phys. Lett.* B224 (1989) 237.

[7] F.A. Berends and W.T. Giele, *Nucl. Phys.* B306 (1988) 759.

[8] F.A. Berends and W.T. Giele, *Nucl. Phys.* B313 (1989) 595.

[9] A.D. Martin, R.G. Roberts and W.J. Stirling, *Phys. Lett.* B206 (1988) 327.

[10] R. Kleiss and W.J. Stirling, *Z. Phys.* C40 (1988) 419.

[11] S.D. Ellis, R. Kleiss and W.J. Stirling, *Phys. Lett.* B154 (1985) 435.

[12] R. Kleiss, A.D. Martin and W.J. Stirling, *Z. Phys.* C39 (1988) 393;
S. Gupta and D.P. Roy, *Z. Phys.* C39 (1988) 417;
F. Halzen, C.S. Kim and A.D. Martin, *Mod. Phys. Lett.* A4 (1989) 1531;
P. Agrawal and S.D. Ellis, *Phys. Lett.* B221 (1989) 393;
J.L. Rosner, *Phys. Rev.* D39 (1989) 3297; *erratum:* D40 (1989) 1701.

[13] F. Abe et al., *Phys. Rev. Lett.* 64 (1990) 147;
G.P. Yeh, FERMILAB-CONF-90/138-E, in the proceedings of 'Les Rencontres de Physique de la Vallée d'Aoste', ed. M. Greco, (Editions Frontières, Gif-sur-Yvette, 1990).

[14] H. Baer, V. Barger and R.J.N. Phillips, *Phys. Lett.* B221 (1989) 398;
W.T. Giele and W.J. Stirling, *Nucl. Phys.* B343 (1990) 14.

Chapter 3

Recognizing the top quark in multijet events

3.1 Introduction

The present direct top mass limit of $m_t > 91$ GeV from the CDF collaboration used an integrated luminosity of roughly 5 pb^{-1} [1]. Based on indirect constraints obtained from the standard model using a combination of measurements, in particular the combined LEP data [2], the top mass is likely to be in the range $m_t = 132\ ^{+45}_{-50}$ GeV. This means the current collider run at Fermilab, yielding at least 25 pb^{-1} of integrated luminosity, should produce enough events to establish the existence of the top quark.

Given the above top quark mass limit and expected top mass, the dominant production process of top quarks is direct $t\bar{t}$ production. The top quark will subsequently decay into a b quark and a W boson, resulting in the following signatures which can be used in the top search

$$p\bar{p} \rightarrow t\bar{t} \rightarrow b\bar{b}\, W^+W^- \rightarrow b\bar{b}\, jj\, jj \tag{3.1.1}$$

$$p\bar{p} \rightarrow t\bar{t} \rightarrow b\bar{b}\, W^+W^- \rightarrow b\bar{b}\, l\nu\, jj \tag{3.1.2}$$

$$p\bar{p} \rightarrow t\bar{t} \rightarrow b\bar{b}\, W^+W^- \rightarrow b\bar{b}\, l\nu\, l'\nu' \tag{3.1.3}$$

where j denotes the jet originating from the hadronic W decays.

Other authors have investigated single top quark production [3], but that does not yield promising results for the Fermilab collider. We shall denote the various channels by the number of hard isolated charged leptons in the event.

The highest event rate is given by the zero lepton process (3.1.1) with its relative branching fraction of $\left(\frac{2}{3}\right) \times \left(\frac{2}{3}\right)$. Unfortunately this multijet final state suffers from a huge QCD background and seems only usable when one of the b-jets can be tagged. Even then the background is still much larger than the signal. We refer to refs. [4, 5] for a more detailed discussion.

The single lepton channel (3.1.2) has a smaller event rate with a relative weight of $2 \times \left(\frac{2}{9}\right) \times \left(\frac{2}{3}\right)$ (counting both electron/positron and muon/antimuon final states). However the QCD background is strongly reduced by the presence of the isolated lepton, making it possible to get a signal over background ratio of order one. The main

purpose of this chapter is to study this one lepton signature and its background in more detail than in chapter 2. In particular it will be shown how specific distributions can greatly improve the extraction of the signal. Depending on the mass difference of the top and the W vector boson the signal (3.1.2) can show up as one lepton with 2, 3 or 4 jets. With an increasing number of jets the calculation of the exact background cross section

$$p\overline{p} \rightarrow W + n \text{ jets} \tag{3.1.4}$$

becomes more and more involved. The $n = 3$ case was considered in refs. [7, 8] and the $n = 4$ case in ref. [6]. Some discussion of top signal versus background was given in ref. [6] and also in ref. [9], but in the latter a shower Monte Carlo was used to estimate (3.1.4) and not the exact evaluation. All the results for the single lepton channel in this chapter refer to the sum of e^+ and e^- signals. For muons the results are, of course, the same.

The unlike two lepton channel (3.1.3) only gives a contribution of $2 \times \left(\frac{1}{9}\right) \times \left(\frac{1}{9}\right)$ (not counting final states with tau leptons). The remainder consists of more difficult final states involving tau leptons, electron-positron or muon-antimuon pairs.

The two lepton signal has the clear advantage of a low background. It has been discussed in detail in refs. [9, 10]. However, due to the presence of two neutrinos, it is not possible to reconstruct the top mass. For a top search in this signal one has to rely on the event rates and compare them directly with the theoretically calculated $t\bar{t}$ cross section. This results in a top mass with a theoretical error which is not known. The usefulness of the two lepton signal will increase when accompanying jets are measured, but it will become clear that for the discovery of the top quark the study of the one lepton signature, besides the two lepton signature is crucial.

The outline of the chapter is as follows. In section 3.2 the production cross sections and their uncertainties are discussed. In section 3.3 some methods to determine the top mass which are not sensitive to the absolute value of the cross sections are proposed. Section 3.4 presents the conclusions.

3.2 The production cross section and backgrounds

With the use of theoretical calculations, the most important consideration is the expected uncertainty in the answer due to the fixed order perturbative calculation. For the top production both signal and background have their uncertainties which affect the applicability of the calculation. Existing next-to-leading order calculations show that the shapes of differential cross sections are already predicted reasonably well by leading order calculations, but their normalizations are uncertain.

A common way to estimate the order of magnitude of the uncalculated higher order corrections is by studying the sensitivity to the renormalization and factorization scales. In this chapter, we shall always choose the renormalization scale and the factorization scale to be equal. For the background we shall make the three scale choices

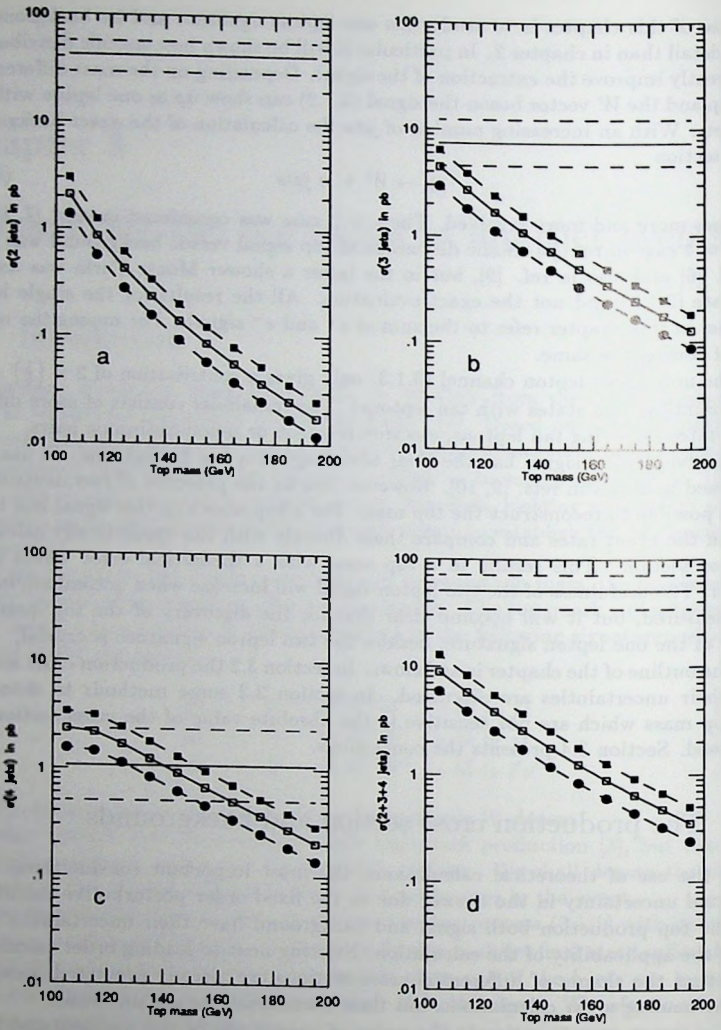

Fig. 3.1. a, b and c: The cross sections for $p\bar{p} \rightarrow$ lepton + 2, 3, and 4 jets, respectively. The curves show the $t\bar{t}$ signal, the horizontal lines are the QCD background. Fig. 1d shows the total $p\bar{p} \rightarrow$ lepton + jets cross section.

1. $\mu = M_W$

2. $\mu = \frac{1}{2} M_W$

3. $\mu = 2\sqrt{M_W^2 + p_{T,W}^2}$,

where $p_{T,W}$ is the transverse momentum of the W. For the signal we use

1. $\mu = m_t$

2. $\mu = \frac{1}{2} m_t$

3. $\mu = 2\sqrt{m_t^2 + p_{T,t}^2}$,

where $p_{T,t}$ is the average of the transverse momenta of the two tops. The results are given in Fig. 3.1 for the single lepton plus jet final state. The solid lines correspond with the first scale choice, the dashed lines with the second (upper line) and third (lower line). Both signal and background are leading order estimates of the cross section. The jet definitions and kinematical cuts used are given in Table 3.1. Note that the signal and background are comparable up to a top mass of around 150 GeV only when one demands that the final state contains both a lepton and four jets.

The normalization uncertainty in the background is relatively unimportant when we use distributions. However in the two lepton signal the ability to predict the theoretical cross section as a function of the top mass is crucial. From Fig. 3.2 it is clear that using the leading order prediction for

$$p\bar{p} \to t\bar{t} \tag{3.2.1}$$

has a large uncertainty and would make it virtually impossible to determine the top mass using the two lepton signal which relies on the total cross section.

For process (3.2.1) also the next-to-leading order contributions have been calculated [11]. The next-to-leading order cross section has a reduced sensitivity to the scale choices. This is demonstrated in Fig. 3.3 where we show the scale choice sensitivity with the same choices as in leading order. For comparison we also plotted the leading order result with the same choices.

One could now in principle use the next-to-leading order calculation with its much smaller theoretical uncertainty to relate the value of the cross section to the top mass. However, in view of the large corrections to the Born cross sections, which amount to about 30%, one should worry about even higher order contributions. The latter can be approximated by calculating the soft gluon corrections, which has been done in ref. [12]. If we apply this technique to approximate the next-to-leading order contribution we recover the exact next-to-leading order result within about 10% (see Fig. 3.4), well within the theoretical uncertainty. Now we can apply the soft gluon approximation to obtain an estimate of the next-to-next-to-leading order contribution, this gives still a large positive correction of 25%. The results are summarized in Fig. 3.5, from which it is clear that the estimate of the theoretical

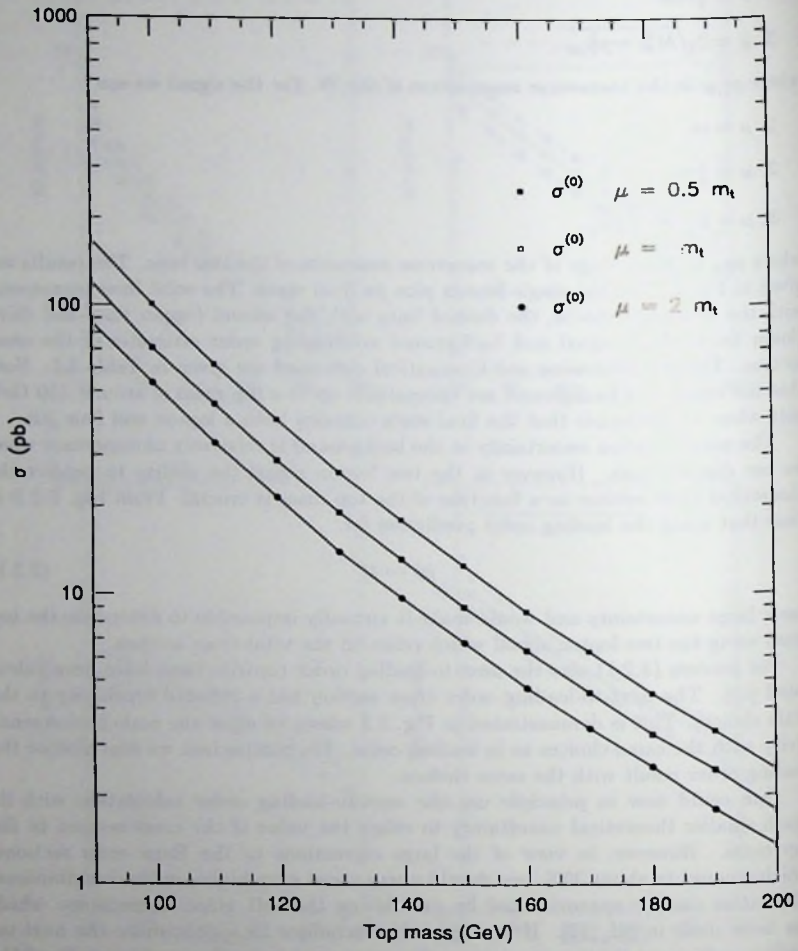

Fig. 3.2. The Born approximation to the total $p\bar{p} \to t\bar{t}$ cross section using the MRSB structure functions.

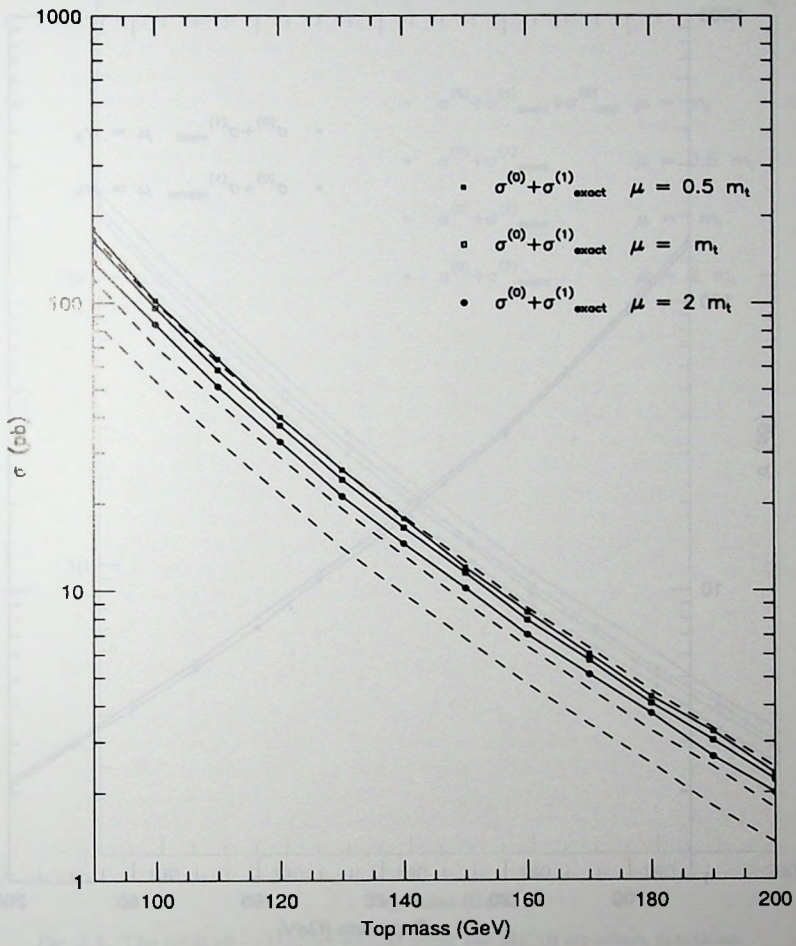

Fig. 3.3. Solid lines: the next-to-leading order $p\bar{p} \to t\bar{t}$ cross section using the MRSB structure functions. Dashed lines: the Born cross section.

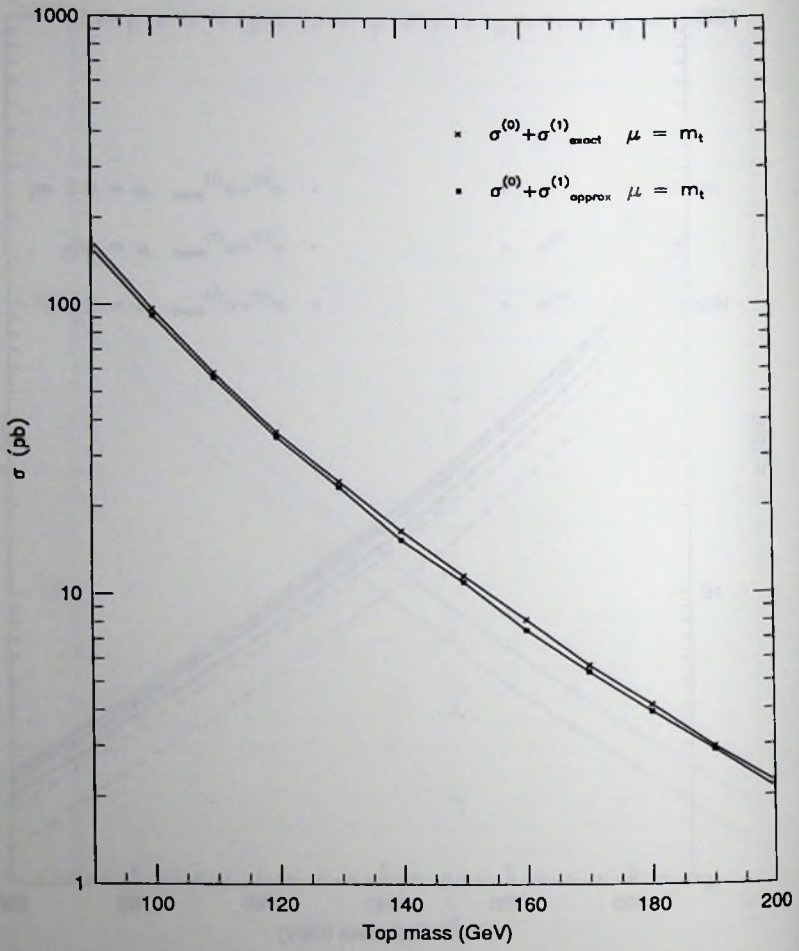

Fig. 3.4. A comparison of the exact next-to-leading order $p\bar{p} \to t\bar{t}$ cross section and the soft gluon approximation using the MRSB structure functions.

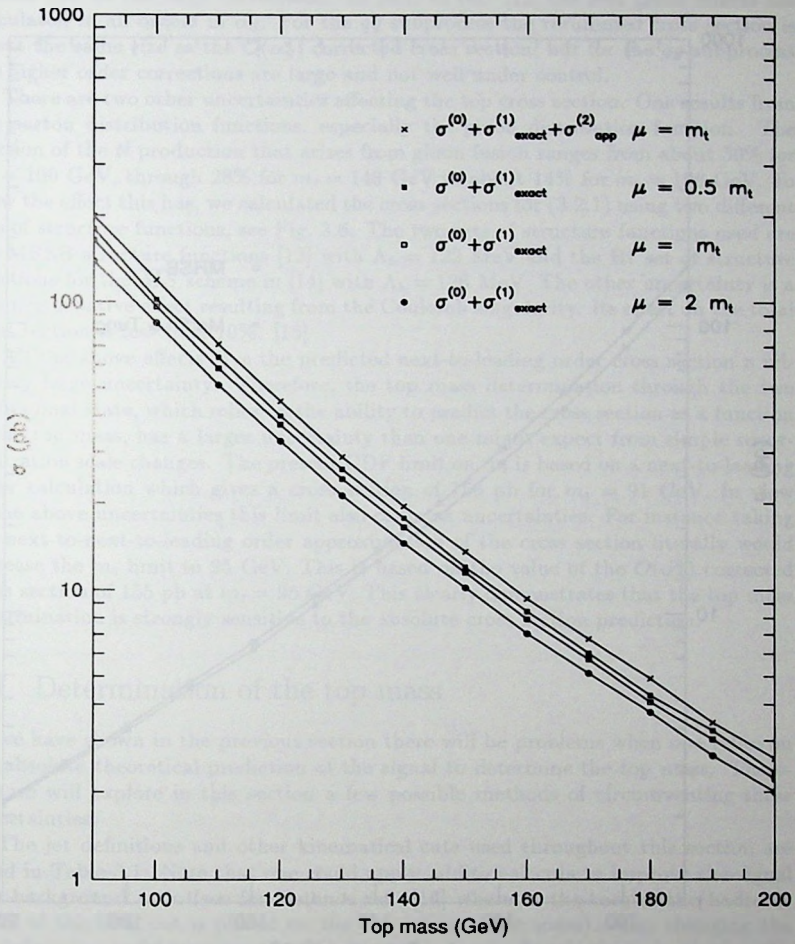

Fig. 3.5. The total $p\bar{p} \to t\bar{t}$ cross section using the MRSB structure functions. The top curve includes the $\mathcal{O}(\alpha_S^2)$ contribution in the soft gluon approximation; the other curves are the exact $\mathcal{O}(\alpha_S)$ corrected cross sections for three choices of the scale μ.

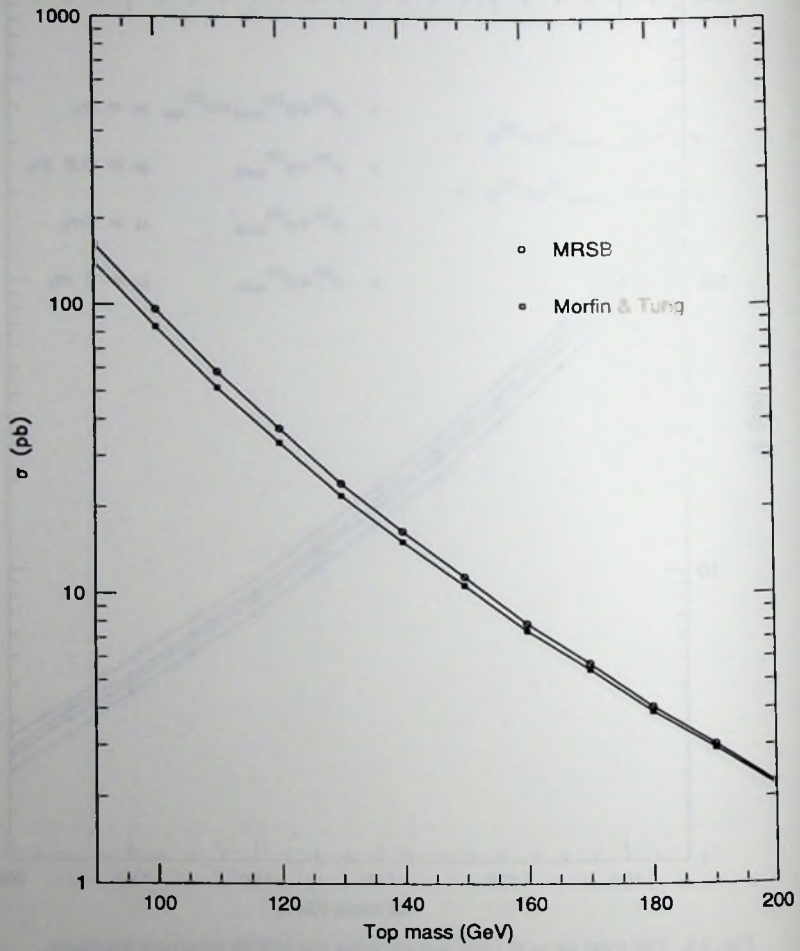

Fig. 3.6. The total $\mathcal{O}(\alpha_S)$ corrected $p\bar{p} \to t\bar{t}$ cross section using two different sets of structure functions.

uncertainty by changing the scale is not a good method for this particular cross section due to the large corrections. In fact, in ref. [12] the soft gluon effects are calculated to all orders in α_S. For the $q\bar{q}$ subprocess the resummed cross section is about the same size as the $\mathcal{O}(\alpha_S^2)$ corrected cross section, but for the gg subprocess the higher order corrections are large and not well under control.

There are two other uncertainties affecting the top cross section. One results from the parton distribution functions, especially the gluon distribution function. The fraction of the $t\bar{t}$ production that arises from gluon fusion ranges from about 50% for $m_t = 100$ GeV, through 28% for $m_t = 140$ GeV to about 14% for $m_t = 190$ GeV. To show the effect this has, we calculated the cross sections for (3.2.1) using two different sets of structure functions, see Fig. 3.6. The two sets of structure functions used are the MRSB structure functions [13] with $\Lambda_5 = 122$ MeV and the B1 set of structure functions for the $\overline{MS}$ scheme in [14] with $\Lambda_5 = 126$ MeV. The other uncertainty is a non-perturbative effect resulting from the Coulomb singularity. Its effect on the total cross section is less than 10%. [15]

All the above effects give the predicted next-to-leading order cross section a relatively large uncertainty. Therefore, the top mass determination through the two lepton final state, which relies on the ability to predict the cross section as a function of the top mass, has a larger uncertainty than one might expect from simple renormalization scale changes. The present CDF limit on m_t is based on a next-to-leading order calculation which gives a cross section of 156 pb for $m_t = 91$ GeV. In view of the above uncertainties this limit also contains uncertainties. For instance taking the next-to-next-to-leading order approximation of the cross section literally would increase the m_t limit to 95 GeV. This is based on the value of the $\mathcal{O}(\alpha_S^2)$ corrected cross section of 155 pb at $m_t = 95$ GeV. This clearly demonstrates that the top mass determination is strongly sensitive to the absolute cross section prediction.

3.3 Determination of the top mass

As we have shown in the previous section there will be problems when one relies on the absolute theoretical prediction of the signal to determine the top mass. Therefore we will explore in this section a few possible methods of circumventing these uncertainties.

The jet definitions and other kinematical cuts used throughout this section are listed in Table 3.1. Note that one could apply additional cuts to improve the signal over background ratio (see for instance ref. [16] where in the case of the hadronic decay of the W a cut is placed on the two jet invariant mass). Also changing the jet definitions could improve the signal over background ratio (e.g. increasing the $E_t^{min}(jet)$). However all these types of additional cuts or changes in the cuts will reduce the number of top events in the final sample and should, therefore, only be applied when needed. As we will show, using the minimal set of cuts listed in Table 3.1, which are dictated by detector properties, one already gets very reasonable results.

$\sqrt{s}$	1800 GeV
Structure Function	MRSB
Jet rapidity coverage	2
Leptonic rapidity coverage	2
$E_t^{min}(jet)$	15 GeV
$E_t^{min}(lepton)$	20 GeV
$E_t^{min}(missing)$	20 GeV
Jet-Jet separation ΔR	0.7
Jet-lepton separation	none

Table 3.1. The parameters and cuts used for the one lepton signal and background. For the two lepton signal and background the same parameters and cuts are used, except that no cut is imposed on the missing momentum.

The first method uses the fact that the signal can have various numbers of jets in the final state. Differentiating between these jet final states enables us to form ratios of cross sections with different number of jets. In the approximation that the top is produced on shell the production cross section (3.2.1) factorizes with respect to the subsequent decay of the top and cancels in the ratio, thus the uncertainties in the production process are removed. Because the energy of the b quark is strongly related to the top mass there will be a strong dependence in the jet fractions and ratios on the top mass.

However this way to cancel the normalization uncertainty in the top cross section only works when the background is negligible. This means the method can only be applied to the two lepton signal and not to the single lepton plus multijets signal. By measuring the 0, 1 or 2 jets arising from energetic b quarks in the top pair decay, we can define jet fractions f_0, f_1 and f_2 by

$$f_i = \frac{\sigma_i}{\sigma_0 + \sigma_1 + \sigma_2} \tag{3.3.1}$$

where σ_i is the cross section for $p\bar{p} \rightarrow 2$ leptons $+$ i jets. As can be seen from Fig. 3.7 these fractions have a marked top mass dependence, while there is almost no dependence on the scale. A measurement of such fractions gives an indication of the top mass without relying on the absolute event rates.

The single lepton plus multijets final state offers a more direct possibility of determining the top mass. This is because the top mass is reconstructible from the final state using distributions. Possible uncertainties in the event rates are relatively unimportant provided that the signal to background ratio is at least of order unity. In ref. [17] several distributions were examined in the lepton plus three jet final state. However the lepton plus four jet final state offers a better possibility since the signal to background ratio is expected to be much more favorable (see Fig. 3.1).

In order to extract the top mass from the signal we will use two simple directly measurable quantities, the three jet invariant mass and the cluster mass. Using the

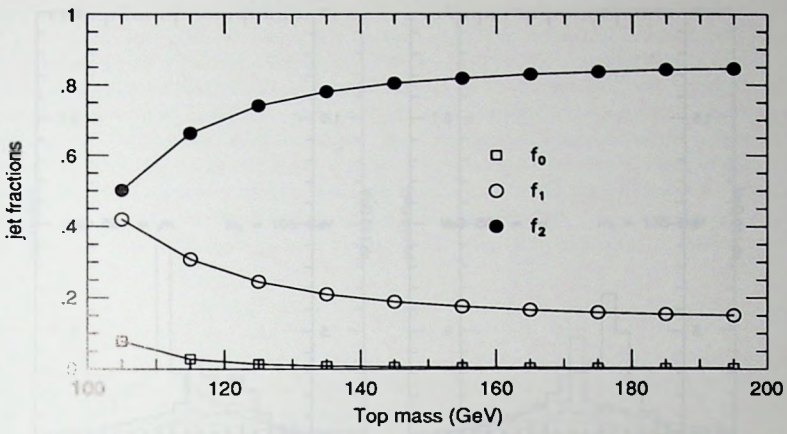

Fig. 3.7. The fractions of all $p\bar{p} \to t\bar{t} \to$ 2 leptons + jets events with 0, 1 and 2 jets.

momentum of one of the four jets, the momentum of the charged lepton and the missing transverse momentum, the cluster mass is defined as:

$$m_c(j,l;\nu)^2 = \left[p_T^0(jl) + p_T(\nu)\right]^2 - \left[\mathbf{p}_T(jl) + \mathbf{p}_T(\nu)\right]^2 \tag{3.3.2}$$

where

$$p_T^0(jl) = \sqrt{\mathbf{p}_T(jl)^2 + m(jl)^2}, \tag{3.3.3}$$

$$\mathbf{p}_T(jl) = \mathbf{p}_T(j) + \mathbf{p}_T(l), \tag{3.3.4}$$

$$m(jl)^2 = [E(j) + E(l)]^2 - [\mathbf{p}(j) + \mathbf{p}(l)]^2. \tag{3.3.5}$$

The 3 jet mass is defined using the momenta of three of the four jets:

$$m(j_1, j_2, j_3) = \sqrt{[E(j_1) + E(j_2) + E(j_3)]^2 - [\mathbf{p}(j_1) + \mathbf{p}(j_2) + \mathbf{p}(j_3)]^2}. \tag{3.3.6}$$

All the following calculations are performed with scale 1. The results refer to the sum of the e^+ and e^- signals. In Fig. 3.8 the average cluster mass distributions (one entry for each of the four possible cluster masses) are shown due to signal and background. The histogram due to background alone is indicated with a dashed line. Four top mass cases are presented: 105, 135, 165 and 195 GeV. For the latter two cases the top mass is not visible anymore, for the others a sharp drop indicates the top mass position.

A better signal is obtained by using the the 3 jet mass distributions which are shown in Fig. 3.9 for both signal and background. Again the background contribution

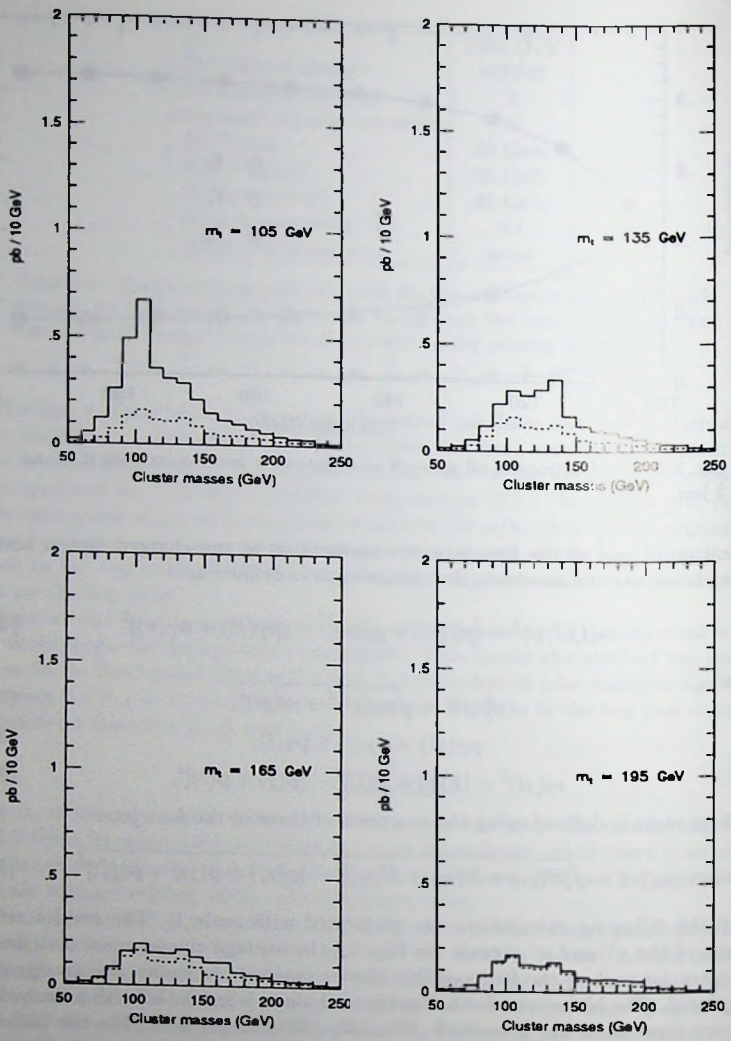

Fig. 3.8. Cluster mass distributions for four values of m_t. The solid lines show the signal plus the background; the dotted lines show the background contribution.

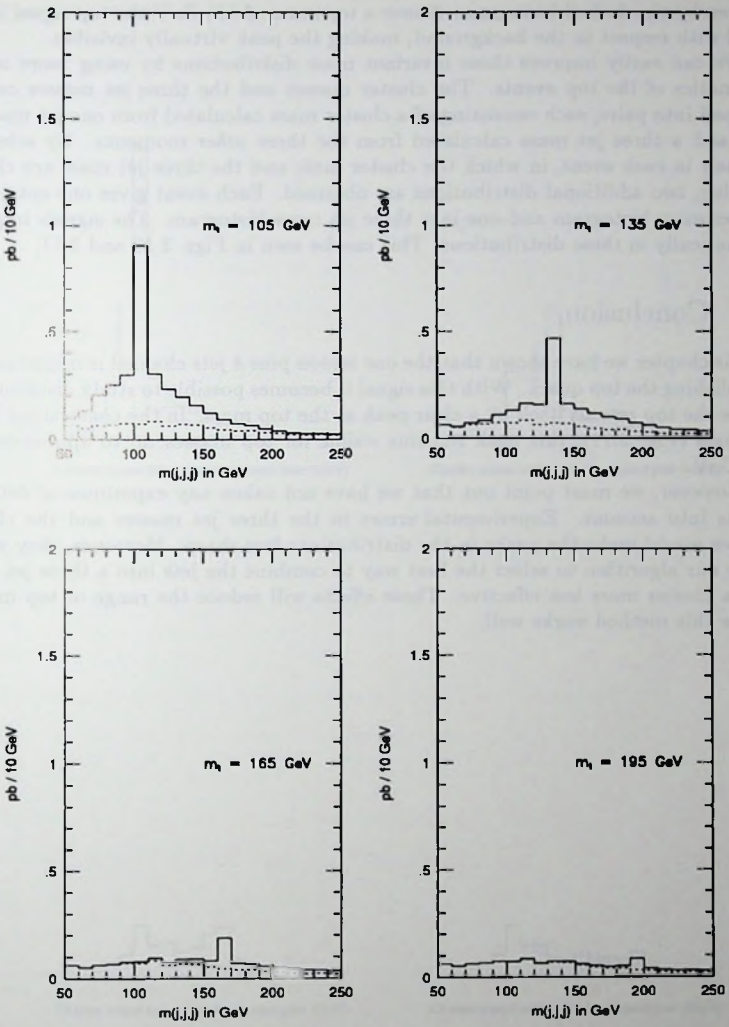

Fig. 3.9. Three-jet-mass distributions for four values of m_t. The solid lines show the signal plus the background; the dotted lines show the background contribution.

is given by the dashed histogram. Above a top mass of 165 GeV the top signal is too small with respect to the background, making the peak virtually invisible.

We can easily improve these invariant mass distributions by using more of the kinematics of the top events. The cluster masses and the three jet masses can be grouped into pairs, each consisting of a cluster mass calculated from one jet momentum and a three jet mass calculated from the three *other* momenta. By selecting the pair in each event, in which the cluster mass and the three jet mass are closest in value, two additional distributions are obtained. Each event gives one entry in a cluster mass histogram and one in a three jet mass histogram. The signals improve dramatically in these distributions. This can be seen in Figs. 3.10 and 3.11.

3.4 Conclusion

In this chapter we have shown that the one lepton plus 4 jets channel is important for establishing the top quark. With this signal it becomes possible to study distributions where the top reveals itself by a clear peak at the top mass. In the constrained three jet mass (Fig. 3.11), this peak remains visible for top masses up to approximately 165 GeV.

However, we must point out that we have not taken any experimental detector effects into account. Experimental errors in the three jet masses and the cluster masses would make the peaks in the distributions less sharp. Moreover, they would make our algorithm to select the best way to combine the jets into a three jet mass and a cluster mass less effective. These effects will reduce the range of top masses where this method works well.

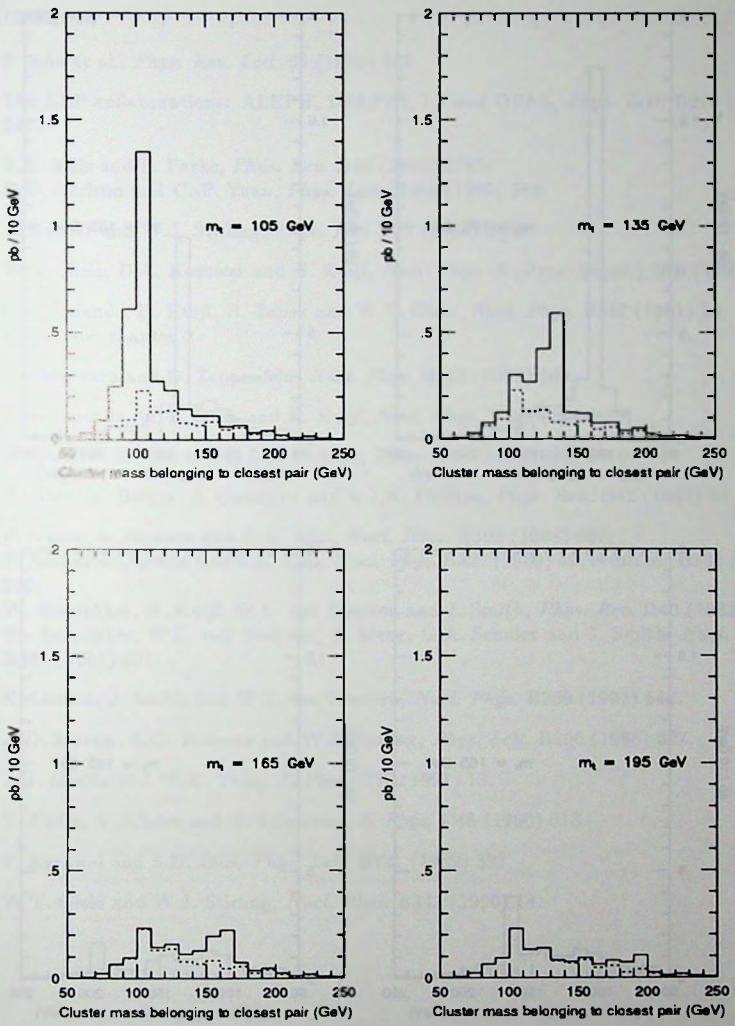

Fig. 3.10. The distribution of the cluster mass belonging to the selected pair for four values of m_t. The solid lines show the signal plus the background; the dotted lines show the background contribution.

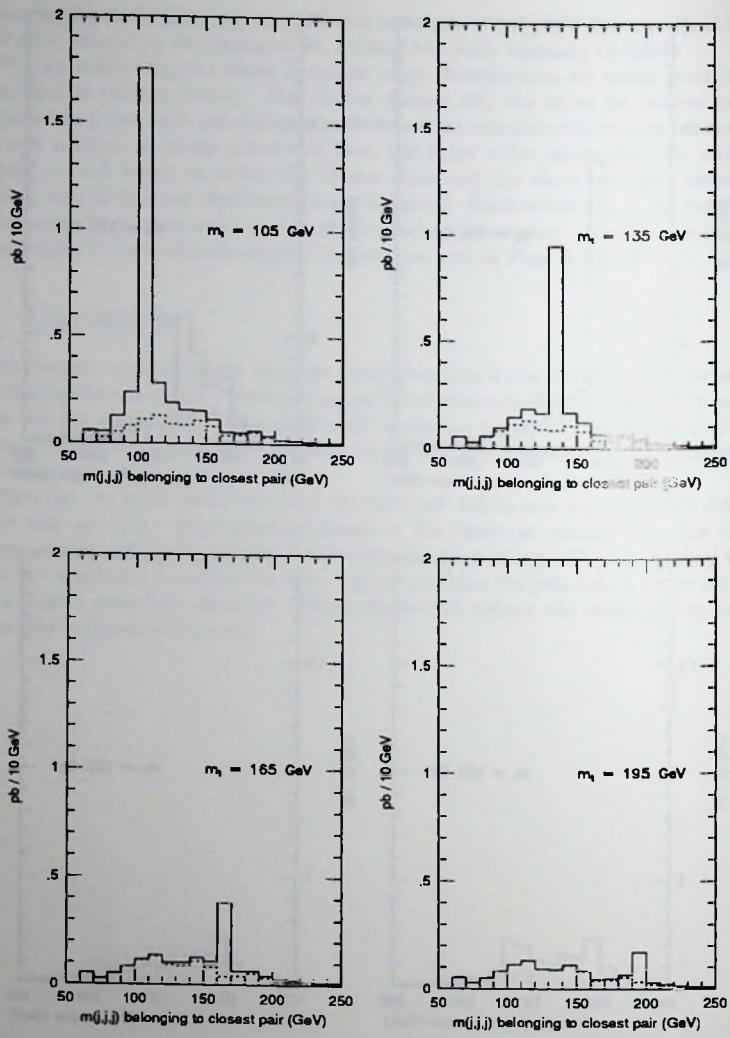

Fig. 3.11. The distribution of the three-jet-mass belonging to the selected pair for four values of m_t. The solid lines show the signal plus the background; the dotted lines show the background contribution.

References

[1] F. Abe et al., *Phys. Rev. Lett.* 68 (1992) 447.

[2] The LEP collaborations: ALEPH, DELPHI, L3 and OPAL, *Phys. Lett.* B276 (1992) 247.

[3] R.K. Ellis and S. Parke, *Phys. Rev.* D46 (1992) 3785;
D.O. Carlson and C.-P. Yuan, *Phys. Lett.* B306 (1993) 386.

[4] Z. Kunszt and W.J. Stirling, *Phys. Rev.* D37 (1988) 2439.

[5] W.T. Giele, D.A. Kosower and H. Kuijf, *Nucl. Phys. B* (Proc. Suppl.) 23B (1991) 22.

[6] F.A. Berends, H. Kuijf, B. Tausk and W.T. Giele, *Nucl. Phys.* B357 (1991) 32; this thesis, chapter 2.

[7] K. Hagiwara and D. Zeppenfeld, *Nucl. Phys.* B313 (1989) 560.

[8] F.A. Berends, W.T. Giele and H. Kuijf, *Nucl. Phys.* B321 (1989) 39.

[9] H. Baer, V. Barger and R.J.N. Phillips, *Phys. Rev.* D39 (1989) 3310.

[10] H. Baer, V. Barger, J. Ohnemus and R.J.N. Phillips, *Phys. Rev.* D42 (1990) 54.

[11] P. Nason, S. Dawson and R.K. Ellis, *Nucl. Phys.* B303 (1988) 607;
P. Nason, S. Dawson and R.K. Ellis, *Nucl. Phys.* B327 (1989) 49; *erratum:* B335 (1990) 260;
W. Beenakker, H. Kuijf, W.L. van Neerven and J. Smith, *Phys. Rev.* D40 (1989) 54;
W. Beenakker, W.L. van Neerven, R. Meng, G.A. Schuler and J. Smith, *Nucl. Phys.* B351 (1991) 507.

[12] E. Laenen, J. Smith and W.L. van Neerven, *Nucl. Phys.* B369 (1992) 543.

[13] A.D. Martin, R.G. Roberts and W.J. Stirling, *Phys. Lett.* B206 (1988) 327.

[14] J.G. Morfín and W.K. Tung, *Z. Phys.* C52 (1991) 13.

[15] V. Fadin, V. Khoze and T. Sjöstrand, *Z. Phys.* C48 (1990) 613.

[16] P. Agrawal and S.D. Ellis, *Phys. Lett.* B221 (1989) 393.

[17] W.T. Giele and W.J. Stirling, *Nucl. Phys.* B343 (1990) 14.

Chapter 4

Two-loop self-energy diagrams with massless fermions

4.1 Introduction

In order to calculate the self-energies of the photon and the W and Z bosons at the two-loop level, two ingredients are needed. The first is an extension of the Passarino Veltman scheme [1] for reducing tensor integrals to scalar integrals. This is now available for two-point functions [2]. Secondly, one must compute the scalar integrals. In the electroweak sector, this is complicated by the presence of massive internal particles, and a general method to calculate these integrals analytically is not known. In this chapter, we will limit ourselves to a class of more simple scalar integrals, namely the ones that occur in two-loop diagrams in which one of the loops represents a massless fermion.

In section 4.2 we introduce our notation for two-loop scalar integrals and give a list of all cases required for our purpose. In section 4.3 we explain the method we use to calculate them, which is based on their analytic properties as functions of the external momentum squared. They have a branch cut along the positive real axis. The discontinuity across this cut is given by Cutkosky's rules. The functions themselves are then obtained through a dispersion relation. The discontinuities can be interpreted as two- and three-particle phase space integrals, which we study in section 4.4. After discussing a simple example in section 4.5, we list the results in section 4.6. In the final section we comment on some possible applications.

4.2 Definitions

In ref. [2], it is shown that all two-loop Feynman diagrams contributing to gauge boson self-energies in the standard model can be expressed in terms of a limited set of scalar integrals. Each of these scalar integrals can be represented graphically by a scalar diagram.

The two basic topologies are shown in Fig. 4.1. All other topologies which are needed for the gauge boson self-energies can be derived from these by cancelling

propagators. Apart from reducible topologies generated in this way there are four remaining irreducible ones as shown in Fig. 4.2.

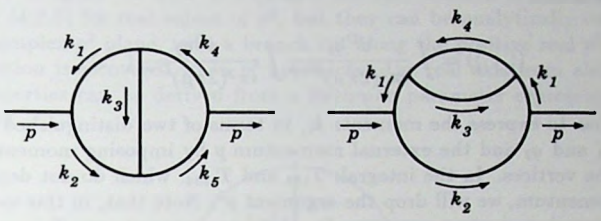

Fig. 4.1. The two basic topologies: T_{12345} (left) and T_{11234} (right).

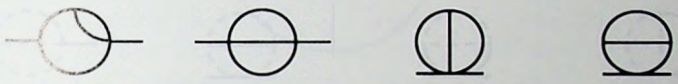

Fig. 4.2. The irreducible topologies that can be derived from the two basic topologies by cancelling propagators.

The reducible topologies represent simply a product of two one-loop integrals, and can be calculated from the following basic integrals, expanded up to terms of order δ.

$$A_0(m^2) = \langle \frac{1}{q^2 - m^2} \rangle \,, \tag{4.2.1}$$

$$B_0(p^2; m_1^2, m_2^2) = \langle \frac{1}{[q^2 - m_1^2]\left[(p+q)^2 - m_2^2\right]} \rangle \,, \tag{4.2.2}$$

$$B_0'(p^2; m_1^2, m_2^2) = \frac{\partial}{\partial(m_1^2)} B_0(p^2; m_1^2, m_2^2) \,. \tag{4.2.3}$$

Here the one-loop integration is symbolized by a bracket

$$\langle \ldots \rangle = \int \frac{d^D q}{i\pi^2 (2\pi\mu)^{D-4}} (\ldots) \,. \tag{4.2.4}$$

$D = 4 - 2\delta$ is the dimension of space-time and μ is an arbitrary reference mass. We use dimensional regularization for both ultraviolet and infrared divergences.

For the scalar integrals associated with the irreducible topologies we will use the notation of ref. [2], which is well suited for computeralgebraic manipulations. An integral with ℓ internal lines is denoted by

$$T_{i_1 i_2 \ldots i_\ell}\left(p^2; m_1^2, m_2^2, \ldots, m_\ell^2\right) = \langle\langle \frac{1}{\left[k_{i_1}^2 - m_1^2\right]\left[k_{i_2}^2 - m_2^2\right] \ldots \left[k_{i_\ell}^2 - m_\ell^2\right]} \rangle\rangle \,, \tag{4.2.5}$$

where the momenta k_{i_j} for $j = 1, \ldots, \ell$ are members of the set of all momenta $\{k_1, \ldots, k_5\}$ of the basic topologies of Fig. 4.1. The two-loop integration is symbolized by double brackets

$$\langle\langle \ldots \rangle\rangle = \int \frac{d^D q_1}{i\pi^2 (2\pi\mu)^{D-4}} \int \frac{d^D q_2}{i\pi^2 (2\pi\mu)^{D-4}} (\ldots) \,, \tag{4.2.6}$$

where one has to express the momenta k_{i_j} in terms of two distinguished integration momenta q_1 and q_2 and the external momentum p by imposing momentum conservation at the vertices. In the integrals T_{134} and T_{1134}, which do not depend on the external momentum, we will drop the argument p^2. Note that, in this system, there are often several equivalent notations for the same integral, eg. $T_{234} = T_{135}$. This becomes obvious when one draws the corresponding diagrams.

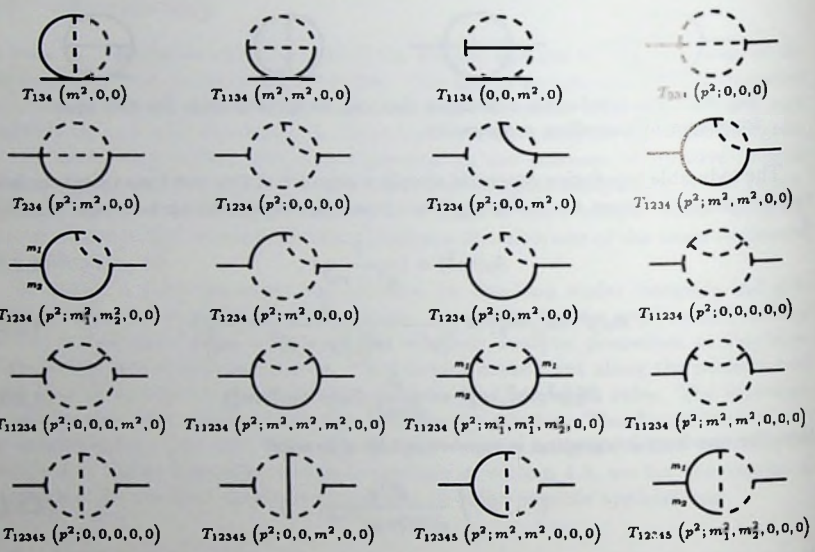

Fig. 4.3. The irreducible scalar integrals given in this chapter. The external lines carry momentum p. The dashed internal lines are massless. The solid internal lines have mass m, except where other masses are indicated.

In this chapter we present analytical results for the two-loop scalar integrals shown in Fig. 4.3, which are all the integrals necessary for the gauge boson self-energy diagrams containing a massless fermion loop.

4.3 The dispersion method

The scalar T-integrals we wish to calculate are only defined in momentum space by equation (4.2.5) for real values of p^2, but they can be analytically continued to the whole complex p^2 plane, with a branch cut along the positive real p^2 axis. The original function is recovered when p^2 approaches the real axis from above. These analytic properties can be derived from a Feynman parameter representation (see, e.g., ref. [3]).

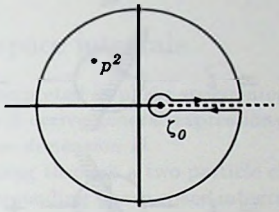

Fig. 4.4. The contour in the complex ζ-plane.

To find a dispersion relation for these T-integrals we apply Cauchy's theorem to the contour $\mathcal{C}$ shown in Fig. 4.4.

$$T(p^2) = \frac{1}{2\pi i}\int_{\mathcal{C}} d\zeta \frac{1}{\zeta - p^2} T(\zeta) \tag{4.3.1}$$

Provided that $T(\zeta)$ goes to zero rapidly enough as $|\zeta| \to \infty$, the contribution from the large circle vanishes in the limit where its radius goes to infinity. We are left with the following integral along the real axis:

$$T(p^2) = \frac{1}{2\pi i}\int_{\zeta_0}^{\infty} d\zeta \frac{1}{\zeta - p^2} \Delta T(\zeta) \tag{4.3.2}$$

where

$$\Delta T(\zeta) = \lim_{\varepsilon \downarrow 0} \{T(\zeta + i\varepsilon) - T(\zeta - i\varepsilon)\} \tag{4.3.3}$$

and ζ_0 is the point on the real axis where the cut starts.

The discontinuity $\Delta T(\zeta)$ can be obtained directly by applying Cutkosky's rules [4]. Then the dispersion relation (4.3.2) is used to find T itself. This is only possible if T goes to zero rapidly enough, but that can always be arranged by reducing the space-time dimension D, if necessary. After the dispersion integration has been carried out, the result is analytically continued in D.

According to the Cutkosky rules, the discontinuity across the branch cut equals a sum of cut diagrams. This is shown in Fig. 4.5. In a cut diagram the lines in the unshaded region (to the left of the cut) represent ordinary propagators:

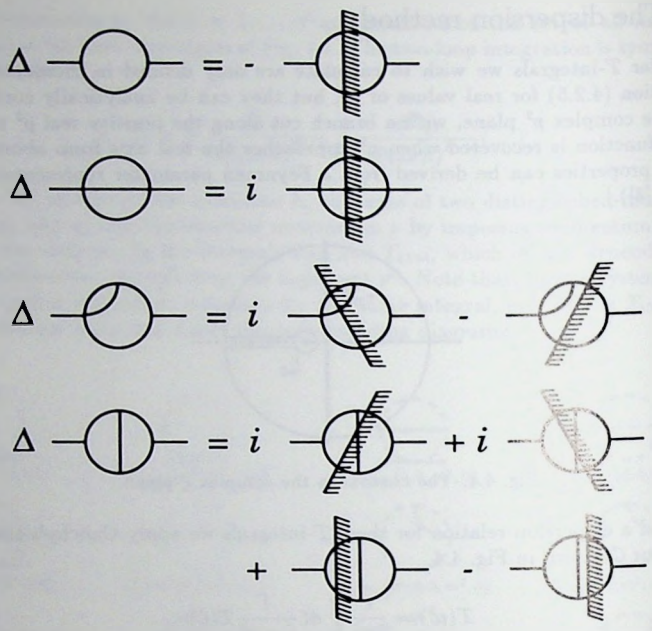

Fig. 4.5. From top to bottom: ΔB_0, ΔT_{234}, ΔT_{1234}, and ΔT_{12345}.

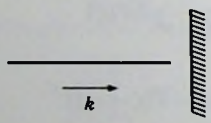

$$\frac{1}{k^2 - m^2 + i\varepsilon}.$$

The lines in the shaded region (to the right of the cut) represent propagators with the opposite sign in front of $i\varepsilon$:

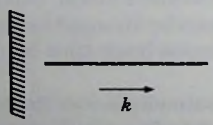

$$\frac{1}{k^2 - m^2 - i\varepsilon}.$$

The lines that cross the cut represent delta functions:

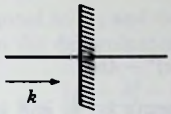

$$2\pi\,\theta(k^0)\,\delta(k^2-m^2)\,,$$

where k is the momentum flowing across the cut from the unshaded into the shaded region. In addition, there are some factors of i and -1 involved, which are given explicitly in Fig. 4.5.

4.4 Massive phase space integrals

The cut diagrams can be interpreted as phase space integrals for two and three body decay processes. Here we will derive general expressions for these integrals that are valid for arbitrary space-time dimension D.

Suppose the momenta going through a two-particle cut are called k_1 and k_2, with $k_1+k_2=p$. Then the corresponding phase space integral will have the form

$$\begin{aligned}&\langle 2\pi\,\theta(k_1^0)\,\delta(k_1^2-m_1^2)\,2\pi\,\theta(k_2^0)\,\delta(k_2^2-m_2^2)\rangle = \\ &\frac{(2\pi)^2}{i\pi^2(2\pi\mu)^{D-4}}\int \mathrm{d}^D k_1\,\theta(k_1^0)\delta(k_1^2-m_1^2)\,\theta(p^0-k_1^0)\delta((p-k_1)^2-m_2^2)\,. \quad (4.4.1)\end{aligned}$$

When $p^2<(m_1+m_2)^2$, this is zero because the on-shell conditions on k_1 and k_2 cannot be solved simultaneously. If $p^2>(m_1+m_2)^2$, we can simplify the calculation by working in the p-rest frame, where

$$p=(p^0,\vec{0}),\;\; k_1=(k_1^0,\vec{k}_1),\;\; k_2=(p^0-k_1^0,-\vec{k}_1)\,. \quad (4.4.2)$$

We use the on-shell condition on k_1 to integrate over k_1^0:

$$\int \mathrm{d}^D k_1\,\theta(k_1^0)\delta(k_1^2-m_1^2)=\int\frac{\mathrm{d}^{D-1}\vec{k}_1}{2k_1^0}\,. \quad (4.4.3)$$

After introducing spherical coordinates,

$$\int\frac{\mathrm{d}^{D-1}\vec{k}_1}{2k_1^0}=\int_0^\infty\frac{|\vec{k}_1|^{D-2}}{2k_1^0}\mathrm{d}|\vec{k}_1|\int \mathrm{d}\Omega_{D-1}(\vec{k}_1)\,, \quad (4.4.4)$$

the $|\vec{k}_1|$-integration can be done using the on-shell condition on k_2. The angular integral gives a factor

$$\int \mathrm{d}\Omega_{D-1}(\vec{k})=\frac{2\pi^{(D-1)/2}}{\Gamma\left(\frac{D-1}{2}\right)}\,. \quad (4.4.5)$$

Using the duplication formula for the Γ-function and expressing p^0 and $|\vec{k}_1|$ in terms of scalar invariants we obtain the following result, which is valid in any frame,

$$\begin{aligned}&\langle 2\pi\,\theta(k_1^0)\,\delta(k_1^2-m_1^2)\,2\pi\,\theta(k_2^0)\,\delta(k_2^2-m_2^2)\rangle = \\ &-2\pi i\,\theta\left(p^2-(m_1+m_2)^2\right)\left(\frac{p^2}{4\pi\mu^2}\right)^{-\delta}\frac{\Gamma(1-\delta)}{\Gamma(2-2\delta)}\left[\frac{\lambda(p^2,m_1^2,m_2^2)}{(p^2)^2}\right]^{1/2-\delta}, \quad (4.4.6)\end{aligned}$$

where λ is the Källén function:

$$\lambda(a,b,c) = (a-b-c)^2 - 4bc\,. \tag{4.4.7}$$

Now consider a three-particle cut with momenta k_1, k_2 and k_3 going through it, such that $k_1 + k_2 + k_3 = p$. It will have the following structure:

$$I(p^2) = \langle\langle 2\pi\,\theta(k_1^0)\,\delta(k_1^2 - m_1^2)\,2\pi\,\theta(k_2^0)\,\delta(k_2^2 - m_2^2)\,2\pi\,\theta(k_3^0)\,\delta(k_3^2 - m_3^2)\,f\,(s_{12}, s_{23}, s_{31})\rangle\rangle\,, \tag{4.4.8}$$

where f is the product of all the uncut propagators, which only depend on the scalar invariants

$$s_{12} = (k_1 + k_2)^2\,, \quad s_{23} = (k_2 + k_3)^2\,, \quad s_{31} = (k_3 + k_1)^2\,. \tag{4.4.9}$$

Only two of these variables are independent, because

$$s_{12} + s_{23} + s_{31} = p^2 + m_1^2 + m_2^2 + m_3^2. \tag{4.4.10}$$

We will rewrite eq. (4.4.8) as a two dimensional integral over s_{12} and s_{23}:

$$I(p^2) = \int \mathrm{d}s_{12}\mathrm{d}s_{23} J(s_{12}, s_{23}; p^2) f\,(s_{12}, s_{23}, s_{31}) \tag{4.4.11}$$

with

$$\begin{aligned} J(s_{12}, s_{23}; p^2) &= \langle\langle 2\pi\,\theta(k_1^0)\,\delta(k_1^2 - m_1^2)\,2\pi\,\theta(k_2^0)\,\delta(k_2^2 - m_2^2)\,2\pi\,\theta(k_3^0)\,\delta(k_3^2 - m_3^2) \\ &\quad \delta\left((k_1 + k_2)^2 - s_{12}\right)\,\delta\left((k_2 + k_3)^2 - s_{23}\right)\rangle\rangle \\ &= \frac{(2\pi)^3}{[i\pi^2(2\pi\mu)^{D-4}]^2} \int \mathrm{d}^D k_1 \int \mathrm{d}^D k_3 \theta(k_1^0)\delta(k_1^2 - m_1^2)\theta(k_3^0)\delta(k_3^2 - m_3^2) \\ &\quad \delta((p - k_1)^2 - s_{23})\,\delta((p - k_3)^2 - s_{12}) \\ &\quad \theta(p^0 - k_1^0 - k_3^0)\,\delta((p - k_1 - k_3)^2 - m_2^2)\,. \end{aligned} \tag{4.4.12}$$

$I(p^2)$ is zero when $p^2 < (m_1 + m_2 + m_3)^2$. For $p^2 > (m_1 + m_2 + m_3)^2$, we will again work in the p-rest frame,

$$p = (p^0, \vec{0}), \quad k_i = (k_i^0, \vec{k}_i) \quad i = 1, 2, 3\,. \tag{4.4.13}$$

We use four of the delta functions to reduce (4.4.12) to two angular integrals,

$$\begin{aligned} J(s_{12}, s_{23}; p^2) &= \frac{(2\pi)^3}{[i\pi^2(2\pi\mu)^{D-4}]^2} \frac{1}{4p^0} |\vec{k}_1|^{D-3} \int \mathrm{d}\Omega_{D-1}(\vec{k}_1) \frac{1}{4p^0} |\vec{k}_3|^{D-3} \int \mathrm{d}\Omega_{D-1}(\vec{k}_3) \\ &\quad \delta\left((p^0 - k_1^0 - k_3^0)^2 - |\vec{k}_1|^2 - |\vec{k}_3|^2 - 2|\vec{k}_1||\vec{k}_3|\cos\theta_{13} - m_2^2\right), \end{aligned} \tag{4.4.14}$$

where θ_{13} is the angle between $\vec{k}_1$ and $\vec{k}_3$. The fifth delta function is eliminated by writing

$$\int \mathrm{d}\Omega_{D-1}(\vec{k}_3) = \int_{-1}^{1} (\sin\theta_{13})^{D-4}\,\mathrm{d}\cos\theta_{13} \int \mathrm{d}\Omega_{D-2}(\vec{k}_{3\perp})\,, \tag{4.4.15}$$

where $\vec{k}_{3\perp}$ is orthogonal to $\vec{k}_1$, and carrying out the $\cos\theta_{13}$ integration. This brings a factor of $2|\vec{k}_1||\vec{k}_3|$ in the denominator, provided that

$$-1 < \frac{(p^0 - k_1^0 - k_3^0)^2 - |\vec{k}_1|^2 - |\vec{k}_3|^2 - m_2^2}{2|\vec{k}_1||\vec{k}_3|} < 1 . \tag{4.4.16}$$

The remaining angular integrations are independent and both of the form of (4.4.5). Combining the results, we find

$$J(s_{12}, s_{23}; p^2) = \frac{-2\pi}{\Gamma(D-2)} \left(\frac{1}{2\pi\mu^2}\right)^{D-4} \frac{1}{(p^0)^2} \left[|\vec{k}_1||\vec{k}_3| \sin\theta_{13}\right]^{D-4} . \tag{4.4.17}$$

In the p-rest frame one can show that

$$\vec{k}_1^2 \vec{k}_3^2 \sin^2\theta_{13} = \frac{det}{p^2} , \tag{4.4.18}$$

where

$$det \equiv \begin{vmatrix} k_1^2 & k_1 \cdot k_2 & k_1 \cdot k_3 \\ k_2 \cdot k_1 & k_2^2 & k_2 \cdot k_3 \\ k_3 \cdot k_1 & k_3 \cdot k_2 & k_3^2 \end{vmatrix} . \tag{4.4.19}$$

This gives the following Lorentz invariant expression for $I(p^2)$:

$$I(p^2) = \frac{-2\pi}{\Gamma(2-2\delta)} \left(\frac{1}{2\pi\mu^2}\right)^{-2\delta} \int_{\Omega(p^2)} ds_{12} ds_{23} \frac{1}{p^2} \left[\frac{det}{p^2}\right]^{-\delta} f(s_{12}, s_{23}, s_{31}) . \tag{4.4.20}$$

In (4.4.19), all the scalar products are functions of s_{12}, s_{23}, m_1^2, m_2^2, m_3^2 and p^2. The integration region $\Omega(p^2)$ is the part of the s_{12}-s_{23}-plane where:

$$s_{12} > (m_1 + m_2)^2 , \quad s_{23} > (m_2 + m_3)^2 , \quad s_{31} > (m_3 + m_1)^2 , \tag{4.4.21}$$

and

$$det > 0 . \tag{4.4.22}$$

This follows from the condition (4.4.16).

It is interesting to see how the factor $(det/p^2)^{-\delta}$ can regularize both infrared and ultraviolet singularities. Infrared singularities are caused by poles in the uncut propagators f on the edge of the phase space. This is exactly where det goes to zero. The poles are cancelled by the factor $(det/p^2)^{-\delta}$ if we make δ negative. On the other hand, if we have an ultraviolet singularity, it will appear as a divergence when we insert $I(p^2)$ in the dispersion integral:

$$\frac{1}{2\pi i} \int_{\zeta_0}^{\infty} d\zeta \frac{1}{\zeta - p^2} I(\zeta) . \tag{4.4.23}$$

This divergence is regularized by giving δ a positive value. Then the factor $(det/p^2)^{-\delta}$ helps to suppress $I(p^2)$ as $p^2 \to \infty$.

In the general massive case, it is the curved boundary of the phase space, determined by $det = 0$, that makes these integrals difficult. If we try to calculate (4.4.23), we run into integrals involving square roots of quartic polynomials, that cannot be removed by a transformation of variables, unless either one of the masses is zero, or p^2 is zero or equal to one of the following (pseudo)thresholds:

$$(m_1+m_2+m_3)^2, \quad (m_1+m_2-m_3)^2, \quad (m_1-m_2+m_3)^2, \quad (-m_1+m_2+m_3)^2. \tag{4.4.24}$$

These are exactly the same conditions as found in [5], where a proof is given that if a two-loop integral contains any three-particle cut where none of these conditions is true, then it cannot be expressed in terms of polylogarithms.

However, this problem does not occur in the diagrams with massless fermions where, in each three-particle cut, at least two of the masses are zero. All the integrals of Fig. 4.3 can be calculated analytically in terms of logarithms, dilogarithms and trilogarithms. In the next section, we will show how this is done for a simple example.

4.5 An example

In this section, we will calculate $T_{1234}(p^2; 0, 0, m^2, 0)$, but first, let us consider the more general case: $T_{1234}(p^2; m_1^2, m_2^2, m_3^2, m_4^2)$. For this calculation, it is convenient to define all momenta k_1 to k_4 flowing from left to right, as in Fig. 4.6.

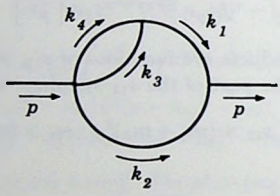

Fig. 4.6. T_{1234}

The discontinuity ΔT is the sum of a two and a three-particle cut, which we will denote by $\Delta T^{(2)}$ and $\Delta T^{(3)}$, respectively. The two-particle cut is given by

$$\Delta T^{(2)}(p^2) = -\langle\langle 2\pi\theta(k_1^0)\,\delta(k_1^2-m_1^2)\,2\pi\theta(k_2^0)\,\delta(k_2^2-m_2^2)\frac{1}{[k_3^2-m_3^2+i\varepsilon]\,[k_4^2-m_4^2+i\varepsilon]}\rangle\rangle. \tag{4.5.1}$$

We write the one-loop subintegral containing propagators 3 and 4 as $B_0(k_1^2; m_3^2, m_4^2)$. Then we note that, due to the factor $\delta(k_1^2-m_1^2)$, we can replace it with $B_0(m_1^2; m_3^2, m_4^2)$. The remaining loop integral equals the discontinuity of another B_0:

$$-\langle 2\pi\,\theta(k_1^0)\,\delta(k_1^2-m_1^2)\,2\pi\,\theta(k_2^0)\,\delta(k_2^2-m_2^2)\rangle = \Delta B_0(p^2; m_1^2, m_2^2). \tag{4.5.2}$$

So, we find

$$\Delta T^{(2)}(p^2) = \Delta B_0(p^2; m_1^2, m_2^2) B_0(m_1^2; m_3^2, m_4^2)\,. \tag{4.5.3}$$

Inserting this result in the dispersion integral (4.3.2) with $\zeta_0 = (m_1 + m_2)^2$ gives

$$\begin{aligned} T^{(2)}(p^2) &\equiv \frac{1}{2\pi i}\int_{\zeta_0}^{\infty} \mathrm{d}\zeta \frac{1}{\zeta - p^2}\Delta T^{(2)}(\zeta) \\ &= \frac{1}{2\pi i}\int_{\zeta_0}^{\infty} \mathrm{d}\zeta \frac{1}{\zeta - p^2}\Delta B_0(\zeta; m_1^2, m_2^2)\; B_0(m_1^2; m_3^2, m_4^2) \\ &= B_0(p^2; m_1^2, m_2^2)\; B_0(m_1^2; m_3^2, m_4^2), \end{aligned} \tag{4.5.4}$$

a product of two one-loop integrals, for which we can use the expressions (4.6.13)–(4.6.15) given in section 4.6.

Now we turn to the contribution from the three-particle cut:

$$T^{(3)}(p^2) \equiv \frac{1}{2\pi i}\int_{\zeta_0}^{\infty} \mathrm{d}\zeta \frac{1}{\zeta - p^2}\Delta T^{(3)}(\zeta)\,, \tag{4.5.5}$$

with $\zeta_0 = (m_3 + m_4)^2$. At this point we will restrict ourselves to the special case: $m_1 = m_2 = m_4 = 0$, $m_3 = m$. The three-particle phase space integral is now given by

$$\Delta T^{(3)}(p^2) = i\langle\langle 2\pi\,\theta(k_2^0)\,\delta(k_2^2)\,2\pi\,\theta(k_3^0)\,\delta(k_3^2 - m^2)\,2\pi\,\theta(k_4^0)\,\delta(k_4^2)\,\frac{1}{k_1^2 - i\varepsilon}\rangle\rangle\,. \tag{4.5.6}$$

First, we note that, in this particular case, k_1^2 is always positive, since

$$k_1^2 = (k_3 + k_4)^2 > m^2\,. \tag{4.5.7}$$

Therefore, we can drop the $i\varepsilon$ in (4.5.6). Next, we reduce $\Delta T^{(3)}(p^2)$ to a two dimensional integral using (4.4.20). The Gram determinant (4.4.19) can be written as:

$$det = \frac{m^6}{4}(ab - c)c\,, \tag{4.5.8}$$

with

$$a = \frac{2k_3\cdot k_4}{m^2},\; b = \frac{2k_2\cdot k_3}{m^2},\; c = \frac{2k_2\cdot k_4}{m^2}\,. \tag{4.5.9}$$

Inserting the resulting expression in the dispersion integral (4.5.5) and introducing the dimensionless variables $\xi = \zeta/m^2$ and $x = p^2/m^2$, we obtain the following three dimensional integral for $T^{(3)}$:

$$\begin{aligned} T^{(3)}(p^2) \;=\; & \frac{-1}{\Gamma(2-2\delta)}\left(\frac{m^2}{4\pi\mu^2}\right)^{-2\delta}\int_1^{\infty}\mathrm{d}\xi\frac{1}{\xi - x}\times \\ & \int_0^{\xi-1}\mathrm{d}a\int_{\frac{\xi-a-1}{a+1}}^{\xi-a-1}\mathrm{d}b\frac{1}{\xi(a+1)}\left[\frac{(ab-\xi+a+b+1)(\xi-a-b-1)}{\xi}\right]^{-\delta}. \end{aligned} \tag{4.5.10}$$

Before calculating this integral for general values of p^2, we will do the special case $p^2 = 0$. The b-integration yields a beta-function:

$$\mathrm{B}(\alpha,\beta) = \int_0^1 \mathrm{d}t\, t^{\alpha-1}(1-t)^{\beta-1} = \frac{\Gamma(\alpha)\,\Gamma(\beta)}{\Gamma(\alpha+\beta)}\,. \tag{4.5.11}$$

We find

$$\int_{\frac{\xi-a-1}{a+1}}^{\xi-a-1} \mathrm{d}b \left[\left(\frac{a+1}{\xi}\right)(\xi-a-1-b)\left(b-\frac{\xi-a-1}{a+1}\right)\right]^{-\delta} = \frac{\Gamma^2(1-\delta)}{\Gamma(2-2\delta)}\xi^{\delta}(\xi-a-1)^{1-2\delta}a^{1-2\delta}(a+1)^{-1+\delta}\,. \tag{4.5.12}$$

The next step is to interchange the a- and ξ-integrations, after which they can easily be done, yielding two more beta-functions. The final result for $T^{(3)}(0)$ is:

$$T^{(3)}(0) = -\frac{\Gamma^2(1-\delta)\,\Gamma(\delta)\,\Gamma(2\delta)}{\Gamma(2-\delta)}\left(\frac{m^2}{4\pi\mu^2}\right)^{-2\delta}\,. \tag{4.5.13}$$

In the general case when $p^2 \neq 0$, we write

$$T^{(3)}(p^2) = \left(T^{(3)}(p^2) - T^{(3)}(0)\right) + T^{(3)}(0)\,. \tag{4.5.14}$$

The first term in (4.5.14) is finite, so we can calculate it with $\delta = 0$, as follows:

$$\begin{aligned} T^{(3)}(p^2) - T^{(3)}(0) &= -\int_1^{\infty} \mathrm{d}\xi \left(\frac{1}{\xi-x}-\frac{1}{\xi}\right)\int_0^{\xi-1}\mathrm{d}a \int_{\frac{\xi-a-1}{a+1}}^{\xi-a-1}\mathrm{d}b\,\frac{1}{\xi(a+1)} \\ &= -\int_1^{\infty} \mathrm{d}\xi \left(\frac{1}{\xi-x}-\frac{1}{\xi}\right)\int_0^{\xi-1}\mathrm{d}a\,\frac{(\xi-a-1)\,a}{\xi(a+1)^2} \\ &= -\int_1^{\infty} \mathrm{d}\xi \left(\frac{1}{\xi-x}-\frac{1}{\xi}\right)\frac{1}{\xi}\left((\xi+1)\ln(\xi)+2(1-\xi)\right) \\ &= 3 - 2\frac{x-1}{x}\ln(1-x) - \frac{x+1}{x}\mathrm{Li}_2(x)\,. \end{aligned} \tag{4.5.15}$$

As a check we may verify that (4.5.15) is indeed an analytic function of p^2 in the whole complex plane, except for a branch cut along the real axis from m^2 to infinity. The discontinuity across the cut is

$$\Delta T^{(3)}(p^2) = 2\pi i\left\{2\frac{x-1}{x} - \frac{x+1}{x}\ln(x)\right\} \quad (x>1)\,. \tag{4.5.16}$$

Another way to check the result is by writing the factor $1/(\xi - x)$ in the integral (4.5.10) as a geometric series

$$\sum_{n=0}^{\infty} x^n\left(\frac{1}{\xi}\right)^{n+1}\,. \tag{4.5.17}$$

By integrating each term separately, we obtain a power series for $T^{(3)}(p^2)$, which converges in the region $|p^2| < m^2$. This series can then be compared with the series we get when we expand (4.5.15) in p^2.

Our final result for $T_{1234}(p^2; 0, 0, m^2, 0)$ is obtained by adding (4.5.15), (4.5.13) and (4.5.4) and expanding the Γ functions in δ. It is given in section 4.6.

Most of the other integrals can be calculated and checked in a similar way. However, there are some differences which we will now briefly discuss. In the case of T_{234}, the discontinuity is given by just one cut diagram (see Fig. 4.5). To isolate the divergent part, we make the following substitution in the dispersion integral (4.3.2)

$$\frac{1}{\zeta - p^2} = \frac{(p^2)^2}{\zeta^2(\zeta - p^2)} + \frac{p^2}{\zeta^2} + \frac{1}{\zeta}. \tag{4.5.18}$$

The integral containing the first term is now finite for $D = 4$. The other terms can easily be calculated for arbitrary D.

The integral T_{12345} is finite, so we may set $D = 4$ from the beginning. There are two three-particle cuts and two two-particle cuts. To compute the contributions from the two-particle cuts, we must first calculate a one-loop three-point integral and then insert the result in the dispersion integral. This is more complicated than in the case of T_{1234}, because there is no factorization analogous to (4.5.4).

The dispersion method cannot be applied directly to T_{134} and T_{1134}, because they do not depend on the external momentum. However, these integrals can be obtained in an indirect way by noting that they are equal to T_{234} and T_{1234}, respectively, when the latter are evaluated at $p = 0$.

An additional trick is needed in the case of T_{11234}. Applying the Cutkosky rules to this integral would give cut diagrams containing the ill defined expression

$$\delta(k_1^2 - m_1^2)\frac{1}{[k_1^2 - m_1^2]}, \tag{4.5.19}$$

when one of the propagators with momentum k_1 is cut and the other is not. To avoid this problem, we first calculate T_{1234}, and then obtain T_{11234} by using

$$T_{11234}(p^2; m_1^2, m_1^2, m_2^2, m_3^2, m_4^2) = \frac{\partial}{\partial m_1^2} T_{1234}(p^2; m_1^2, m_2^2, m_3^2, m_4^2). \tag{4.5.20}$$

4.6 Results

In this section, a list of analytical expressions for the two-loop integrals shown in Fig. 4.3 is presented. They are given up to $\mathcal{O}(1)$ in δ, where $D = 4 - 2\delta$ is the dimension of space-time. In cases where they exist, closed expressions in terms of Γ-functions that are valid for arbitrary values of δ are included. The one-loop integrals A_0, B_0 and B_0' of (4.2.1)–(4.2.3) are also given, up to $\mathcal{O}(\delta)$. The results were derived for real values of the masses. The momentum p^2 is assumed to have a positive infinitesimal imaginary part.

Some of the simpler two-loop integrals are well known, but they are included for the sake of completeness. Three of the more complicated cases were also considered in ref. [6] and improved in ref. [7].[1]

We use the principal branch of the logarithm $\ln(z)$ with a cut along the negative real axis in z. For a, b and ab not on the real axis one defines the η-function

$$\begin{aligned} \eta(a,b) &= \ln(ab) - \ln(a) - \ln(b) \\ &= 2\pi i \left\{ \theta(-\mathrm{Im}a)\theta(-\mathrm{Im}b)\theta(\mathrm{Im}(ab)) \right. \\ &\qquad \left. -\theta(\mathrm{Im}a)\theta(\mathrm{Im}b)\theta(-\mathrm{Im}(ab)) \right\} . \end{aligned} \tag{4.6.1}$$

The principal branches of the dilogarithm $\mathrm{Li}_2(z)$ and the trilogarithm $\mathrm{Li}_3(z)$ are defined by

$$\mathrm{Li}_2(z) = -\int_0^1 dt \frac{\ln(1-zt)}{t} , \tag{4.6.2}$$

$$\mathrm{Li}_3(z) = \int_0^1 dt \frac{\mathrm{Li}_2(zt)}{t} . \tag{4.6.3}$$

Both have a cut along the positive real axis for $z > 1$. For special values of the argument they involve the values $\zeta(2) = \pi^2/6$ and $\zeta(3)$ of the Riemann zeta function. For properties of polylogarithms like functional equations, etc. we refer to Lewin [8].

A useful list of integrals that can be expressed in terms of these functions is presented in ref. [9]. One has to be careful, however, in extending these formulae to complex values of the arguments. The η-function comes in handy in this respect.

We will use the following abbreviations,

$$\begin{aligned} L_m &= \gamma_E + \ln\left(\frac{m^2}{4\pi\mu^2}\right) , \\ L_{m_{1,2}} &= \gamma_E + \ln\left(\frac{m_{1,2}^2}{4\pi\mu^2}\right) , \\ L_p &= \gamma_E + \ln\left(\frac{-p^2}{4\pi\mu^2}\right) , \end{aligned} \tag{4.6.4}$$

where γ_E is Euler's constant.

In the results for integrals that depend on two different masses m_1 and m_2, the dimensionless variables x and y are defined by

$$x = \frac{p^2}{m_2^2} , \quad y = \frac{m_1^2}{m_2^2} . \tag{4.6.5}$$

We also need the roots r_1 and r_2 of the equation

$$m_2^2 r + \frac{m_1^2}{r} = m_1^2 + m_2^2 - p^2 . \tag{4.6.6}$$

[1]The integrals $\mathcal{A}_{1m}$ and $\mathcal{E}_1$ are in agreement with our formulae (4.6.23) and (4.6.29), respectively. However, we disagree with the integral $\mathcal{L}_1$, corresponding to (4.6.34).

They satisfy

$$r_1 r_2 = y\,, \quad (1-r_1)(1-r_2) = x\,. \tag{4.6.7}$$

Since the results are always invariant under $r_1 \leftrightarrow r_2$, it does not matter which root is chosen to be called r_1 and which one r_2. Note that (4.6.13) and (4.6.36) are also invariant under $m_1 \leftrightarrow m_2$; this corresponds to

$$y \leftrightarrow 1/y\,, \; x \leftrightarrow x/y\,, \; r_1 \leftrightarrow 1/r_1\,, \; r_2 \leftrightarrow 1/r_2\,. \tag{4.6.8}$$

In the results for integrals that only depend on one mass m, we use

$$x = \frac{p^2}{m^2}\,, \tag{4.6.9}$$

and the roots r_1 and r_2 of

$$m^2\left(r + \frac{1}{r}\right) = 2m^2 - p^2. \tag{4.6.10}$$

The latter satisfy the relations

$$r_1 r_2 = 1\,, \quad (1-r_1)(1-r_2) = x\,. \tag{4.6.11}$$

The one-loop integrals are given by (see [10])

$$\begin{aligned} \frac{1}{m^2} A_0(m^2) &= -\left(\frac{m^2}{4\pi\mu^2}\right)^{-\delta} \Gamma(\delta-1) \\ &= \frac{1}{\delta} + 1 - L_m + \delta\left\{\frac{1}{2}\zeta(2) + \frac{1}{2}L_m^2 - L_m + 1\right\} \end{aligned} \tag{4.6.12}$$

$$\begin{aligned} &B_0(p^2; m_1^2, m_2^2) = \\ \frac{1}{\delta} \; - \; & \left\{\frac{1}{2}(L_{m_1} + L_{m_2}) - 2 + \frac{1}{2}\frac{y-1}{x}\ln(y) - \frac{1}{2}\frac{r_1 - r_2}{x}(\ln(r_1) - \ln(r_2))\right\} \\ + \; & \frac{\delta}{2}\left\{\zeta(2) + 8 + \frac{1}{4}(L_{m_1} + L_{m_2})^2 + \frac{1}{4}\ln^2(y)\right. \\ & + (L_{m_1} + L_{m_2}) \times \left(-2 + \frac{1}{2}\frac{y-1}{x}\ln(y) - \frac{1}{2}\frac{r_1 - r_2}{x}(\ln(r_1) - \ln(r_2))\right) \\ & -2\frac{y-1}{x}\ln(y) + \frac{r_1 - r_2}{x}\left(2\ln(r_1) - 2\ln(r_2)\right. \\ & + \ln\left(\frac{1-r_1}{r_2 - r_1}\right)\ln\left(\frac{r_1(1-r_2)}{r_1 - r_2}\right) - \ln\left(\frac{1-r_2}{r_1 - r_2}\right)\ln\left(\frac{r_2(1-r_1)}{r_2 - r_1}\right) \\ & \left.\left. + \mathrm{Li}_2\left(\frac{r_1(1-r_2)}{r_1 - r_2}\right) - \mathrm{Li}_2\left(\frac{r_2(1-r_1)}{r_2 - r_1}\right) - \mathrm{Li}_2\left(\frac{1-r_2}{r_1 - r_2}\right) + \mathrm{Li}_2\left(\frac{1-r_1}{r_2 - r_1}\right)\right)\right\} \end{aligned} \tag{4.6.13}$$

The next two special cases are used in section 4.5.

$$B_0(0;m^2,0) = \frac{1}{m^2}A_0(m^2) \tag{4.6.14}$$

$$\begin{aligned} B_0(p^2;0,0) &= \left(\frac{-p^2}{4\pi\mu^2}\right)^{-\delta}\frac{\Gamma(\delta)\,\Gamma^2(1-\delta)}{\Gamma(2-2\delta)} \\ &= \frac{1}{\delta}+2-L_p+\delta\left\{4-\frac{1}{2}\zeta(2)+\frac{1}{2}L_p^2-2L_p\right\} \end{aligned} \tag{4.6.15}$$

$$\begin{aligned} &p^2\,B_0'\left(p^2;m_1^2,m_2^2\right) = \\ &\left\{1-\frac{\delta}{2}\left(L_{m_1}+L_{m_2}\right)\right\}\times\left\{-\frac{1}{2}\ln(y)+\frac{1}{2}\frac{x-y+1}{r_2-r_1}\left(\ln(r_1)-\ln(r_2)\right)\right\} \\ &+\frac{\delta}{2}\frac{x-y+1}{r_2-r_1}\left\{\ln\left(\frac{1-r_1}{r_2-r_1}\right)\ln\left(\frac{r_1(1-r_2)}{r_1-r_2}\right)-\ln\left(\frac{1-r_2}{r_1-r_2}\right)\ln\left(\frac{r_2(1-r_1)}{r_2-r_1}\right)\right. \\ &\left.+\mathrm{Li}_2\left(\frac{r_1(1-r_2)}{r_1-r_2}\right)-\mathrm{Li}_2\left(\frac{r_2(1-r_1)}{r_2-r_1}\right)-\mathrm{Li}_2\left(\frac{1-r_2}{r_1-r_2}\right)+\mathrm{Li}_2\left(\frac{1-r_1}{r_2-r_1}\right)\right\} \end{aligned} \tag{4.6.16}$$

The results for the two-loop integrals are

$$\begin{aligned} \frac{1}{m^2}T_{134}\left(m^2,0,0\right) &= -\left(\frac{m^2}{4\pi\mu^2}\right)^{-2\delta}\frac{\Gamma^2(1-\delta)\,\Gamma(\delta)\,\Gamma(-1+2\delta)}{\Gamma(2-\delta)} \\ &= \frac{1}{2\delta^2}+\frac{1}{\delta}\left\{\frac{3}{2}-L_m\right\}+\frac{7}{2}+\frac{3}{2}\zeta(2)+L_m^2-3\,L_m \end{aligned} \tag{4.6.17}$$

$$\begin{aligned} T_{1134}\left(m^2,m^2,0,0\right) &= \left(\frac{m^2}{4\pi\mu^2}\right)^{-2\delta}\frac{\Gamma^2(1-\delta)\,\Gamma(\delta)\,\Gamma(2\delta)}{\Gamma(2-\delta)} \\ &= \frac{1}{2\delta^2}+\frac{1}{\delta}\left\{\frac{1}{2}-L_m\right\}+\frac{1}{2}+\frac{3}{2}\zeta(2)+L_m^2-L_m \end{aligned} \tag{4.6.18}$$

$$\begin{aligned} T_{1134}\left(0,0,m^2,0\right) &= -\left(\frac{m^2}{4\pi\mu^2}\right)^{-2\delta}\frac{\Gamma^2(1-\delta)\,\Gamma(\delta)\,\Gamma(2\delta)}{\Gamma(2-\delta)} \\ &= -\frac{1}{2\delta^2}+\frac{1}{\delta}\left\{-\frac{1}{2}+L_m\right\}-\frac{1}{2}-\frac{3}{2}\zeta(2)-L_m^2+L_m \end{aligned} \tag{4.6.19}$$

$$\begin{aligned} \frac{1}{p^2}T_{234}\left(p^2;0,0,0\right) &= \left(\frac{-p^2}{4\pi\mu^2}\right)^{-2\delta}\frac{\Gamma^3(1-\delta)\,\Gamma(-1+2\delta)}{\Gamma(3-3\delta)} \\ &= -\frac{1}{4\delta}-\frac{13}{8}+\frac{1}{2}L_p \end{aligned} \tag{4.6.20}$$

$$\frac{1}{m^2}T_{234}\left(p^2;m^2,0,0\right)=\frac{1}{2\delta^2}-\frac{1}{\delta}\left\{-\frac{3}{2}+L_m+\frac{x}{4}\right\}+3+\frac{3}{2}\zeta(2)+L_m^2+\left(-3+\frac{x}{2}\right)L_m$$
$$-\frac{13}{8}x-\frac{1}{2}\left(\frac{1}{x}-x\right)\ln(1-x)+\mathrm{Li}_2(x) \qquad (4.6.21)$$

$$\begin{aligned}T_{1234}\left(p^2;0,0,0,0\right) &= -\left(\frac{-p^2}{4\pi\mu^2}\right)^{-2\delta}\frac{\Gamma^3(1-\delta)\,\Gamma(-1+2\delta)}{\delta\,\Gamma(2-3\delta)}\\ &= \frac{1}{2\delta^2}+\frac{1}{\delta}\left\{\frac{5}{2}-L_p\right\}+\frac{19}{2}-\frac{1}{2}\zeta(2)+L_p^2-5L_p \qquad (4.6.22)\end{aligned}$$

$$\begin{aligned}T_{1234}\left(p^2;0,0,m^2,0\right) &= \frac{1}{2\delta^2}+\frac{1}{\delta}\left\{\frac{5}{2}-L_m-\ln(-x)\right\}\\ &+\frac{19}{2}-\frac{3}{2}\zeta(2)+L_m^2+(-5+2\ln(-x))\,L_m+\frac{1}{2}\ln^2(-x)\\ &-3\ln(-x)-2\frac{x-1}{x}\ln(1-x)-\frac{x+1}{x}\mathrm{Li}_2(x) \qquad (4.6.23)\end{aligned}$$

$$\begin{aligned}T_{1234}\left(p^2;m^2,m^2,0,0\right) &= \frac{1}{2\delta^2}+\frac{1}{\delta}\left\{\frac{5}{2}-L_m+\frac{r_1-r_2}{x}\ln(r_1)\right\}\\ &+\frac{19}{2}+\frac{3}{2}\zeta(2)+L_m^2-\left(5+2\,\frac{r_1-r_2}{x}\ln(r_1)\right)L_m\\ &+\frac{1-x}{x}\ln(1-x)+\frac{1}{2}\mathrm{Li}_2(x)\\ &+\frac{1}{2}\frac{r_1-r_2}{x}\left\{8\ln(r_1)+\ln^2(1+r_2)-\ln^2(1+r_1)\right.\\ &+2\mathrm{Li}_2\left(\frac{1}{1+r_2}\right)-2\mathrm{Li}_2\left(\frac{1}{1+r_1}\right)-\mathrm{Li}_2(1-r_1)+\mathrm{Li}_2(1-r_2)\\ &-\mathrm{Li}_2(r_2(1-r_2))-\eta(1-x,r_2)\ln(r_2(1-r_2))\\ &\left.+\mathrm{Li}_2(r_1(1-r_1))+\eta(1-x,r_1)\ln(r_1(1-r_1))\right\} \qquad (4.6.24)\end{aligned}$$

$$\begin{aligned}T_{1234}\left(p^2;m_1^2,m_2^2,0,0\right) &= \frac{1}{2\delta^2}+\frac{1}{2\delta}\left\{5-2\,L_{m_2}-\left(1+\frac{y-1}{x}\right)\ln(y)\right.\\ &\left.+\frac{r_1-r_2}{x}\left(\ln(r_1)-\ln(r_2)\right)\right\}+L_{m_2}^2\\ &+\left(-5+\left(1+\frac{y-1}{x}\right)\ln(y)-\frac{r_1-r_2}{x}\left(\ln(r_1)-\ln(r_2)\right)\right)L_{m_2}\\ &+\frac{19}{2}+\frac{3}{2}\zeta(2)+\frac{1}{2}\left(1+\frac{y-1}{x}\right)\ln^2(y)\\ &+\left(-2\left(1+\frac{y-1}{x}\right)-\frac{3}{4}\frac{r_1-r_2}{x}\left(\ln(r_1)-\ln(r_2)\right)\right)\ln(y)\\ &+\frac{1-x}{x}\ln(1-x)+\frac{1}{2}\left(\frac{1-y+x}{x}\right)\mathrm{Li}_2(x)\end{aligned}$$

$$
\begin{aligned}
&+\frac{1}{2}\frac{r_1-r_2}{x}\Bigg\{4\ln(r_1)-4\ln(r_2)\\
&+\ln\left(\frac{1-r_1}{r_2-r_1}\right)\ln\left(\frac{r_1(1-r_2)}{r_1-r_2}\right)-\ln\left(\frac{1-r_2}{r_1-r_2}\right)\ln\left(\frac{r_2(1-r_1)}{r_2-r_1}\right)\\
&+\mathrm{Li}_2\left(\frac{r_1(1-r_2)}{r_1-r_2}\right)-\mathrm{Li}_2\left(\frac{r_2(1-r_1)}{r_2-r_1}\right)\\
&-\mathrm{Li}_2\left(\frac{1-r_2}{r_1-r_2}\right)+\mathrm{Li}_2\left(\frac{1-r_1}{r_2-r_1}\right)-\mathrm{Li}_2(1-r_1)+\mathrm{Li}_2(1-r_2)\\
&-\mathrm{Li}_2\left(\frac{r_2(1-r_1)}{-r_1}\right)-\eta\left(1-x,\frac{1}{r_1}\right)\ln\left(\frac{r_2(1-r_1)}{-r_1}\right)\\
&+\mathrm{Li}_2\left(\frac{r_1(1-r_2)}{-r_2}\right)+\eta\left(1-x,\frac{1}{r_2}\right)\ln\left(\frac{r_1(1-r_2)}{-r_2}\right)\Bigg\}
\end{aligned}
\tag{4.6.25}
$$

$$
\begin{aligned}
T_{1234}(p^2;m^2,0,0,0) &= \frac{1}{2\delta^2}+\frac{1}{2\delta}\left\{5-2L_m+2\left(\frac{1-x}{x}\right)\ln(1-x)\right\}\\
&+\frac{19}{2}+\frac{3}{2}\zeta(2)+L_m^2-L_m\left(5+2\left(\frac{1-x}{x}\right)\ln(1-x)\right)\\
&-\ln(-x)+\left(\frac{x-1}{x}\right)\left\{2\,\mathrm{Li}_2(x)+\ln^2(1-x)\right.\\
&\left.+\ln(-x)\ln(1-x)-4\ln(1-x)\right\}\,.
\end{aligned}
\tag{4.6.26}
$$

$$
\begin{aligned}
T_{1234}(p^2;0,m^2,0,0) &= \frac{1}{2\delta^2}+\frac{1}{2\delta}\left\{5-2L_m+2\left(\frac{1-x}{x}\right)\ln(1-x)\right\}\\
&+\frac{19}{2}+\frac{3}{2}\zeta(2)+L_m^2-L_m\left(5+2\left(\frac{1-x}{x}\right)\ln(1-x)\right)\\
&+5\left(\frac{1-x}{x}\right)\ln(1-x)+\left(2-\frac{1}{x}\right)\mathrm{Li}_2(x)\\
&+2\left(1-\frac{1}{x}\right)\ln^2(1-x)\,.
\end{aligned}
\tag{4.6.27}
$$

Note that $T_{1234}(p^2;m^2,0,0,0)-T_{1234}(p^2;0,m^2,0,0)$ is finite.

$$
\begin{aligned}
p^2\,T_{11234}\left(p^2;0,0,0,0,0\right) &= \left(\frac{-p^2}{4\pi\mu^2}\right)^{-2\delta}\frac{\Gamma^2(1-\delta)\,\Gamma(-1-\delta)\,\Gamma(-1+2\delta)}{\Gamma(1-3\delta)}\\
&= -\frac{1}{2\delta^2}+\frac{1}{\delta}\left\{-\frac{1}{2}+L_p\right\}-\frac{3}{2}+\frac{1}{2}\zeta(2)-L_p^2+L_p
\end{aligned}
\tag{4.6.28}
$$

$$
\begin{aligned}
p^2\,T_{11234}\left(p^2;0,0,0,m^2,0\right) &= -\frac{1}{\delta^2}+\frac{1}{\delta}\left\{-1+L_p+L_m\right\}-\frac{3}{2}-\frac{1}{2}\left(L_p+L_m\right)^2+L_p+L_m\\
&-\frac{1}{2}x\ln(-x)+\frac{1}{2}\left(x-\frac{1}{x}\right)\ln(1-x)+\mathrm{Li}_2(x)
\end{aligned}
\tag{4.6.29}
$$

$$
\begin{aligned}
& m^2 T_{11234}\left(p^2; m^2, m^2, m^2, 0, 0\right) = \\
& \left\{\frac{1}{\delta} - 2L_m + x - 2\right\} \frac{\ln(r_1)}{r_2 - r_1} - \frac{1}{2x} \operatorname{Li}_2(x) + \frac{1-x}{x} \ln(1-x) \\
& + \frac{1}{2} \frac{1}{r_2 - r_1} \left\{\ln^2(1+r_2) - \ln^2(1+r_1)\right. \\
& + 2 \operatorname{Li}_2\left(\frac{1}{1+r_2}\right) - 2 \operatorname{Li}_2\left(\frac{1}{1+r_1}\right) - \operatorname{Li}_2(1-r_1) + \operatorname{Li}_2(1-r_2) \\
& - \operatorname{Li}_2(r_2(1-r_2)) - \eta(1-x, r_2) \ln(r_2(1-r_2)) \\
& \left. + \operatorname{Li}_2(r_1(1-r_1)) + \eta(1-x, r_1) \ln(r_1(1-r_1))\right\}
\end{aligned} \tag{4.6.30}
$$

$$
\begin{aligned}
& p^2 T_{11234}\left(p^2; m_1^2, m_1^2, m_2^2, 0, 0\right) = \\
& \left\{\frac{1}{2\delta} - L_{m_2}\right\} \times \left\{-\ln(y) + \frac{x-y+1}{r_2 - r_1} (\ln(r_1) - \ln(r_2))\right\} \\
& + \frac{1}{2} \ln^2(y) + \frac{1}{2} \frac{x-y-1}{y} \ln(y) - \frac{3}{4} \frac{x-y+1}{r_2 - r_1} \ln(y) (\ln(r_1) - \ln(r_2)) \\
& + \frac{1}{2} \frac{(x-y-1)(x+y-1)}{y(r_2 - r_1)} (\ln(r_1) - \ln(r_2)) - \frac{1}{2} \operatorname{Li}_2(x) + \frac{1-x}{y} \ln(1-x) \\
& + \frac{1}{2} \frac{x-y+1}{r_2 - r_1} \left\{\ln\left(\frac{1-r_1}{r_2 - r_1}\right) \ln\left(\frac{-r_1(1-r_2)}{r_2 - r_1}\right) - \ln\left(\frac{1-r_2}{r_1 - r_2}\right) \ln\left(\frac{-r_2(1-r_1)}{r_1 - r_2}\right)\right. \\
& + \operatorname{Li}_2\left(\frac{-r_1(1-r_2)}{r_2 - r_1}\right) - \operatorname{Li}_2\left(\frac{-r_2(1-r_1)}{r_1 - r_2}\right) \\
& - \operatorname{Li}_2\left(\frac{1-r_2}{r_1 - r_2}\right) + \operatorname{Li}_2\left(\frac{1-r_1}{r_2 - r_1}\right) - \operatorname{Li}_2(1-r_1) + \operatorname{Li}_2(1-r_2) \\
& - \operatorname{Li}_2\left(\frac{r_2(1-r_1)}{-r_1}\right) - \eta\left(1-x, \frac{1}{r_1}\right) \ln\left(\frac{r_2(1-r_1)}{-r_1}\right) \\
& \left. + \operatorname{Li}_2\left(\frac{r_1(1-r_2)}{-r_2}\right) + \eta\left(1-x, \frac{1}{r_2}\right) \ln\left(\frac{r_1(1-r_2)}{-r_2}\right)\right\}
\end{aligned} \tag{4.6.31}
$$

When $m_2 = 0$, eq. (4.6.31) reduces to

$$
\begin{aligned}
p^2 T_{11234}(p^2; m^2, m^2, 0, 0, 0) = & \left\{\frac{1}{\delta} - 2L_m\right\} \ln(1-x) - x \ln(-x) + (1+x) \ln(1-x) \\
& - 2 \operatorname{Li}_2(x) - \ln^2(1-x) - \ln(-x) \ln(1-x) \,.
\end{aligned} \tag{4.6.32}
$$

$$
\begin{aligned}
& p^2 T_{12345}\left(p^2; 0, 0, 0, 0, 0\right) \\
= \quad & \left(\frac{-p^2}{4\pi\mu^2}\right)^{-2\delta} \frac{1}{\delta^3} \frac{\Gamma^3(1-\delta)}{\Gamma(2-2\delta)} \left\{\frac{\Gamma(1-\delta)\Gamma^2(1+\delta)}{\Gamma(1-2\delta)} - \frac{\Gamma(1-2\delta)\Gamma(1+2\delta)}{\Gamma(1-3\delta)}\right\} \\
= \quad & 6\zeta(3)
\end{aligned} \tag{4.6.33}
$$

$$
\begin{aligned}
&p^2\, T_{12345}\left(p^2;0,0,m^2,0,0\right) = \\
&\quad -\zeta(3) - 2\zeta(2)\left(\ln(-x) - \ln(1-x)\right) + \ln^2(-x)\ln(1+x) - \frac{2}{3}\ln^3(1-x) \\
&\quad + \left(2\ln(-x) - 4\ln(1-x)\right)\mathrm{Li}_2(1+x) + 4\,\mathrm{Li}_3(1+x) + 2\,\mathrm{Li}_3(-x) \\
&\quad +4\,\mathrm{Li}_3\left(\frac{1}{1-x}\right) + 2\,\mathrm{Li}_3(x) - 4\,\mathrm{Li}_3\left(\frac{1+x}{1-x}\right) + 4\,\mathrm{Li}_3\left(\frac{x+1}{x-1}\right)
\end{aligned}
\tag{4.6.34}
$$

$$
\begin{aligned}
&p^2\, T_{12345}\left(p^2;m^2,m^2,0,0,0\right) = \\
&\quad 2\,\mathrm{Li}_3(x) + 4\,\mathrm{Li}_3\left(\frac{-x}{1-x}\right) + 6\,\mathrm{Li}_3(1-r_1) + 6\,\mathrm{Li}_3(1-r_2) + \frac{2}{3}\ln^3(1-x) \\
&\quad -4\,\mathrm{Li}_3\left(\frac{1-r_2}{1-r_1-r_2}\right) - 2\,\mathrm{Li}_3(r_2(1-r_2)) \\
&\quad +\eta(1-x,r_2)\left\{2\ln^2\left(\frac{1-r_2}{1-r_1-r_2}\right) - \ln^2(r_2(1-r_2))\right\} \\
&\quad -4\,\mathrm{Li}_3\left(\frac{1-r_1}{1-r_1-r_2}\right) - 2\,\mathrm{Li}_3(r_1(1-r_1)) \\
&\quad +\eta(1-x,r_1)\left\{2\ln^2\left(\frac{1-r_1}{1-r_1-r_2}\right) - \ln^2(r_1(1-r_1))\right\} \\
&\quad -2\ln(1-x)\ln^2(r_2) - \ln(-x)\ln^2(r_2) \\
&\quad +2\ln(r_2)\left\{\mathrm{Li}_2(1-r_1) - \mathrm{Li}_2(1-r_2)\right\}
\end{aligned}
\tag{4.6.35}
$$

$$
\begin{aligned}
&p^2\, T_{12345}(p^2;m_1^2,m_2^2,0,0,0) = \\
&\left(\ln(-x) - \frac{1}{2}\ln(y)\right)\ln(r_1)\ln(r_2) \\
&+3\,\mathrm{Li}_3(1-r_1) + 3\,\mathrm{Li}_3(1-1/r_1) + 3\,\mathrm{Li}_3(1-r_2) + 3\,\mathrm{Li}_3(1-1/r_2) \\
&+\ln(y)\left(\frac{3}{2}\mathrm{Li}_2(1-r_1) - \frac{3}{2}\mathrm{Li}_2(1-1/r_1) + \frac{3}{2}\mathrm{Li}_2(1-r_2)\right. \\
&\qquad \left. - \frac{3}{2}\mathrm{Li}_2(1-1/r_2) - \frac{1}{2}\mathrm{Li}_2(1-y) + \frac{1}{2}\mathrm{Li}_2(1-1/y)\right) \\
&-\ln(r_1)\left(\mathrm{Li}_2(1-r_1) - \mathrm{Li}_2(1-1/r_1)\right) - \ln(r_2)\left(\mathrm{Li}_2(1-r_2) - \mathrm{Li}_2(1-1/r_2)\right) \\
&-\frac{1}{2}\ln(y)\left(\mathrm{Li}_2\left(\frac{-r_2(1-r_1)}{1-r_2}\right) - \mathrm{Li}_2\left(\frac{1-r_1}{-r_1(1-r_2)}\right)\right. \\
&\qquad \left. + \mathrm{Li}_2\left(\frac{-r_1(1-r_2)}{1-r_1}\right) - \mathrm{Li}_2\left(\frac{1-r_2}{-r_2(1-r_1)}\right)\right) \\
&-\frac{1}{4}\ln^2(y)\left(\ln\left(\frac{1-y}{1-r_2}\right) + \ln\left(\frac{1-y}{r_1(1-r_2)}\right) + \ln\left(\frac{1-y}{1-r_1}\right) + \ln\left(\frac{1-y}{r_2(1-r_1)}\right)\right) \\
&+\frac{1}{3}\ln^3(1-x) + \frac{1}{3}\ln^3(1-x/y) \\
&+\mathrm{Li}_3(x) + \mathrm{Li}_3(x/y) + 2\,\mathrm{Li}_3\left(\frac{-x}{1-x}\right) + 2\,\mathrm{Li}_3\left(\frac{-x}{y-x}\right)
\end{aligned}
$$

$$
\begin{aligned}
&-2\ln(1-x)\,\mathrm{Li}_2(x) - 2\ln(1-x/y)\,\mathrm{Li}_2(x/y)\\
&-\ln(y)\left(\ln^2(1-x) - \ln^2(1-x/y)\right)\\
&+\left(\ln(1-x) + \ln(1-x/y)\right)\left(\ln^2(r_1) + \ln^2(r_2)\right)\\
&-\mathrm{Li}_3\left(\frac{r_2(1-r_1)}{-r_1}\right) - 2\,\mathrm{Li}_3\left(\frac{1-x-r_1}{1-x}\right) + 2\ln(1-x)\,\mathrm{Li}_2\left(\frac{r_2(1-r_1)}{-r_1}\right)\\
&-\eta(r_2, 1-x)\left(\frac{1}{2}\ln^2\left(\frac{r_2(1-r_1)}{-r_1}\right) - \ln^2\left(\frac{1-x-r_1}{1-x}\right) - 2\ln(1-x)\ln\left(\frac{r_2(1-r_1)}{-r_1}\right)\right)\\
&-\mathrm{Li}_3\left(\frac{1-r_1}{r_2}\right) - 2\,\mathrm{Li}_3\left(\frac{y-x-r_2}{y-x}\right) + 2\ln(1-x/y)\,\mathrm{Li}_2\left(\frac{1-r_1}{r_2}\right)\\
&-\eta(r_1, y-x)\left(\frac{1}{2}\ln^2\left(\frac{1-r_1}{r_2}\right) - \ln^2\left(\frac{y-x-r_2}{y-x}\right) - 2\ln(1-x/y)\ln\left(\frac{1-r_1}{r_2}\right)\right)\\
&-\mathrm{Li}_3\left(\frac{r_1(1-r_2)}{-r_2}\right) - 2\,\mathrm{Li}_3\left(\frac{1-x-r_2}{1-x}\right) + 2\ln(1-x)\,\mathrm{Li}_2\left(\frac{r_1(1-r_2)}{-r_2}\right)\\
&-\eta(r_1, 1-x)\left(\frac{1}{2}\ln^2\left(\frac{r_1(1-r_2)}{-r_2}\right) - \ln^2\left(\frac{1-x-r_2}{1-x}\right) - 2\ln(1-x)\ln\left(\frac{r_1(1-r_2)}{-r_2}\right)\right)\\
&-\mathrm{Li}_3\left(\frac{1-r_2}{r_1}\right) - 2\,\mathrm{Li}_3\left(\frac{y-x-r_1}{y-x}\right) + 2\ln(1-x/y)\,\mathrm{Li}_2\left(\frac{1-r_2}{r_1}\right)\\
&-\eta(r_2, y-x)\left(\frac{1}{2}\ln^2\left(\frac{1-r_2}{r_1}\right) - \ln^2\left(\frac{y-x-r_1}{y-x}\right) - 2\ln(1-x/y)\ln\left(\frac{1-r_2}{r_1}\right)\right)
\end{aligned}
\tag{4.6.36}
$$

In eqs. (4.6.25) and (4.6.31), $\mathrm{Li}_2(x)$ can be eliminated using

$$
\begin{aligned}
\mathrm{Li}_2(x) \;=\;& \mathrm{Li}_2(1-r_1) + \mathrm{Li}_2(1-r_2)\\
&+\mathrm{Li}_2\left(\frac{r_1(1-r_2)}{-r_2}\right) + \eta\left(1-x, \frac{1}{r_2}\right)\ln\left(\frac{r_1(1-r_2)}{-r_2}\right)\\
&+\mathrm{Li}_2\left(\frac{r_2(1-r_1)}{-r_1}\right) + \eta\left(1-x, \frac{1}{r_1}\right)\ln\left(\frac{r_2(1-r_1)}{-r_1}\right)\\
&+\ln^2(r_1) + \ln^2(r_2) - \frac{1}{2}\ln^2(y)\,.
\end{aligned}
\tag{4.6.37}
$$

In some results, the number of dilogarithms can obviously be reduced by using identities such as e.g.

$$
\mathrm{Li}_2(1-y) + \mathrm{Li}_2(1-1/y) = -\frac{1}{2}\ln^2(y)\,, \tag{4.6.38}
$$

and

$$
\mathrm{Li}_2\left(\frac{1-r_1}{r_2-r_1}\right) + \mathrm{Li}_2\left(\frac{1-r_2}{r_1-r_2}\right) = \zeta(2) - \ln\left(\frac{1-r_1}{r_2-r_1}\right)\ln\left(\frac{1-r_2}{r_1-r_2}\right)\,, \tag{4.6.39}
$$

but this has not been done in cases where it would hide the symmetries.

4.7 Conclusion

In this chapter, we presented analytical expressions for all the scalar integrals required for the calculation of two-loop self-energy diagrams containing a massless fermion loop. We obtained their discontinuities by applying Cutkosky's rules. Then we calculated the integrals themselves through a dispersion relation, using dimensional regularization for both ultraviolet and infrared divergences. We checked that the results agree with an independent calculation using Feynman parameters [3]. Other checks included verifying the analytic structure of the results, and, in the case of T_{12345}, a comparison with a numerical program based on [11].

Note that the mass configurations considered here are different from those required in QED and QCD, for which analytical results can be found in refs. [12, 13, 14, 15]. With the results of this chapter and the tensor integral reduction algorithm of ref. [2], one can now study the light fermion contributions to gauge boson self-energies in the standard model in the approximation where the fermion masses are neglected.

Some of the integrals of this chapter can also be used for a different purpose. In chapter 6, we will discuss a method to calculate T_{234}, T_{1234} and T_{11234} in the general mass case. This will be done by first subtracting combinations of integrals from them which are known analytically, such that the remainders are finite in $D = 4$. Then they can be integrated numerically in the same way as T_{12345} is calculated in ref. [11].

References

[1] G.Passarino and M.Veltman, *Nucl. Phys.* B160 (1979) 151.

[2] G. Weiglein, R. Mertig, R. Scharf, and M. Böhm, in "New Computing Techniques in Physics Research II" , ed. D. Perret-Gallix, World Scientific 1992, p.617;
G. Weiglein, R. Scharf and M. Böhm, Reduction of general two-loop self-energies to standard scalar integrals, to be published.

[3] R. Scharf, J.B. Tausk, Scalar two-loop integrals for gauge boson self-energy diagrams with a massless fermion loop, University of Leiden preprint INLO–PUB–7/93 (1993).

[4] R.E. Cutkosky, *J. Math. Phys.* 1 (1960) 429;
M. Veltman, *Physica* 29 (1963) 186;
G. 't Hooft and M. Veltman, Diagrammar, CERN Yellow Report 73-9.

[5] R. Scharf, Diplom Thesis, Würzburg, 1991.

[6] P.N. Maher, University of Wisconsin–Madison thesis (1991).

[7] L. Durand, P.N. Maher and K. Riesselmann, University of Wisconsin–Madison preprint MAD–TH/93–1 (1993).

[8] L. Lewin, *Polylogarithms and associated functions* (North Holland, 1981).

[9] A. Devoto and D.W. Duke, *Riv. del Nuovo Cim.* 7 (1984) N.6.

[10] U. Nierste, D. Müller and M. Böhm, *Z.Phys.* C57 (1993) 605.

[11] D. Kreimer, Phys.Lett. B273 (1991) 277.

[12] D.J. Broadhurst, *Phys.Lett.* B101 (1981) 423; D.J. Broadhurst, *Z.Phys.* C47 (1990) 115.

[13] G. Rufa, University of Mainz thesis MZ–TH/85–16 (1985).

[14] A. Djouadi, *Nuovo Cim.* 100A (1988) 357.

[15] B.A. Kniehl, *Nucl.Phys.* B347 (1990) 86.

Chapter 5

Series expansions of two-loop self-energy diagrams

5.1 Introduction

In chapter 4 analytical expressions in terms of polylogarithms were given for all scalar integrals needed for computing the contributions to vector boson self-energies from two-loop diagrams containing massless fermions. That was possible because all three particle cuts in such diagrams contain at least two massless particles. However, the full self-energies also get contributions from diagrams that do not possess this property. These are the diagrams containing top quarks, whose mass can definitely not be neglected, and the purely bosonic diagrams containing W, Z or Higgs bosons. Since many of these diagrams cannot be expressed in terms of polylogarithms, we are forced to calculate them by other methods.

In this chapter, we will study two series expansions of two-loop self-energy diagrams with arbitrary internal masses: one for small external momenta and one for large external momenta. Since the coefficients can be calculated analytically, the first few terms of the expansions give approximate results for these diagrams, provided the value of the external momentum is inside the region where the series converge. This happens to be true in a number of cases of physical interest. On the other hand, there are also diagrams with intermediate values of the external momentum, where both series fail to converge. For those diagrams other techniques will have to be developed. The series expansions described in this chapter could then be used as checks on such new techniques.

The scalar integrals we will consider correspond to the diagram in Fig. 5.1 and will be written as

$$J(\nu_1,\ldots,\nu_5;m_1,\ldots,m_5;k) \equiv \iint \frac{\mathrm{d}^n p\ \mathrm{d}^n q}{((k-p)^2-m_1^2)^{\nu_1}\,((k-q)^2-m_2^2)^{\nu_2}\,((p-q)^2-m_3^2)^{\nu_3}\,(p^2-m_4^2)^{\nu_4}\,(q^2-m_5^2)^{\nu_5}}, \tag{5.1.1}$$

where k is the external momentum (note that J really depends on k^2) and n is the

space-time dimension (in the framework of dimensional regularization [1, 2]). Here and below the usual causal way of dealing with denominators in pseudo-Euclidean momentum space ($k^2 \leftrightarrow k^2 + i0$) is understood. This notation, which allows us to consider integrals with arbitrary powers of denominators ν_i, will prove to be very useful during our calculation of the coefficients of the expansions. Occasionally, we will use the shorter notation $J(\{\nu_i\}; \{m_i\}; k)$ instead of $J(\nu_1, ..., \nu_5; m_1, ..., m_5; k)$.

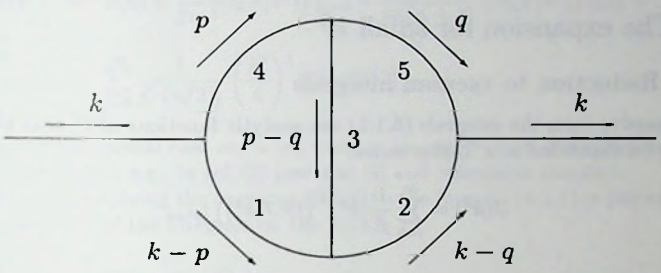

Fig. 5.1. The two-loop self-energy diagram of eq. (5.1.1). Note that the propagators are labeled in a different way than in chapter 4.

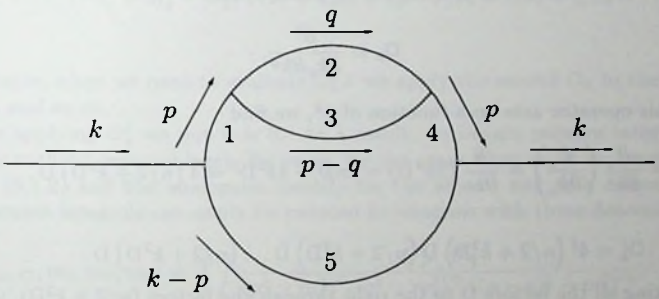

Fig. 5.2.

More simple two-loop diagrams which contain four or three internal lines as well as products of one-loop diagrams, can be obtained from (5.1.1) by putting some of the powers of denominators ν_i equal to zero. Moreover, the integral corresponding to Fig. 5.2 can also be expressed in terms of (5.1.1) (for the case of integer values of ν_1 and ν_4) by use of the obvious decomposition formula

$$\frac{1}{(p^2 - m_1^2)(p^2 - m_4^2)} = \frac{1}{m_1^2 - m_4^2}\left(\frac{1}{p^2 - m_1^2} - \frac{1}{p^2 - m_4^2}\right). \tag{5.1.2}$$

So, in general it is sufficient to consider the scalar integrals (5.1.1) with different powers of denominators ν_i.

The rest of this chapter is organized as follows. In section 5.2 we study the expansion for small k^2. Then, in section 5.3 we discuss the expansion for large k^2. A number of formulae we need for massless two-point integrals and for massive vacuum integrals are collected in appendices A and B, respectively.

5.2 The expansion for small k^2

5.2.1 Reduction to vacuum integrals

In the massive case, the integrals (5.1.1) are analytic functions of k^2 near $k^2 = 0$, so they can be expanded in a Taylor series:

$$J(k^2) = \sum_{j=0}^{\infty} \frac{1}{j!} \left(k^2\right)^j \left(\mathrm{D}^j J(k^2)\right)|_{k^2=0}\,, \tag{5.2.1}$$

where

$$\mathrm{D} \equiv \partial/\partial(k^2)\,. \tag{5.2.2}$$

In order to calculate the derivatives with respect to k^2, it is convenient to express them in terms of the momentum space d'Alembertian,

$$\Box_k \equiv \frac{\partial^2}{\partial k_\mu \partial k^\mu}\,. \tag{5.2.3}$$

When this operator acts on a function of k^2, we find

$$\Box_k = \frac{\partial}{\partial k^\mu}\left(\frac{\partial}{\partial k_\mu}\right) = \frac{\partial}{\partial k^\mu}\left(2k^\mu \mathrm{D}\right) = 2n\mathrm{D} + 4k^2\mathrm{D}^2 = 4\left(n/2 + k^2\mathrm{D}\right)\mathrm{D}\,, \tag{5.2.4}$$

so

$$\Box_k^j = 4^j \left(n/2 + k^2\mathrm{D}\right)\mathrm{D}\left(n/2 + k^2\mathrm{D}\right)\mathrm{D}\ldots\left(n/2 + k^2\mathrm{D}\right)\mathrm{D}\,. \tag{5.2.5}$$

Commuting all the factors D to the right through the factors $(n/2 + k^2\mathrm{D})$, using the rule:

$$\mathrm{D}\left(n/2 + l + k^2\mathrm{D}\right) = \left(n/2 + l + 1 + k^2\mathrm{D}\right)\mathrm{D} \qquad l = 0, 1, 2, \ldots \tag{5.2.6}$$

leads to

$$\Box_k^j = 4^j \left(n/2 + k^2\mathrm{D}\right)\left(n/2 + 1 + k^2\mathrm{D}\right)\ldots\left(n/2 + j - 1 + k^2\mathrm{D}\right)\mathrm{D}^j\,. \tag{5.2.7}$$

Setting $k^2 = 0$ in this equation gives the following identity:

$$\Box_k^j J(k^2) = 4^j (n/2)_j\, \mathrm{D}^j J(k^2) \quad \text{at } k^2 = 0\,, \tag{5.2.8}$$

where

$$(a)_j \equiv \frac{\Gamma(a+j)}{\Gamma(a)} \tag{5.2.9}$$

is the Pochhammer symbol. By substituting eq. (5.2.8) in the Taylor series (5.2.1) we finally obtain:

$$\begin{aligned} J(k^2) &= J(0) + \frac{k^2}{2n}\left(\Box_k J(k^2)\right)|_{k=0} + \frac{(k^2)^2}{8n(n+2)}\left(\Box_k^2 J(k^2)\right)|_{k=0} + \ldots \\ &= \sum_{j=0}^{\infty} \frac{1}{j!\,(n/2)_j}\left(\frac{k^2}{4}\right)^j \left(\Box_k^j J(k^2)\right)|_{k=0}\,. \end{aligned} \tag{5.2.10}$$

Note that for the special case $m_1 = m_2 = m_4 = m_5$, $m_3 = 0$ an analogous expansion has been considered, e.g., in ref. [3] (see also [4] and references therein).

The result of applying the operator (5.2.3) to the integral (5.1.1) is (we only write shifted arguments of the integrals on the r.h.s.):

$$\begin{aligned} &\Box_k J(\nu_1, \ldots, \nu_3; m_1, \ldots, m_5; k) \\ &\quad = 4\,\{(\nu_1+\nu_2+1-n/2)\,(\nu_1\, J(\nu_1+1) + \nu_2\, J(\nu_2+1)) \\ &\quad +\nu_1(\nu_1+1)m_1^2\, J(\nu_1+2) + \nu_2(\nu_2+1)m_2^2\, J(\nu_2+2) \\ &\quad +\nu_1\nu_2\left((m_1^2+m_2^2-m_3^2)\, J(\nu_1+1,\nu_2+1) - J(\nu_1+1,\nu_2+1,\nu_3-1)\right)\}\,. \end{aligned} \tag{5.2.11}$$

For example, when we need to evaluate $\Box_k^2 J$ we apply the second $\Box_k$ to the r.h.s. of (5.2.11), and so on.

After applying $\Box_k^j$ we put $k = 0$. As a result, we obtain vacuum integrals (i.e. diagrams without external legs). By using, for the cases when $m_1 \neq m_4$ or $m_2 \neq m_5$, formula (5.1.2) and the analogous identity for the second and fifth denominators, these vacuum integrals can easily be reduced to integrals with three denominators,

$$I(\nu_1,\nu_2,\nu_3; m_1,m_2,m_3) \equiv \int\!\!\int \frac{\mathrm{d}^n p\;\; \mathrm{d}^n q}{(p^2-m_1^2)^{\nu_1}\,(q^2-m_2^2)^{\nu_2}\,((p-q)^2-m_3^2)^{\nu_3}}, \tag{5.2.12}$$

(see Fig. 5.3). Of course, in these integrals we may have m_4 instead of m_1 or m_5 instead of m_2. So, the coefficients of the momentum expansion (5.2.10) of the integrals (5.1.1) can be expressed in terms of vacuum integrals (5.2.12) with various values of ν_1, ν_2, ν_3.

When one of the indices ν_i is zero the result corresponds to the product of two massive tadpoles and can be represented in terms of gamma functions (see eq. (5B.1)). For example:

$$I(\nu_1,\nu_2,0) = -\pi^n(-1)^{\nu_1+\nu_2}(m_1^2)^{n/2-\nu_1}(m_2^2)^{n/2-\nu_2}\frac{\Gamma(\nu_1-n/2)\Gamma(\nu_2-n/2)}{\Gamma(\nu_1)\Gamma(\nu_2)}\,. \tag{5.2.13}$$

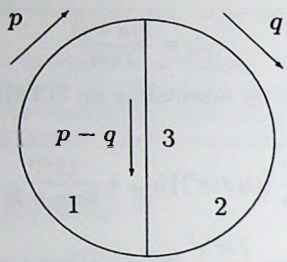

Fig. 5.3.

Note that when we apply operator (5.2.3) to (5.1.1) we may also obtain negative values of ν_3. This means that in this case we have

$$\left((p-q)^2 - m_3^2\right)^{|\nu_3|} = \left(p^2 + q^2 - m_3^2 - 2(pq)\right) \tag{5.2.14}$$

in the numerator. The squared momenta p^2 and q^2 can be represented in terms of denominators. The integrals containing $(pq)^\alpha$ vanish for odd α, and for even α we use

$$\int\int \frac{\mathrm{d}^n p \;\; \mathrm{d}^n q \;\; (pq)^{2j}}{(p^2 - m_1^2)^{\nu_1}\,(q^2 - m_2^2)^{\nu_2}} = \frac{(2j)!}{4^j\, j!\,(n/2)_j} \int \frac{\mathrm{d}^n p\,(p^2)^j}{(p^2 - m_1^2)^{\nu_1}} \int \frac{\mathrm{d}^n q\,(q^2)^j}{(q^2 - m_2^2)^{\nu_2}}. \tag{5.2.15}$$

Finally, we arrive at a representation of integrals with negative ν_3 in terms of tadpole integrals (5.2.13). This property is well known, and we presented formula (5.2.15) only for completeness.

So, the main problem in obtaining the coefficients of the expansion of (5.1.1) in k^2 is to evaluate the integrals (5.2.12) for positive integer values of ν_1, ν_2 and ν_3. We will do this in three stages. In sections 5.2.2 and 5.2.3 we will consider two different mass combinations and derive explicit formulae for the case $\nu_1 = \nu_2 = \nu_3$. Then, in section 5.2.4, the results will be extended to the general ν_1, ν_2, ν_3 case.

5.2.2 Vacuum integrals with two different masses

We start the examination of the vacuum integrals (5.2.12) with the case when two of the masses are equal: $m_1 = m_2 \equiv m$, $m_3 \equiv M$. The case when all three masses are unequal will be discussed in the next section.

To obtain the result for the case of arbitrary values of ν_1, ν_2, ν_3 and n, it is convenient to use the method of evaluating massive Feynman integrals [5, 6] based on the Mellin-Barnes representation of massive denominators,

$$\frac{1}{(k^2 - M^2)^\nu} = \frac{1}{\Gamma(\nu)} \frac{1}{2\pi i} \int_{-i\infty}^{i\infty} \mathrm{d}s\, \frac{(-M^2)^s}{(k^2)^{\nu+s}}\, \Gamma(-s)\, \Gamma(\nu+s). \tag{5.2.16}$$

In this formula we remember that $(k^2 \leftrightarrow k^2 + i0)$. The contours in Mellin-Barnes representations are chosen so as to separate the left and right series of poles of gamma functions occurring in the integrand.

In our case, it is sufficient to apply formula (5.2.16) to the third denominator in eq. (5.2.12) only. Then the obtained vacuum integral with one massless line (with shifted power of denominator) can be evaluated in terms of gamma functions (see eq. (5B.4)), and we arrive at the following Mellin-Barnes representation:

$$I(\nu_1, \nu_2, \nu_3; m, m, M) = -\pi^n (-1)^{\nu_1+\nu_2+\nu_3} (m^2)^{n-\nu_1-\nu_2-\nu_3} \frac{1}{\Gamma(\nu_1)\Gamma(\nu_2)\Gamma(\nu_3)\Gamma(n/2)}$$

$$\times \frac{1}{2\pi i} \int_{-i\infty}^{i\infty} du \left(\frac{M^2}{m^2}\right)^u \Gamma(-u)\, \Gamma(n/2 - \nu_3 - u)$$

$$\times \frac{\Gamma(\nu_3 + u)\Gamma(\nu_1 + \nu_3 - n/2 + u)\Gamma(\nu_2 + \nu_3 - n/2 + u)\Gamma(\nu_1 + \nu_2 + \nu_3 - n + u)}{\Gamma(\nu_1 + \nu_2 + 2\nu_3 - n + 2u)}. \tag{5.2.17}$$

In the following, it will be convenient to use the dimensionless variable

$$z \equiv \frac{M^2}{4m^2}\,. \tag{5.2.18}$$

For $|z| < 1$ we close the integration contour in (5.2.17) to the right and obtain

$$I(\nu_1, \nu_2, \nu_3; m, m, M) = -\pi^n (-1)^{\nu_1+\nu_2+\nu_3} (m^2)^{n-\nu_1-\nu_2-\nu_3}$$

$$\times \left\{ \frac{\Gamma(n/2 - \nu_3)\Gamma(\nu_1 + \nu_3 - n/2)\Gamma(\nu_2 + \nu_3 - n/2)\Gamma(\nu_1 + \nu_2 + \nu_3 - n)}{\Gamma(n/2)\Gamma(\nu_1)\Gamma(\nu_2)\Gamma(\nu_1 + \nu_2 + 2\nu_3 - n)} \right.$$

$$\times {}_4F_3 \left(\begin{array}{c} \nu_3,\ \nu_1 + \nu_3 - n/2,\ \nu_2 + \nu_3 - n/2,\ \nu_1 + \nu_2 + \nu_3 - n \\ (\nu_1 + \nu_2 + 2\nu_3 - n)/2,\ (\nu_1 + \nu_2 + 2\nu_3 - n + 1)/2,\ \nu_3 - n/2 + 1 \end{array} \middle| z \right)$$

$$+ (4z)^{n/2-\nu_3} \frac{\Gamma(\nu_3 - n/2)\Gamma(\nu_1 + \nu_2 - n/2)}{\Gamma(\nu_3)\Gamma(\nu_1 + \nu_2)}$$

$$\left. \times {}_4F_3 \left(\begin{array}{c} \nu_1,\ \nu_2,\ \nu_1 + \nu_2 - n/2,\ n/2 \\ (\nu_1 + \nu_2)/2,\ (\nu_1 + \nu_2 + 1)/2,\ n/2 - \nu_3 + 1 \end{array} \middle| z \right) \right\}, \tag{5.2.19}$$

where we have used the standard notation for the generalized hypergeometric function of one variable (see, e.g., [7]),

$${}_PF_Q \left(\begin{array}{c} a_1,\ \dots a_P \\ c_1,\ \dots c_Q \end{array} \middle| z \right) \equiv \sum_{j=0}^{\infty} \frac{z^j}{j!} \frac{(a_1)_j \dots (a_P)_j}{(c_1)_j \dots (c_Q)_j}, \tag{5.2.20}$$

where $(a)_j$ is the Pochhammer symbol (5.2.9).

In the case $\nu_1 = \nu_2 = \nu_3 = 1$ the ${}_4F_3$ functions reduce to ${}_2F_1$ functions. Expanding them in $\varepsilon = (4-n)/2$ and keeping the singular and $\mathcal{O}(1)$ terms only, we get

$$\begin{aligned} I(1,1,1;m,m,M) &= \pi^{4-2\varepsilon}(m^2)^{1-2\varepsilon}\, A(\varepsilon) \\ &\times \left\{-\frac{1}{\varepsilon^2}(1+2z) + \frac{1}{\varepsilon}(4z\ln(4z)) - 2z\ln^2(4z) + 2(1-z)\Phi(z)\right\} \end{aligned} \tag{5.2.21}$$

where

$$\begin{aligned} \Phi(z) &= 4z\left[(2-\ln(4z))\ {}_2F_1\left(\begin{matrix}1,1\\3/2\end{matrix}\middle|\, z\right)\right. \\ &\left. -\partial_a\, {}_2F_1\left(\begin{matrix}1,1\\3/2\end{matrix}\middle|\, z\right) - \partial_c\, {}_2F_1\left(\begin{matrix}1,1\\3/2\end{matrix}\middle|\, z\right)\right], \end{aligned} \tag{5.2.22}$$

$$\begin{aligned} A(\varepsilon) &\equiv \frac{\Gamma^2(1+\varepsilon)}{(1-\varepsilon)(1-2\varepsilon)} \\ &= 1 + \varepsilon(3-2\gamma_E) + \varepsilon^2\left(7 - 6\gamma_E + 2\gamma_E^2 + \frac{\pi^2}{6}\right) + \mathcal{O}(\varepsilon^3), \end{aligned} \tag{5.2.23}$$

and $\gamma_E = 0.57721566...$ is Euler's constant. In formula (5.2.22) we used the following notation for the derivatives of the hypergeometric function with respect to the parameters a and c:

$$\begin{aligned} \partial_a\, {}_2F_1\left(\begin{matrix}a,b\\c\end{matrix}\middle|\, z\right) &\equiv \frac{\partial}{\partial a}\, {}_2F_1\left(\begin{matrix}a,b\\c\end{matrix}\middle|\, z\right) \\ &= \sum_{j=0}^{\infty}\frac{z^j}{j!}\frac{(a)_j\,(b)_j}{(c)_j}(\psi(a+j)-\psi(a)), \end{aligned} \tag{5.2.24}$$

$$\begin{aligned} \partial_c\, {}_2F_1\left(\begin{matrix}a,b\\c\end{matrix}\middle|\, z\right) &\equiv \frac{\partial}{\partial c}\, {}_2F_1\left(\begin{matrix}a,b\\c\end{matrix}\middle|\, z\right) \\ &= -\sum_{j=0}^{\infty}\frac{z^j}{j!}\frac{(a)_j\,(b)_j}{(c)_j}(\psi(c+j)-\psi(c)), \end{aligned} \tag{5.2.25}$$

where $\psi(a) \equiv (d/da)\ln(\Gamma(a))$. The combinations of ψ functions of integer and half-integer arguments occurring on the r.h.s.'s of (5.2.24) and (5.2.25) (for $a = b = 1$, $c = 3/2$) are known rational numbers. Many useful properties of the functions (5.2.24) and (5.2.25) (integral representations, analytic continuation formulae, etc.) can be obtained by differentiating appropriate formulae for ${}_2F_1$ with respect to parameters. Note that the same functions as in (5.2.22) also occurred in ref. [8], where the QCD radiative correction to Higgs decay into two quarks was considered.

Equation (5.2.22) is useful for studying the behaviour of $\Phi(z)$ in the region $z \approx 0$. For larger values of z, it is more convenient to use other expressions which will be given below.

For the region $0 \leq z < 1$ we use the following formulae, which can easily be obtained from a parametric integral representation for the ${}_2F_1$ function and its parametric derivatives:

$$ {}_2F_1\left(\begin{matrix}1,1\\3/2\end{matrix}\middle|\, z\right) = \frac{\arcsin\sqrt{z}}{\sqrt{z(1-z)}}, \tag{5.2.26}$$

$$\partial_a\, {}_2F_1\left(\begin{matrix}1,1\\3/2\end{matrix}\middle|\, z\right) + \partial_c\, {}_2F_1\left(\begin{matrix}1,1\\3/2\end{matrix}\middle|\, z\right) - 2\, {}_2F_1\left(\begin{matrix}1,1\\3/2\end{matrix}\middle|\, z\right)$$

$$= -\frac{1}{\sqrt{z(1-z)}}\left\{\ln(4z)\arcsin\sqrt{z} + \mathrm{Cl}_2\left(2\arcsin\sqrt{z}\right)\right\}, \tag{5.2.27}$$

where Cl_2 is Clausen's integral function (see, e.g., [9]),

$$\mathrm{Cl}_2(\theta) = -\int_0^\theta d\theta\, \ln\left|2\sin\frac{\theta}{2}\right|. \tag{5.2.28}$$

As a result, we get

$$\Phi(z) = 4\sqrt{\frac{z}{1-z}}\,\mathrm{Cl}_2\left(2\arcsin\sqrt{z}\right). \tag{5.2.29}$$

It should be noted that an analogous representation (in terms of Lobachevsky's function) has been obtained in ref. [10].

In particular, if $M = m$ $(z = 1/4)$ we have

$$I(1,1,1;m,m,m) = \pi^{4-2\varepsilon}(m^2)^{1-2\varepsilon}A(\varepsilon)\left\{-\frac{3}{2\varepsilon^2} + \frac{27}{2}S_2\right\} \tag{5.2.30}$$

with (we follow the notation of ref. [11])

$$S_2 = \frac{4}{9\sqrt{3}}\mathrm{Cl}_2\left(\frac{\pi}{3}\right) = 0.2604341\ldots, \tag{5.2.31}$$

where $\mathrm{Cl}_2(\pi/3) = 1.0149417\ldots$ corresponds to the maximum of Clausen's integral [9] and cannot be represented in terms of other known transcendental constants. This constant has appeared before in two-loop massive calculations (see, e.g., [12, 11, 10]). Note that in ref. [13] results for the integrals (5.2.12) have been obtained in the form of hypergeometric series which follow from (5.2.19) if we take $M = m$ $(z = 1/4)$. After extraction of singularities in ε, these expressions are numerical series. A numerical comparison shows that they coincide with the results expressed in terms of (5.2.31).

To obtain an expression for $\Phi(z)$ in the region $z > 1$, we go back to the hypergeometric representation (5.2.22) and use the following analytic continuation formulae

from z to $(1-z)$ (see, e.g., [8]):

$$ {}_2F_1\left(\begin{array}{c}1,1\\3/2\end{array}\middle|1-z\right)=\frac{\pi}{2}\frac{1}{\sqrt{z(1-z)}}-{}_2F_1\left(\begin{array}{c}1,1\\3/2\end{array}\middle|z\right), \tag{5.2.32}$$

$$\partial_a\,{}_2F_1\left(\begin{array}{c}1,1\\3/2\end{array}\middle|1-z\right)=-\frac{\pi}{2}\frac{\ln(4z)}{\sqrt{z(1-z)}}$$

$$+2\,{}_2F_1\left(\begin{array}{c}1,1\\3/2\end{array}\middle|z\right)-\partial_a\,{}_2F_1\left(\begin{array}{c}1,1\\3/2\end{array}\middle|z\right)-\partial_c\,{}_2F_1\left(\begin{array}{c}1,1\\3/2\end{array}\middle|z\right). \tag{5.2.33}$$

Formula (5.2.33) can be obtained by differentiation of the usual analytic continuation formula for ${}_2F_1$ with respect to the parameter a. Using these formulae we get

$$\Phi(z)=4z\left[\ln(4z)\,{}_2F_1\left(\begin{array}{c}1,1\\3/2\end{array}\middle|1-z\right)+\partial_a\,{}_2F_1\left(\begin{array}{c}1,1\\3/2\end{array}\middle|1-z\right)\right]. \tag{5.2.34}$$

This formula gives us the expansion near $z=1$.

The region $z>1$ corresponds to negative values of the arguments of the hypergeometric functions in (5.2.34). In this case the function (5.2.32) can be represented in terms of logarithms while the function (5.2.33) contains a dilogarithm (Spence function) [9], defined by

$$\mathrm{Li}_2(\xi)=-\int_0^1 dt\frac{\ln(1-\xi t)}{t}. \tag{5.2.35}$$

Finally, we obtain from (5.2.34)

$$\Phi(z)=\frac{1}{\lambda}\left[-4\,\mathrm{Li}_2\left(\frac{1-\lambda}{2}\right)+2\ln^2\left(\frac{1-\lambda}{2}\right)-\ln^2(4z)+\frac{\pi^2}{3}\right], \tag{5.2.36}$$

where

$$\lambda(z)=\sqrt{1-\frac{1}{z}}. \tag{5.2.37}$$

So, we have representations of $I(1,1,1;m,m,M)$ for all values of the masses.

5.2.3 Vacuum integrals with three different masses

Let us now consider the general case of (5.2.12) when all three masses m_1, m_2 and m_3 are different. This time, we use the Mellin-Barnes representation (5.2.16) for the first and second denominators. Substituting eq. (5B.3) yields

$$I(\nu_1,\nu_2,\nu_3;m_1,m_2,m_3)=-\pi^n(-1)^{\nu_1+\nu_2+\nu_3}(m_3^2)^{n-\nu_1-\nu_2-\nu_3}\frac{1}{\Gamma(\nu_1)\Gamma(\nu_2)\Gamma(\nu_3)\Gamma(n/2)}$$

$$\times\frac{1}{(2\pi i)^2}\int_{-i\infty}^{i\infty}\int_{-i\infty}^{i\infty}ds\,dt\,x^s\,y^t\Gamma(-s)\Gamma(-t)\Gamma(n/2-\nu_1-s)\Gamma(n/2-\nu_2-t)$$

$$\times\Gamma(\nu_1+\nu_2-n/2+s+t)\Gamma(\nu_1+\nu_2+\nu_3-n+s+t), \tag{5.2.38}$$

where the two dimensionless variables

$$x \equiv \frac{m_1^2}{m_3^2} \quad \text{and} \quad y \equiv \frac{m_2^2}{m_3^2} \tag{5.2.39}$$

are used. Closing the contours to the right we get (for arbitrary ν_1, ν_2, ν_3 and n)

$$\begin{aligned}
I(\nu_1,\nu_2,\nu_3;m_1,m_2,m_3) &= -\pi^n(-1)^{\nu_1+\nu_2+\nu_3}(m_3^2)^{n-\nu_1-\nu_2-\nu_3}\frac{1}{\Gamma(\nu_1)\Gamma(\nu_2)\Gamma(\nu_3)\Gamma(n/2)} \\
&\times\Big\{\Gamma(n/2-\nu_1)\Gamma(n/2-\nu_2)\Gamma(\nu_1+\nu_2-n/2)\Gamma(\nu_1+\nu_2+\nu_3-n) \\
&\quad\times F_4(\nu_1+\nu_2+\nu_3-n,\ \nu_1+\nu_2-n/2;\ \nu_1-n/2+1,\ \nu_2-n/2+1\,|\,x,\ y) \\
&\quad+y^{n/2-\nu_2}\Gamma(n/2-\nu_1)\Gamma(\nu_2-n/2)\Gamma(\nu_1)\Gamma(\nu_1+\nu_3-n/2) \\
&\quad\times F_4(\nu_1,\ \nu_1+\nu_3-n/2;\ \nu_1-n/2+1,\ n/2-\nu_2+1\,|\,x,\ y) \\
&\quad+x^{n/2-\nu_1}\Gamma(\nu_1-n/2)\Gamma(n/2-\nu_2)\Gamma(\nu_2)\Gamma(\nu_2+\nu_3-n/2) \\
&\quad\times F_4(\nu_2,\ \nu_2+\nu_3-n/2;\ n/2-\nu_1+1,\ \nu_2-n/2+1\,|\,x,\ y) \\
&\quad+x^{n/2-\nu_1}\,y^{n/2-\nu_2}\Gamma(\nu_1-n/2)\Gamma(\nu_2-n/2)\Gamma(\nu_3)\Gamma(n/2) \\
&\quad\times F_4(\nu_3,\ n/2;\ n/2-\nu_1+1,\ n/2-\nu_2+1\,|\,x,\ y)\Big\}\ ,
\end{aligned} \tag{5.2.40}$$

where

$$F_4(a,b;c,d|x,y) = \sum_{j=0}^{\infty}\sum_{l=0}^{\infty}\frac{x^j\,y^l}{j!\,l!}\,\frac{(a)_{j+l}\,(b)_{j+l}}{(c)_j\,(d)_l} \tag{5.2.41}$$

is Appell's hypergeometric function of two variables (see, e.g., [7]) and $(a)_j$ is defined by (5.2.9). Formula (5.2.40) gives us the expansion in x and y for the case $\sqrt{x}+\sqrt{y} \le 1$ (this corresponds to the region of convergence of the F_4 functions).

For the important special case $\nu_1 = \nu_2 = \nu_3 = 1$ ($n \equiv 4-2\varepsilon$), we can use known reduction formulae for F_4-functions (see, e.g., [14, p.102] or [15, p.453]). As a result, we find

$$\begin{aligned}
I(1,1,1;m_1,m_2,m_3) &= \pi^{4-2\varepsilon}(m_3^2)^{1-2\varepsilon}\frac{1}{\Gamma(2-\varepsilon)} \\
&\times\left\{\Gamma^2(1-\varepsilon)\Gamma(\varepsilon)\Gamma(-1+2\varepsilon)\left(\frac{1-wz}{(1-w)(1-z)}\right)^{1-2\varepsilon}\right. \\
&\quad+\Gamma(1-\varepsilon)\Gamma(-1+\varepsilon)\Gamma(\varepsilon)\left(\frac{-z}{(1-w)(1-z)}\right)^{1-\varepsilon} \\
&\quad\times(1-w)\,{}_2F_1\left(\begin{matrix}\varepsilon,\ 1\\ 2-\varepsilon\end{matrix}\,\middle|\,-\frac{z(1-w)}{1-z}\right)
\end{aligned}$$

$$+\Gamma(1-\varepsilon)\Gamma(-1+\varepsilon)\Gamma(\varepsilon)\left(\frac{-w}{(1-w)(1-z)}\right)^{1-\varepsilon}$$

$$\times(1-z)\,{}_2F_1\left(\begin{array}{c}\varepsilon,\ 1\\ 2-\varepsilon\end{array}\middle|-\frac{w(1-z)}{1-w}\right)$$

$$+\Gamma(2-\varepsilon)\Gamma^2(-1+\varepsilon)\left(\frac{-z}{(1-w)(1-z)}\right)^{1-\varepsilon}\left(\frac{-w}{(1-w)(1-z)}\right)^{1-\varepsilon}$$

$$\times(1-w)\,(1-z)\,{}_2F_1\left(\begin{array}{c}\varepsilon,\ 1\\ 2-\varepsilon\end{array}\middle|wz\right)\Bigg\}, \tag{5.2.42}$$

where

$$w=\frac{1}{2y}\left(-1+x+y+\lambda\right)\ ,\ z=\frac{1}{2x}\left(-1+x+y+\lambda\right)\ , \tag{5.2.43}$$

with

$$\lambda(x,y)\equiv\sqrt{(1-x-y)^2-4xy}\ . \tag{5.2.44}$$

This formula can be connected with the result obtained in [18] by using analytic continuation formulae that express ${}_2F_1$ functions of ξ in terms of ${}_2F_1$ functions of $1-\xi$. By use of the parametric integral representation for the ${}_2F_1$ function occurring in (5.2.42) it is easy to obtain the following expansion as $\varepsilon\to 0$ (keeping terms up to $\mathcal{O}(\varepsilon^2)$ only):

$${}_2F_1\left(\begin{array}{c}\varepsilon,\ 1\\ 2-\varepsilon\end{array}\middle|\xi\right)\simeq\frac{1-\varepsilon}{1-2\varepsilon}\left\{1+\frac{1-\xi}{\xi}\left(\varepsilon\ln(1-\xi)-\varepsilon^2\left(\ln^2(1-\xi)+\mathrm{Li}_2(\xi)\right)\right)\right\}. \tag{5.2.45}$$

Using this expansion and some well-known relations for dilogarithms [9] we get the following result for the integral with $\nu_1=\nu_2=\nu_3=1$ (as $n\to 4$):

$$I(1,1,1;m_1,m_2,m_3)=\pi^{4-2\varepsilon}(m_3^2)^{1-2\varepsilon}\frac{A(\varepsilon)}{2}$$

$$\times\left\{-\frac{1}{\varepsilon^2}(1+x+y)+\frac{2}{\varepsilon}(x\ln x+y\ln y)\right.$$

$$\left.-x\ln^2 x-y\ln^2 y+(1-x-y)\ln x\ln y-\lambda^2\Phi(x,y)\right\}\ , \tag{5.2.46}$$

where

$$\Phi(x,y)\ =\ \frac{1}{\lambda}\left\{2\ln\left(\frac{1+x-y-\lambda}{2}\right)\ln\left(\frac{1-x+y-\lambda}{2}\right)-\ln x\ln y\right.$$

$$\left.-2\,\mathrm{Li}_2\left(\frac{1+x-y-\lambda}{2}\right)-2\,\mathrm{Li}_2\left(\frac{1-x+y-\lambda}{2}\right)+\frac{\pi^2}{3}\right\} \tag{5.2.47}$$

The functions $\lambda(x,y)$ and $\Phi(x,y)$ coincide with $\lambda(z)$ (5.2.37) and $\Phi(z)$ (5.2.36) when $x=y=1/(4z)$.

Note that these results were obtained in the region $\lambda^2 \geq 0$ and $\sqrt{x} + \sqrt{y} \leq 1$. By permutation of m_1, m_2, m_3 we can also obtain results for the region $\sqrt{x} - \sqrt{y} \geq 1$ and the region $\sqrt{y} - \sqrt{x} \geq 1$.

It is interesting to note that the function $\Phi(x,y)$ (5.2.47) is the same as in the case of the massless triangle diagram (see, e.g., [17]) where x and y are constructed from external momenta squared instead of masses. So, all results for $\Phi(x,y)$ obtained here are also applicable to that case.

The analytic continuation to the region $\lambda^2 < 0$ can be done by use of the quadratic transformation,

$$ {}_2F_1\left(\begin{matrix} a,\ b \\ a-b+1 \end{matrix} \middle| \xi \right) = (1-\xi)^{-a}\ {}_2F_1\left(\begin{matrix} a/2,\ (a+1)/2-b \\ a-b+1 \end{matrix} \middle| -\frac{4\xi}{(1-\xi)^2} \right), \quad (5.2.48) $$

which we apply to the ${}_2F_1$ functions occurring in (5.2.42). Then the transition to inverse arguments yields

$$ \begin{aligned} I(1,1,1;m_1,m_2,m_3) &= \pi^{4-2\varepsilon}(m_3^2)^{1-2\varepsilon}A(\varepsilon) \\ &\times \frac{1}{2\varepsilon^2}\left\{ x^{-\varepsilon}y^{-\varepsilon}(1-x-y)\ {}_2F_1\left(\begin{matrix} \varepsilon,\ 1 \\ 1/2+\varepsilon \end{matrix} \middle| -\frac{\lambda^2}{4xy} \right) \right. \\ &-x^{-\varepsilon}(1+x-y)\ {}_2F_1\left(\begin{matrix} \varepsilon,\ 1 \\ 1/2+\varepsilon \end{matrix} \middle| -\frac{\lambda^2}{4x} \right) \\ &\left. -y^{-\varepsilon}(1-x+y)\ {}_2F_1\left(\begin{matrix} \varepsilon,\ 1 \\ 1/2+\varepsilon \end{matrix} \middle| -\frac{\lambda^2}{4y} \right) \right\}. \end{aligned} \quad (5.2.49) $$

This formula can be used to examine the behaviour of $I(1,1,1;m_1,m_2,m_3)$ near $\lambda^2 = 0$. It is valid for arbitrary n because we did not expand in ε. Using the definition of x and y (5.2.39) we see that it is completely symmetric in m_1, m_2, m_3. However, it is only valid outside the region bounded by the lines $1-x-y=0$ $(0<x<1)$, $1+x-y=0$ $(x>0)$ and $1-x+y=0$ $(x>1)$, where the arguments of the corresponding ${}_2F_1$ functions are equal to one. A careful examination of the ${}_2F_1$ functions near these lines shows that if we write an additional term in the braces in (5.2.49),

$$ \left\{ \ldots \right\} \to \left\{ \ldots + 2\pi\varepsilon\frac{\Gamma(1+2\varepsilon)}{\Gamma^2(1+\varepsilon)}(-\lambda^2)^{1/2-\varepsilon}\theta(x+y-1)\theta(1-x+y)\theta(1+x-y) \right\}, \quad (5.2.50) $$

we obtain an expression which is valid for all positive values of x and y. If we consider $\varepsilon \to 0$ the following expansion up to ε^2 terms can be derived:

$$ \begin{aligned} &{}_2F_1\left(\begin{matrix} \varepsilon,\ 1 \\ 1/2+\varepsilon \end{matrix} \middle| \eta \right) \simeq 1 + 2\varepsilon\eta\ {}_2F_1\left(\begin{matrix} 1,\ 1 \\ 3/2 \end{matrix} \middle| \eta \right) \\ &+2\varepsilon^2\eta\left\{ -2\ {}_2F_1\left(\begin{matrix} 1,\ 1 \\ 3/2 \end{matrix} \middle| \eta \right) + \partial_a\ {}_2F_1\left(\begin{matrix} 1,\ 1 \\ 3/2 \end{matrix} \middle| \eta \right) + \partial_c\ {}_2F_1\left(\begin{matrix} 1,\ 1 \\ 3/2 \end{matrix} \middle| \eta \right) \right\} \end{aligned} \quad (5.2.51) $$

Here we obtained the same functions as in equation (5.2.22) for the case of two different masses.

In this case, in the representations (5.2.26) and (5.2.27) it is more convenient to use arccos rather than arcsin in the arguments of Clausen's function. So, we get the following representation for the function $\Phi(x,y)$ in the region $\lambda^2 \leq 0$ ($\sqrt{x}+\sqrt{y} \geq 1$):

$$\Phi(x,y) = \frac{2}{\sqrt{-\lambda^2}}\left\{\mathrm{Cl}_2\left(2\arccos\left(\frac{-1+x+y}{2\sqrt{xy}}\right)\right) + \mathrm{Cl}_2\left(2\arccos\left(\frac{1+x-y}{2\sqrt{x}}\right)\right)\right.$$
$$\left. + \mathrm{Cl}_2\left(2\arccos\left(\frac{1-x+y}{2\sqrt{y}}\right)\right)\right\}. \tag{5.2.52}$$

Note that the result (5.2.46), (5.2.52) is also completely symmetric. This expression can be used inside the parabola which continues the curve $\sqrt{x}+\sqrt{y}=1$. The analogous representation was obtained in ref. [18] in terms of Lobachevsky's function.

5.2.4 Recurrence relations for two-loop vacuum integrals

When we calculate the coefficients of the expansion (5.2.10) we also need vacuum integrals (5.2.12) with higher powers of denominators. Instead of working out eqs. (5.2.19) and (5.2.40), we will construct a recursive procedure for evaluating $I(\nu_1,\nu_2,\nu_3)$ with integer ν's (in this section we omit the arguments m_1, m_2, m_3) by applying the integration-by-parts technique [19]. Our procedure is analogous to the method used in ref. [17] to calculate massless triangle diagrams.

Starting from

$$0 = \int\int \mathrm{d}^n p\, \mathrm{d}^n q \frac{\partial}{\partial p_\mu}\left\{\frac{p_\mu}{(p^2-m_1^2)^{\nu_1}(q^2-m_2^2)^{\nu_2}((p+q)^2-m_3^2)^{\nu_3}}\right\}, \tag{5.2.53}$$

and writing the right hand side in terms of $I(\nu_1,\nu_2,\nu_3)$, we find

$$\begin{aligned} 0 &= -2m_1^2\nu_1 I(\nu_1+1,\nu_2,\nu_3) - (m_1^2-m_2^2+m_3^2)\nu_3 I(\nu_1,\nu_2,\nu_3+1) \\ &\quad +(n-2\nu_1-\nu_3)I(\nu_1,\nu_2,\nu_3) \\ &\quad +\nu_3\left[I(\nu_1,\nu_2-1,\nu_3+1) - I(\nu_1-1,\nu_2,\nu_3+1)\right]. \end{aligned} \tag{5.2.54}$$

By interchanging p, q, and $p+q$ in eq. (5.2.53), we obtain two further identities, similar to (5.2.54). Together they form a system of equations for $I(\nu_1+1,\nu_2,\nu_3)$, $I(\nu_1,\nu_2+1,\nu_3)$ and $I(\nu_1,\nu_2,\nu_3+1)$, whose determinant is proportional to

$$\begin{aligned} \Delta(m_1^2,m_2^2,m_3^2) &= 2(m_1^2m_2^2+m_1^2m_3^2+m_2^2m_3^2) - (m_1^4+m_2^4+m_3^4) \\ &= -m_3^4\lambda^2(x,y), \end{aligned} \tag{5.2.55}$$

where $\lambda(x,y)$ is defined by (5.2.44). Solving these equations yields

$$I(\nu_1+1,\nu_2,\nu_3) = \frac{1}{\nu_1\Delta(m_1^2,m_2^2,m_3^2)}$$

$$\times \quad \Big\{\Big[m_1^2(\nu_1+\nu_2+\nu_3-n)+m_2^2(n-2\nu_1-\nu_3)+m_3^2(n-2\nu_1-\nu_2)\Big]\, I(\nu_1,\nu_2,\nu_3)$$
$$+(m_2^2-m_3^2)\nu_1\,[I(\nu_1+1,\nu_2-1,\nu_3)-I(\nu_1+1,\nu_2,\nu_3-1)]$$
$$+\,m_2^2\nu_2\,[I(\nu_1,\nu_2+1,\nu_3-1)-I(\nu_1-1,\nu_2+1,\nu_3)]$$
$$+m_3^2\nu_3\,[I(\nu_1,\nu_2-1,\nu_3+1)-I(\nu_1-1,\nu_2,\nu_3+1)]\Big\} \tag{5.2.56}$$

and analogous expressions for $I(\nu_1,\nu_2+1,\nu_3)$ and $I(\nu_1,\nu_2,\nu_3+1)$. These results make it possible to evaluate integrals with $\nu_1+\nu_2+\nu_3=\sigma+1$ in terms of integrals with $\nu_1+\nu_2+\nu_3=\sigma$. It can also be noted that there is an additional condition for integrals with the same sum $\nu_1+\nu_2+\nu_3$, which can be used to reduce the number of terms on the r.h.s. of (5.2.56),

$$\Big[\nu_1(m_2^2-m_3^2)+\nu_2(m_3^2-m_1^2)+\nu_3(m_1^2-m_2^2)\Big]\, I(\nu_1,\nu_2,\nu_3)$$
$$=\nu_1 m_1^2\,[I(\nu_1+1,\nu_2-1,\nu_3)-I(\nu_1+1,\nu_2,\nu_3-1)]$$
$$+\nu_2 m_2^2\,[I(\nu_1,\nu_2+1,\nu_3-1)-I(\nu_1-1,\nu_2+1,\nu_3)]$$
$$+\nu_3 m_3^2\,[I(\nu_1-1,\nu_2,\nu_3+1)-I(\nu_1,\nu_2-1,\nu_3+1)]\,. \tag{5.2.57}$$

Using eq. (5.2.56) (and permutations), all integrals $I(\nu_1,\nu_2,\nu_3)$ with positive integer ν's can be reduced to $I(1,1,1)$ and trivial boundary integrals (5.2.13) (when one of ν's is equal to zero).

The recurrence relations can easily be programmed, which we did using the REDUCE system [20]. As an example, it is easy to check that, after some transformations, the result for $I(2,1,1)$ obtained by applying relation (5.2.56) with $\nu_1=\nu_2=\nu_3=1$ coincides with the results presented in refs. [12, 21] in terms of dilogarithms.

In the case $m_1=m_2\equiv m,\ \ m_3\equiv M\ \ (z\equiv M^2/(4m^2))$ we get (at $\varepsilon=0$)

$$I(2,2,1)=\frac{\pi^4}{2m^2}\frac{1}{(1-z)}\left\{(1-2z)\frac{\mathrm{Cl}_2\,(2\arcsin\sqrt{z})}{\sqrt{z(1-z)}}+\ln(4z)\right\},\quad z\le 1, \tag{5.2.58}$$

and for $z\ge 1$:

$$I(2,2,1)=\frac{\pi^4}{2m^2}\frac{1}{(1-z)}\Big\{\ln(4z)$$
$$+\frac{2z-1}{\lambda z}\left[\mathrm{Li}_2\left(\frac{1-\lambda}{2}\right)-\frac{1}{2}\ln^2\left(\frac{1-\lambda}{2}\right)+\frac{1}{4}\ln^2(4z)-\frac{\pi^2}{12}\right]\Big\}\,. \tag{5.2.59}$$

These results give the first term of expansion (5.2.10) for the integral corresponding to the diagram in Fig. 5.1 with $m_1=m_2=m_4=m_5=m,\ m_3=M$. Note that expressions (5.2.58) and (5.2.59) coincide at $z=1$ and yield

$$I(2,2,1)=\frac{\pi^4}{3m^2}(4\ln 2-1),\qquad z=1\qquad (M=2m)\,. \tag{5.2.60}$$

5.2.5 Numerical results

In this section we shall demonstrate our method by considering the integral

$$J(m_1, m_2, m_3, m_4, m_5; k) \equiv J(1,1,1,1,1; m_1, m_2, m_3, m_4, m_5; k). \tag{5.2.61}$$

It is finite and it can be calculated for arbitrary masses by a method described in ref. [22], which involves a two-dimensional numerical integration. We shall approximate the integral (5.2.61) by taking the first few terms of its momentum expansion, and then compare the results with the values we obtain by using the numerical method.

In our first example we take $m_1 = m_2 = m_4 = m_5 = m$ and $m_3 = M$ and write the momentum expansion as:

$$J(m, m, M, m, m; k) = \frac{\pi^4}{m^2} \sum_{j=0}^{\infty} c_j(z) \left(\frac{k^2}{4m^2} \right)^j \tag{5.2.62}$$

with $z = M^2/(4m^2)$. By performing the procedure described in the previous sections we obtain expressions for the coefficients $c_j(z)$ that contain $\ln z$ and $\Phi(z)$. In the denominator they contain powers of z and $(1-z)$, which are introduced when the recurrence relation (5.2.56) is used. To avoid numerical instabilities, we derive expansions of our expressions in z and in $(z-1)$, which we use when z is close to 0 or 1. These expansions can easily be obtained by using the expressions for Φ in terms of hypergeometric functions (5.2.22) and (5.2.34). Near $z = 1$ the coefficients $c_j(z)$ are analytic. The expansions near $z = 0$ contain powers of z, and in addition terms of the form $z^l \ln z$. As can be seen from Fig. 5.4 for the case of $c_0(z)$, the expansions can give good approximations to the exact coefficients in a wide range of z values.

The first six coefficients $c_j(z)$ are plotted in Fig. 5.5. Their exact values are listed in Table 5.1 for three special values of z. For $z = 0$ they coincide with the results given in ref. [11].

Fig. 5.6 shows the first terms of the momentum expansion (5.2.62), and also the value of J obtained by numerical integration, in the region below the threshold at $k^2 = 4m^2$ (the right edge of the plot). In this example we chose $M = M_Z$ and $m = m_t$, the masses of the Z boson and the top quark. For the latter we picked a value which is in the middle of the allowed range of masses. This combination of masses occurs in two-loop corrections to the Z and photon propagators in the standard model. In this particular case only three terms are needed to obtain an accuracy of 1% when $k^2/m_t^2 = 1$. To obtain 1% accuracy when $k^2/m_t^2 = 2$, five terms are needed. When $k^2/m_t^2 = 3$, the sum of the first six terms differs about 5% from the numerical value. These numbers depend on z, but the picture for other values of z is very similar. Notice that if $k^2 \approx M_Z^2$, $k^2/m_t^2 \approx 0.42$, which is still in the region where the momentum expansion approximation works well.

An example involving three different masses is shown in Fig. 5.7, where $m_1 = m_4 = m_t$, $m_2 = m_5 = M_W$ (the W boson mass) and $m_3 = m_b$ (the b quark mass). In this case the first threshold is at $k^2 = 4M_W^2$. If we choose $k^2 \approx M_Z^2$, $k^2/M_W^2 \approx 1.3$,

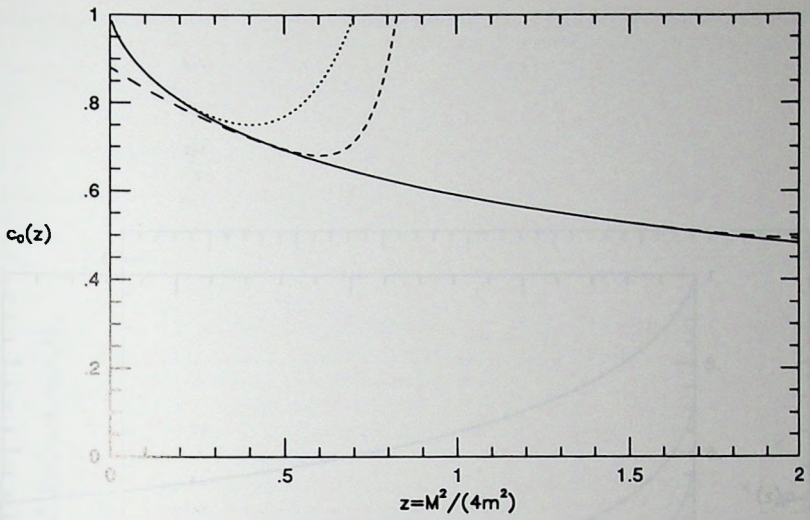

Fig. 5.4. The coefficient $c_0(z)$. The solid curve shows the exact value, the curve with long dashes is the expansion near $z = 1$ including terms up to $\mathcal{O}\left((z-1)^4\right)$, the dotted curve is the expansion near $z = 0$ including terms up to $\mathcal{O}\left(z^4 \ln z\right)$, and the curve with short dashes is the expansion near $z = 0$ including terms up to $\mathcal{O}\left(z^{10} \ln z\right)$.

	$z=0$	$z=\frac{1}{4}\ (M=m)$	$z=1\ (M=2m)$
$c_0(z)$	1	$3S_2$	$\frac{4\ln 2-1}{3}$
$c_1(z)$	$\frac{13}{18}$	$\frac{2(4+9S_2)}{27}$	$\frac{32\ln 2-1}{70}$
$c_2(z)$	$\frac{388}{675}$	$\frac{4(29-36S_2)}{243}$	$\frac{4(1992\ln 2+83)}{31185}$
$c_3(z)$	$\frac{5309}{11025}$	$\frac{8(367-990S_2)}{3645}$	$\frac{7680\ln 2+529}{45045}$
$c_4(z)$	$\frac{206624}{496125}$	$\frac{16(317179-1063440S_2)}{3444525}$	$\frac{32(1417840\ln 2+113193)}{363738375}$
$c_5(z)$	$\frac{13260704}{36018675}$	$\frac{32(566101-2061360S_2)}{6200145}$	$\frac{1312(73920\ln 2+6221)}{1003917915}$

Table 5.1. The first coefficients c_j for $z = 0$, $z = 1/4$ and $z = 1$. The constant S_2 is defined in (5.2.31).

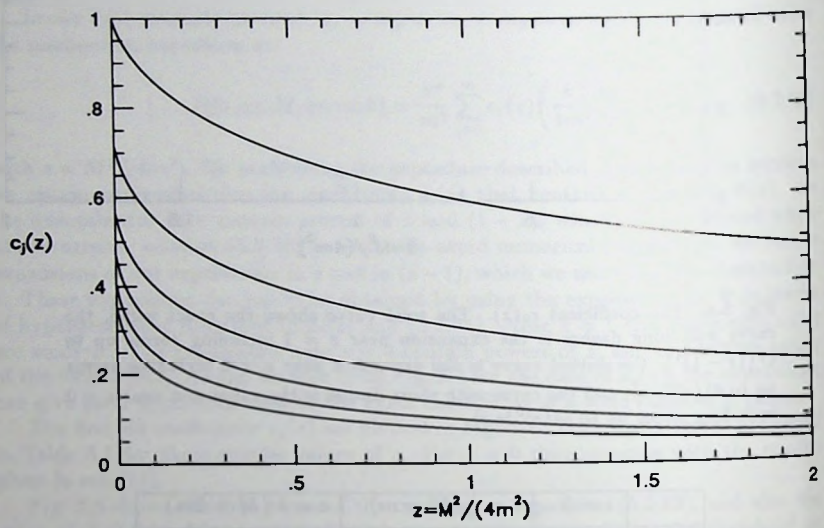

Fig. 5.5. From top to bottom: $c_0(z)$, $c_1(z)$, $c_2(z)$, $c_3(z)$, $c_4(z)$, $c_5(z)$.

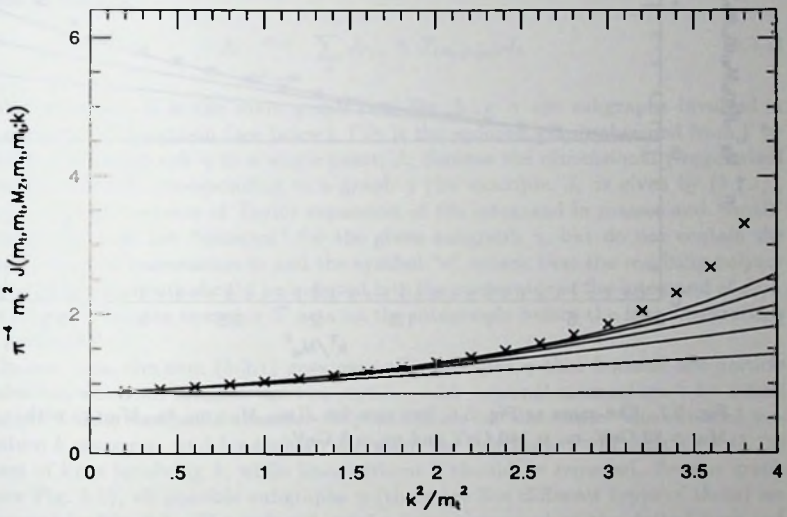

Fig. 5.6. The integral $J(m_t, m_t, M_Z, m_t, m_t; k)$ with $M_Z = 91.16$ GeV and $m_t = 140$ GeV ($z = 0.106$). The crosses are the values obtained by numerical integration. The straight line is the first term of the momentum expansion. The curves show the improvement of the approximation when successive terms of the small k^2 expansion are added.

which is again far below the threshold, so we see that also in this case, the expansion works well.

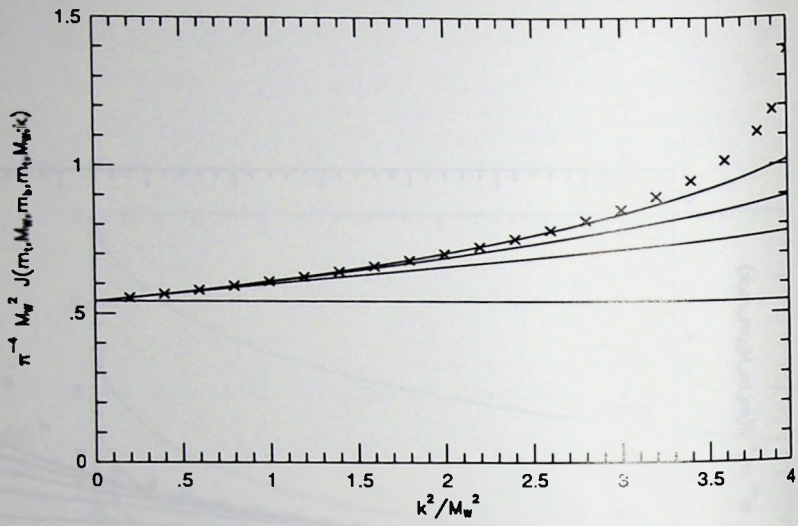

Fig. 5.7. The same as Fig. 5.6, but now for $J(m_t, M_W, m_b, m_t, M_W; k)$ with $M_W = 80$ GeV, $m_t = 140$ GeV and $m_b = 5$ GeV.

5.3 The expansion for large k^2

In this section, we will show how to obtain a series expansion for the integrals (5.1.1) for large external momenta, when k^2 is larger than the highest threshold of the diagram. This expansion is more complicated than the one for small k^2, because it is not a usual Taylor expansion, but also contains logarithms and squared logarithms of $(-k^2)$ (in four dimensions), yielding an imaginary part when the momentum is time-like. The procedure of calculating this diagram in the form of a series in inverse powers of the external momentum (plus logarithms) resembles the standard procedure of analytic continuation of the hypergeometric function (some explicit examples of such a procedure connected with Feynman integrals were presented e.g. in ref. [5]). To obtain this expansion, we shall apply a general mathematical theorem on asymptotic expansions of Feynman integrals in the limit of large momenta. This theorem holds at least in the case when the external momenta are not restricted to a mass shell. However, in our case of a two-point massive diagram, it is valid for any

values of the external momentum. All the coefficients of the expansion have a natural interpretation in terms of Feynman integrals and are analytically calculable in the case we consider. Expansions of this kind were presented in refs. [23, 24, 25, 26] and rigorously proved in ref. [27]. A review is given in ref. [4].

5.3.1 Constructing the asymptotic expansion

When applied to our self-energy diagrams, the asymptotic expansion theorem can be stated as follows:

$$J_\Gamma \underset{k^2\to\infty}{\sim} \sum_\gamma J_{\Gamma/\gamma} \circ \mathcal{T}_{\{m_i\};\{q_i\}} J_\gamma \,. \tag{5.3.1}$$

In this equation, Γ is the main graph (see Fig. 5.1); γ are subgraphs involved in the asymptotic expansion (see below); Γ/γ is the reduced graph obtained from Γ by shrinking the subgraph γ to a single point; J_γ denotes the dimensionally-regularized Feynman integral corresponding to a graph γ (for example, J_Γ is given by (5.1.1)), $\mathcal{T}_{\{m_i\};\{q_i\}}$ is the operator of Taylor expansion of the integrand in masses and "small" momenta q_i, that are "external" for the given subgraph γ, but do not contain the "large" external momentum k; and the symbol "o" means that the resulting polynomial in these momenta should be inserted into the numerator of the integrand of $J_{\Gamma/\gamma}$. It is implied that the operator $\mathcal{T}$ acts on the integrands before the loop integrations are performed.

In our case, the sum (5.3.1) goes over all subgraphs γ that become one-particle irreducible when we connect the two vertices with external momentum k by a line. In other words, we should consider all possibilities to "distribute" the external momentum k among p_i, and for each arrangement the subgraph γ will coincide with the subset of lines involving k, while lines without k should be removed. For our graph Γ (see Fig. 5.1), all possible subgraphs γ (there are five different types of them) are presented in Fig. 5.8. The reduced graphs Γ/γ correspond to the dotted lines and can be obtained by shrinking all solid lines to a point. In such a way, we find that for the second and third type (see Fig. 5.8) $J_{\Gamma/\gamma}$ corresponds to a massive tadpole, for the fourth type we obtain a product of two massive tadpoles, while for the fifth type we get a two-loop massive vacuum integral (with three internal lines).

The Taylor expansion operator $\mathcal{T}$ expands the denominators of the integrand in the following way:

$$\mathcal{T}_m \frac{1}{[p^2-m^2]^\nu} = \frac{1}{[p^2]^\nu} \sum_{j=0}^{\infty} \frac{(\nu)_j}{j!} \left(\frac{m^2}{p^2}\right)^j , \tag{5.3.2}$$

$$\mathcal{T}_{m;q} \frac{1}{[(k-q)^2-m^2]^\nu} = \frac{1}{[k^2]^\nu} \sum_{j=0}^{\infty} \frac{(\nu)_j}{j!} \left(\frac{2(kq)-q^2+m^2}{k^2}\right)^j . \tag{5.3.3}$$

The terms on the right hand side of (5.3.3) should then be sorted according to the total power of m and q. For example, the terms proportional to q^2/k^2 and m^2/k^2

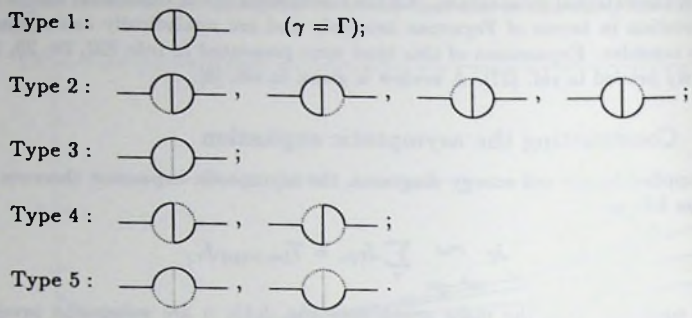

Fig. 5.8. The subgraphs γ (solid lines) contributing to the large k^2 expansion. The dotted lines belong to the reduced graphs Γ/γ.

(from $j = 1$) and the term proportional to $[(kq)/k^2]^2$ (from $j = 2$) should be grouped together. The reason is that when we evaluate the massive vacuum integrals $J_{\Gamma/\gamma}$ with these momenta q in the numerator, the powers of q will be transformed into powers of the masses. If we have several denominators to expand, then we should also collect all terms with the same total power of masses and "small" momenta q_i.

Now we are ready to consider what integrals correspond to different terms of the asymptotic expansion (see Fig. 5.8).

1. In this case, $\gamma = \Gamma$. All denominators of (5.1.1) should be expanded in masses,

$$\mathcal{T}_{\{m_i\}}\, J(\{\nu_i\};\{m_i\};k) = \sum_{j_1,\ldots,j_5=0}^{\infty} \frac{(\nu_1)_{j_1}\ldots(\nu_5)_{j_5}}{j_1!\ldots j_5!}(m_1)^{j_1}\ldots(m_5)^{j_5}\; J(\{\nu_i+j_i\};\{0\};k). \tag{5.3.4}$$

Note that if we consider the case $\nu_1 = \ldots = \nu_5 = 1$, the first term of the expansion (5.3.4) (with $j_1 = \ldots = j_5 = 0$) gives the well-known result: $-6\zeta(3)\pi^4/k^2$. The two-loop massless integrals with higher integer powers of denominators occurring on the r.h.s. of (5.3.4) can be evaluated by use of the integration-by-parts technique [19] (see Appendix A).

2. Let us consider only the first contribution of the second type (see Fig. 5.8), when γ is obtained from Γ by removing line 1. Then we get

$$\int \frac{d^n p}{[p^2-m_1^2]^{\nu_1}}\; \mathcal{T}_{m_2,\ldots,m_5;p} \int \frac{d^n q}{[q^2-m_2^2]^{\nu_2}[(p-q)^2-m_3^2]^{\nu_3}[(k-p)^2-m_4^2]^{\nu_4}[(k-q)^2-m_5^2]^{\nu_5}}. \tag{5.3.5}$$

After expanding the integrand of the q-integral in masses and p, we obtain products of massless one-loop integrals (see Appendix A) and massive tadpoles with numerators that can be calculated by use of eq. (5B.11) (see Appendix B). Other contributions of the second type can be evaluated in the same way.

3. In the case when the central line is removed from γ, we obtain:

$$\int \frac{d^n p}{[p^2-m_3^2]^{\nu_3}} \times \mathcal{T}_{m_1,m_2,m_4,m_5;p} \int \frac{d^n q}{[(k+p-q)^2-m_1^2]^{\nu_1}[(k-q)^2-m_2^2]^{\nu_2}[(p-q)^2-m_4^2]^{\nu_4}[q^2-m_5^2]^{\nu_5}}. \tag{5.3.6}$$

After expansion, we obtain integrals of the same type as in the previous case.

4. There are no loop integrations in the subgraph γ, and we get for the first contribution of the fourth type:

$$\iint \frac{d^n p}{[p^2-m_1^2]^{\nu_1}} \frac{d^n q}{[q^2-m_5^2]^{\nu_5}} \times \mathcal{T}_{m_2,m_3,m_4;p,q} \left(\frac{1}{[(k-q)^2-m_2^2]^{\nu_2}[(k-p-q)^2-m_3^2]^{\nu_3}[(k-p)^2-m_4^2]^{\nu_4}} \right). \tag{5.3.7}$$

As a result, we obtain products of two one-loop tadpoles with numerators (also for the second contribution), which can be evaluated by use of eq. (5B.12) (see Appendix B).

5. In this case we obtain a non-trivial two-loop vacuum integral. For example, the first contribution of the fifth type gives:

$$\iint \frac{d^n p\, d^n q}{[p^2-m_1^2]^{\nu_1}[q^2-m_2^2]^{\nu_2}[(p-q)^2-m_3^2]^{\nu_3}} \times \mathcal{T}_{m_4,m_5;p,q} \left(\frac{1}{[(k-p)^2-m_4^2]^{\nu_4}[(k-q)^2-m_5^2]^{\nu_5}} \right). \tag{5.3.8}$$

Expanding the denominators, we obtain two-loop vacuum integrals with numerators, that can be evaluated by use of eq. (5B.13) presented in Appendix B (the same for the second contribution of the fifth type). Note, that here we obtain the same two-loop vacuum integrals as those involved in the small-k^2 expansion. In particular, for unit powers of denominators the dependence on masses can be expressed in terms of dilogarithms (see (5B.5)–(5B.10)).

So, the total asymptotic expansion is the sum of all terms presented, and we see that all integrals corresponding to the coefficients of the expansion can be evaluated.

5.3.2 Analytical results

In principle, eqs. (5.3.4)–(5.3.8) presented in the previous section (together with the formulae of Appendices A and B) enable one to construct analytical expressions for the coefficients of the large-k^2 expansion. However, in the general case of unequal masses the higher-order coefficients become rather cumbersome. To calculate these coefficients, we used the REDUCE system [20]. The algorithm constructed is applicable to integrals with arbitrary values of masses, space-time dimension and (integer)

powers of denominators. If we are interested in the result near $n = 4$, we perform an expansion in $\varepsilon = (4-n)/2$ to get the divergent and finite parts of the coefficients.

One of the most important examples is the "master" two-loop diagram (presented in Fig. 5.1) in the case $\nu_1 = \ldots = \nu_5 = 1$. In this case, the result should be finite as $n \to 4$ (and it is a non-trivial check of the algorithm that all the divergent contributions from separate terms of (5.3.4)–(5.3.8) cancel in this sum !). A rigorous proof of the finiteness of the expansion was given in [26] (it was based on the so-called R^*-operation [28]).

Let us define

$$\begin{aligned} J(1,\ldots,1;m_1,\ldots,m_5;k)|_{n=4} &\equiv J(m_1,\ldots,m_5;k) \\ &\equiv -\frac{\pi^4}{k^2}\mathcal{M}(m_1,\ldots,m_5;k) \equiv -\frac{\pi^4}{k^2}\sum_{j=0}^{\infty}\frac{\mathcal{M}_j}{(k^2)^j}, \end{aligned} \tag{5.3.9}$$

where the coefficient functions $\mathcal{M}_j$ include the powers of masses and the logarithms of masses and momentum squared. It is easy to see that the only integral contributing to $\mathcal{M}_0$ is $J^{(0)}(1,1,1,1,1)$ in (5.3.4) (see eq. (5A.7) in Appendix A). So we get the obvious result that the expansion starts from

$$\mathcal{M}_0 = 6\zeta(3). \tag{5.3.10}$$

The $\mathcal{M}_1$ term already includes contributions of all terms (5.3.4)–(5.3.8) (with the exception of (5.3.7) that begins to contribute starting from $\mathcal{M}_2$); this yields

$$\begin{aligned} \mathcal{M}_1 = & \frac{m_1^2}{2}\left\{\ln^2\left(-\frac{k^2}{m_1^2}\right) + 4\ln\left(-\frac{k^2}{m_1^2}\right) - \ln\frac{m_2^2}{m_1^2}\ln\frac{m_3^2}{m_1^2} + 6\right\} \\ & + \left\{\text{analogous terms with } m_2^2,\ m_4^2,\ m_5^2\right\} \\ & + \frac{m_3^2}{2}\left\{2\ln^2\left(-\frac{k^2}{m_3^2}\right) + 4\ln\left(-\frac{k^2}{m_3^2}\right) - \ln\frac{m_1^2}{m_3^2}\ln\frac{m_2^2}{m_3^2} - \ln\frac{m_4^2}{m_3^2}\ln\frac{m_5^2}{m_3^2}\right\} \\ & + \frac{1}{2}\left\{F(m_1^2,m_2^2,m_3^2) + F(m_4^2,m_5^2,m_3^2)\right\}, \end{aligned} \tag{5.3.11}$$

where the symmetric function F is defined by (5B.7)–(5B.10) (note that F has the dimension of mass squared). We see that $\mathcal{M}_1$ contains also $\ln(-k^2)$ and $\ln^2(-k^2)$ terms, which means that our expansion (at $n = 4$) is not a usual Taylor expansion. In fact, the highest power of $\ln(-k^2)$ is connected with the highest order of pole in ε (double pole) that can occur in the two-loop integrals involved. Note that for positive k^2 the sign of the imaginary part produced by these logarithms is defined by the "causal" $i0$-prescription,

$$\ln(-k^2 - i0) = \ln(k^2) - i\pi \qquad (k^2 > 0). \tag{5.3.12}$$

Let us also present the result for the next term of the expansion,

$$
\begin{aligned}
\mathcal{M}_2 \;=\; & \frac{m_1^4}{8}\left\{2\ln^2\left(-\frac{k^2}{m_1^2}\right)+4\ln\left(-\frac{k^2}{m_1^2}\right)-2\ln\frac{m_2^2}{m_1^2}\ln\frac{m_3^2}{m_1^2}+7\right\} \\
& \qquad +\left\{\text{analogous terms with } m_2^4,\ m_4^4,\ m_5^4\right\} \\
+\; & \frac{m_3^4}{4}\left\{-2\ln^2\left(-\frac{k^2}{m_3^2}\right)-2\ln\left(-\frac{k^2}{m_3^2}\right)+\ln\frac{m_1^2}{m_3^2}\ln\frac{m_2^2}{m_3^2}+\ln\frac{m_4^2}{m_3^2}\ln\frac{m_5^2}{m_3^2}+6\right\} \\
-\; & \frac{1}{2}(m_1^2m_2^2+m_4^2m_5^2) \\
+\; & \frac{m_1^2m_4^2}{2}\left\{\ln^2\left(-\frac{k^2}{m_1^2}\right)+\ln^2\left(-\frac{k^2}{m_4^2}\right)+4\ln\left(-\frac{k^2}{m_1^2}\right)+4\ln\left(-\frac{k^2}{m_4^2}\right)\right. \\
& \qquad \left.-\ln\frac{m_2^2}{m_1^2}\ln\frac{m_3^2}{m_1^2}-\ln\frac{m_3^2}{m_4^2}\ln\frac{m_5^2}{m_4^2}+8\right\} \\
& \qquad +\left\{\text{analogous term with } m_2^2m_5^2\right\} \\
+\; & \frac{m_1^2m_5^2}{2}\left\{2\ln^2\left(-\frac{k^2}{m_1^2}\right)+2\ln^2\left(-\frac{k^2}{m_5^2}\right)+2\ln\left(-\frac{k^2}{m_1^2}\right)+2\ln\left(-\frac{k^2}{m_5^2}\right)\right. \\
& \qquad \left.-\ln\frac{m_2^2}{m_1^2}\ln\frac{m_3^2}{m_1^2}-\ln\frac{m_3^2}{m_5^2}\ln\frac{m_4^2}{m_5^2}-\ln^2\frac{m_1^2}{m_5^2}+2\right\} \\
& \qquad +\left\{\text{analogous term with } m_2^2m_4^2\right\} \\
+\; & \frac{m_1^2m_3^2}{2}\left\{2\ln^2\left(-\frac{k^2}{m_3^2}\right)-2\ln\left(-\frac{k^2}{m_1^2}\right)-\ln\frac{m_1^2}{m_3^2}\ln\frac{m_2^2}{m_3^2}-\ln\frac{m_4^2}{m_3^2}\ln\frac{m_5^2}{m_3^2}-8\right\} \\
& \qquad +\left\{\text{analogous terms with } m_2^2m_3^2,\, m_4^2m_3^2,\, m_5^2m_3^2\right\} \\
+\; & \frac{1}{4}\left\{\left(m_1^2+m_2^2-m_3^2+2m_4^2+2m_5^2\right)\ F(m_1^2,m_2^2,m_3^2)\right. \\
& \qquad \left.+\left(2m_1^2+2m_2^2-m_3^2+m_4^2+m_5^2\right)\ F(m_4^2,m_5^2,m_3^2)\right\}. \qquad (5.3.13)
\end{aligned}
$$

Higher contributions are more cumbersome, and we do not present them here (but we are going to use them below, when comparing our expansion with the results of numerical integration). By use of the REDUCE system [20], for the general massive case of the integral (5.3.9) (when all five masses are arbitrary) we obtained analytical results for the coefficient functions up to $\mathcal{M}_6$.

There are also some other possibilities to check the correctness of our results (in addition to cancellation of $1/\varepsilon$ poles). For example, in ref. [11] analogous results were presented for some special cases when some of the masses are zero while others are equal (see also ref. [29] where these results were generalised to the case of arbitrary space-time dimension n). In these cases, we compared our results for the coefficients

(at $n = 4$) and found complete agreement.

5.3.3 Numerical results

In this section, we will continue to focus on the "master" two-loop integral corresponding to Fig. 5.1. In general, it has two two-particle thresholds, at $k^2 = (m_1 + m_4)^2$ and $k^2 = (m_2 + m_5)^2$, and two three-particle thresholds at $k^2 = (m_1 + m_3 + m_5)^2$ and $k^2 = (m_2 + m_3 + m_4)^2$. The asymptotic expansion theorem quoted in (5.3.1) provides a series of approximations to this integral of the form (see eq. (5.3.9)):

$$\mathcal{M}^{(N)} \equiv \sum_{j=0}^{N} \frac{\mathcal{M}_j}{(k^2)^j}, \tag{5.3.14}$$

such that the remainder behaves like

$$\mathcal{M} - \mathcal{M}^{(N)} = \mathcal{O}\left((k^2)^{-N-1} \ln^2(-k^2)\right) \tag{5.3.15}$$

as $k^2 \to \infty$.

Strictly speaking, this does not imply convergence of the series for any fixed value of k^2, but from experience with special cases where exact analytical results are known, one would expect the series to converge when $|k^2|$ is larger than the highest threshold. In order to see whether this is true in the general case, and whether the asymptotic expansion can be used as a practical means of calculating these integrals, we made some numerical comparisons for two physical examples.

The first example is:

$$J(M_W, M_W, M_Z, m_t, m_b; k), \tag{5.3.16}$$

where the M_W, M_Z and m_b denote the masses of the W-boson, the Z-boson and the bottom quark. This integral is a contribution to the top quark self-energy. In this case, both the two-particle thresholds coincide. The three-particle thresholds also coincide with each other.

The other example occurs in the photon, the Higgs and the Z-boson self-energies:

$$J(m_t, m_t, M_Z, m_t, m_t; k). \tag{5.3.17}$$

Here m_t is the top quark mass. As in the first example, there are only two distinct thresholds. We calculated (5.3.16) and (5.3.17) numerically using the method of ref. [22]. The values we took for the masses were:

$$M_Z = 91\,\text{GeV}, \quad M_W = 80\,\text{GeV}, \quad m_t = 140\,\text{GeV}, \quad m_b = 5\,\text{GeV}. \tag{5.3.18}$$

The results are displayed in Figs. 5.9 and 5.10. In each plot, the first threshold is exactly on the left edge and the position of the highest threshold is indicated by a dashed vertical line. The dotted horizontal line shows the lowest order asymptotic

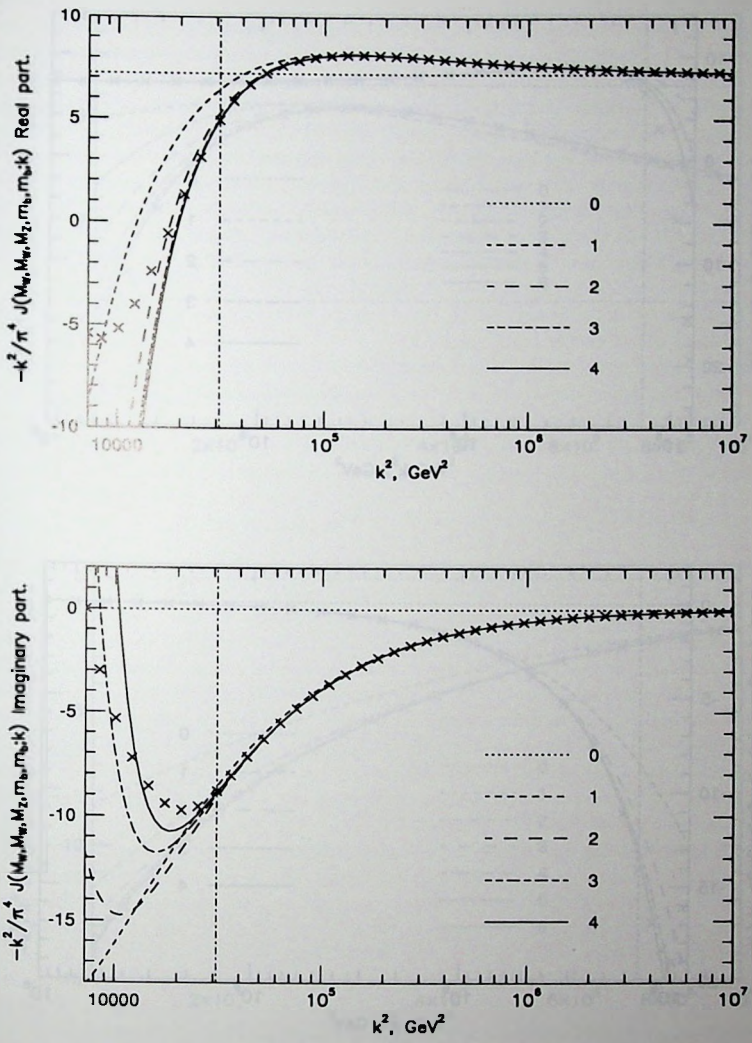

Fig. 5.9. The real and imaginary parts of $J(M_W, M_W, M_Z, m_b, m_b; k)$ for $k^2 \geq (M_W + m_b)^2$. The second threshold is at $(M_W + M_Z + m_b)^2$.

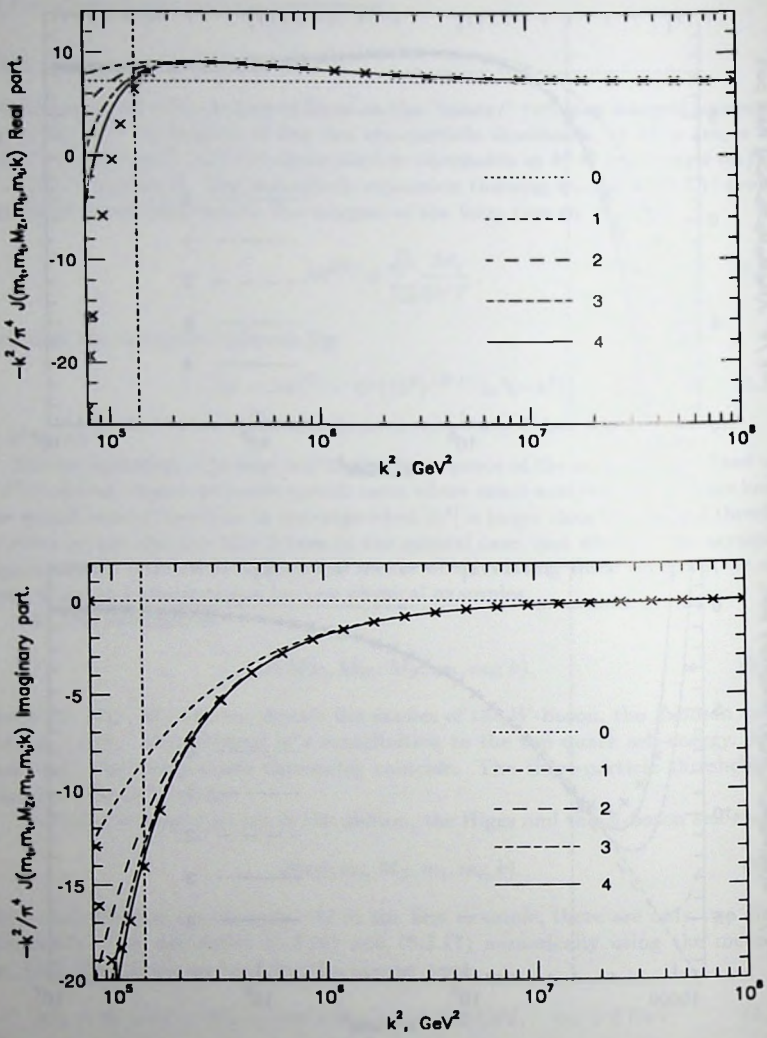

Fig. 5.10. The real and imaginary parts of $J(m_t, m_t, M_Z, m_t, m_t; k)$ for $k^2 \geq 4m_t^2$. The second threshold is at $(2m_t + M_Z)^2$.

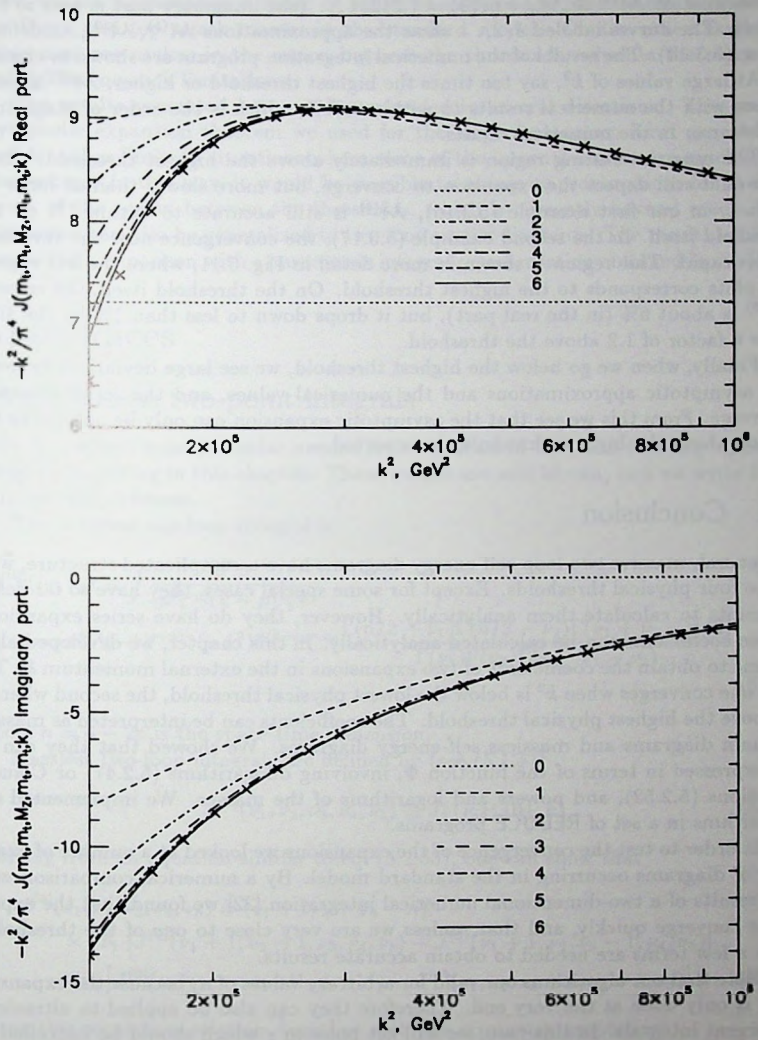

Fig. 5.11. The real and imaginary parts of $J(m_t, m_t, M_Z, m_t, m_t; k)$ for $k^2 \geq (2m_t + M_Z)^2$.

approximation $\mathcal{M}^{(0)} \equiv \mathcal{M}_0 = 6\zeta(3) = 7.21234\ldots$ (the imaginary part is zero to this order). The curves labeled $1, 2, \ldots$ show the approximations $\mathcal{M}^{(1)}, \mathcal{M}^{(2)}, \ldots$ defined by eq. (5.3.14). The results of the numerical integration program are shown as crosses.

At large values of k^2, say ten times the highest threshold or higher, $\mathcal{M}^{(3)}$ already agrees with the numerical results to within 0.01%, which is the order of magnitude of the error in the numerical results.

The most interesting region is immediately above the highest threshold, where we would still expect the expansion to converge, but more slowly than at large k^2. In fact, in our first example (5.3.16), $\mathcal{M}^{(4)}$ is still accurate to within 1% on the threshold itself. In the second example (5.3.17), the convergence near the threshold is less rapid. This region is shown in more detail in Fig. 5.11, where the left edge of the plots corresponds to the highest threshold. On the threshold itself, the error in $\mathcal{M}^{(6)}$ is about 6% (in the real part), but it drops down to less than 1% by the time k^2 is a factor of 1.2 above the threshold.

Finally, when we go below the highest threshold, we see large deviations between the asymptotic approximations and the numerical values, and the series ceases to converge. From this we see that the asymptotic expansion can only be applied to the region above the highest threshold, as expected.

5.4 Conclusion

In general, massive two-loop self-energy diagrams have a complicated structure, with up to four physical thresholds. Except for some special cases, they have so far defied attempts to calculate them analytically. However, they do have series expansions, whose coefficients can be calculated analytically. In this chapter, we developed algorithms to obtain the coefficients of two expansions in the external momentum k. The first one converges when k^2 is below the lowest physical threshold, the second when k^2 is above the highest physical threshold. The coefficients can be interpreted as massive vacuum diagrams and massless self-energy diagrams. We showed that they can all be expressed in terms of the function Φ, involving dilogarithms (5.2.47) or Clausen functions (5.2.52), and powers and logarithms of the masses. We implemented our algorithms in a set of REDUCE programs.

In order to test the convergence of the expansions we looked at a number of examples of diagrams occurring in the standard model. By a numerical comparison with the results of a two-dimensional numerical integration [22] we found that the expansions converge quickly, and that, unless we are very close to one of the thresholds, only a few terms are needed to obtain accurate results.

Note that our algorithms our valid for arbitrary values of n, because the expansion in ε is only done at the very end. Therefore they can also be applied to ultraviolet divergent integrals. In this case, we will get poles in ε which should be cancelled by renormalization counterterms.

The main advantage of series expansions as compared with numerical integrations is that they can be evaluated much faster on a computer. This is especially important

when we are interested in a range of values of some of the parameters, such as e.g. the Higgs and top quark masses in the standard model. On the other hand, our expansions are useless in the region between the thresholds, whereas the numerical method has no such limitations.

The results presented here can be extended in several directions. The general asymptotic expansion theorem we used for the large momentum limit can also be used for other limits in situations where some of the internal masses are much larger than others. In this way, it would be possible to obtain approximations for at least a part of the region between the thresholds, which is currently beyond reach. The expansions can also be generalized to two-loop vertex diagrams. The results could be checked by comparison with a parametric integral representation obtained in ref. [30].

Appendices

5A Massless two-point integrals

Here we present some formulae needed for evaluation of one- and two-loop massless integrals occurring in this chapter. These results are well known, and we write them only for completeness.

The massless one-loop integral is

$$\begin{aligned} I^{(0)}(\nu_1,\nu_2) &\equiv \int \frac{\mathrm{d}^n p}{[p^2]^{\nu_1}[(k-p)^2]^{\nu_2}} \\ &= i\pi^{n/2}(-1)^{\nu_1+\nu_2}(-k^2)^{n/2-\nu_1-\nu_2}\frac{\Gamma(n/2-\nu_1)\Gamma(n/2-\nu_2)\Gamma(\nu_1+\nu_2-n/2)}{\Gamma(\nu_1)\Gamma(\nu_2)\Gamma(n-\nu_1-\nu_2)}, \end{aligned} \tag{5A.1}$$

where $n = 4 - 2\varepsilon$ is the space-time dimension.

Massless two-loop integrals are defined by (see (5.1.1))

$$J^{(0)}(\nu_1,\nu_2,\nu_3,\nu_4,\nu_5) \equiv J(\{\nu_i\};\{0\};k)\,. \tag{5A.2}$$

Starting from an equation similar to eq. (5.2.53), one can show that

$$\begin{aligned} J^{(0)}(\nu_1,\nu_2,\nu_3,\nu_4,\nu_5) &= (\nu_1+2\nu_3+\nu_4-n)^{-1} \\ &\times\Big\{\nu_1\Big[J^{(0)}(\nu_1+1,\nu_2-1,\nu_3,\nu_4,\nu_5)-J^{(0)}(\nu_1+1,\nu_2,\nu_3-1,\nu_4,\nu_5)\Big] \\ &+\nu_4\Big[J^{(0)}(\nu_1,\nu_2,\nu_3,\nu_4+1,\nu_5-1)-J^{(0)}(\nu_1,\nu_2,\nu_3-1,\nu_4+1,\nu_5)\Big]\Big\}\,. \end{aligned} \tag{5A.3}$$

Using this recurrence relation, together with the symmetry properties:

$$\begin{aligned} J^{(0)}(\nu_1,\nu_2,\nu_3,\nu_4,\nu_5) &= J^{(0)}(\nu_4,\nu_5,\nu_3,\nu_1,\nu_2) \\ = J^{(0)}(\nu_2,\nu_1,\nu_3,\nu_5,\nu_4) &= J^{(0)}(\nu_5,\nu_4,\nu_3,\nu_2,\nu_1)\,, \end{aligned} \tag{5A.4}$$

all integrals $J^{(0)}(\nu_1,\nu_2,\nu_3,\nu_4,\nu_5)$ with positive integer ν's can be reduced to the following "boundary" integrals:

$$J^{(0)}(\nu_1,\nu_2,0,\nu_4,\nu_5) = I^{(0)}(\nu_1,\nu_4)\; I^{(0)}(\nu_2,\nu_5); \tag{5A.5}$$

$$J^{(0)}(\nu_1,\nu_2,\nu_3,\nu_4,0) = (k^2)^{\nu_2+\nu_3-n/2}\; I^{(0)}(\nu_2,\nu_3)\; I^{(0)}(\nu_1+\nu_2+\nu_3-n/2,\nu_4). \tag{5A.6}$$

For example,

$$J^{(0)}(1,1,1,1,1) = -\frac{\pi^4}{k^2}\,6\zeta(3) + \mathcal{O}(\varepsilon)\,. \tag{5A.7}$$

Note that $\zeta(3)$ does not occur in the divergent and finite parts of any other integrals $J^{(0)}$ with positive ν's.

5B Massive vacuum integrals

The result for the one-loop massive tadpole integral is well known [1] :

$$K(\nu,m) \equiv \int \frac{\mathrm{d}^n p}{[p^2-m^2]^\nu} = i\pi^{n/2}(-1)^\nu (m^2)^{n/2-\nu}\frac{\Gamma(\nu-n/2)}{\Gamma(\nu)} \tag{5B.1}$$

The massive two-loop vacuum integral is defined by

$$I(\nu_1,\nu_2,\nu_3;m_1,m_2,m_3) \equiv \int\int \frac{\mathrm{d}^n p\;\mathrm{d}^n q}{[p^2-m_1^2]^{\nu_1}[q^2-m_2^2]^{\nu_2}[(p-q)^2-m_3^2]^{\nu_3}}\,. \tag{5B.2}$$

Some special cases were considered in refs. [12, 21, 16, 10, 18]. When $m_1=m_2=0$ or $m_1=m_2=m$, $m_3=0$, it can be expressed in terms of gamma functions,

$$\begin{aligned} I(\nu_1,\nu_2,\nu_3;0,0,m) &= -\pi^n(-1)^{\nu_1+\nu_2+\nu_3}(m^2)^{n-\nu_1-\nu_2-\nu_3} \\ &\times\frac{\Gamma(n/2-\nu_1)\Gamma(n/2-\nu_2)\Gamma(\nu_1+\nu_2+\nu_3-n)\Gamma(\nu_1+\nu_2-n/2)}{\Gamma(\nu_1)\Gamma(\nu_2)\Gamma(\nu_3)\Gamma(n/2)}\,, \end{aligned} \tag{5B.3}$$

$$\begin{aligned} I(\nu_1,\nu_2,\nu_3;m,m,0) &= -\pi^n(-1)^{\nu_1+\nu_2+\nu_3}(m^2)^{n-\nu_1-\nu_2-\nu_3} \\ &\times\frac{\Gamma(\nu_1+\nu_2+\nu_3-n)\Gamma(n/2-\nu_3)\Gamma(\nu_1+\nu_3-n/2)\Gamma(\nu_2+\nu_3-n/2)}{\Gamma(\nu_1)\Gamma(\nu_2)\Gamma(n/2)\Gamma(\nu_1+\nu_2+2\nu_3-n)}\,. \end{aligned} \tag{5B.4}$$

The case where all the masses are non-zero is discussed in detail in sections (5.2.2)-(5.2.4). Here we give a summary of the results for $\nu_1=\nu_2=\nu_3=1$ in a form that clearly shows the symmetry with respect to m_1^2, m_2^2 and m_3^2.

$$\begin{aligned} I(1,1,1;m_1,m_2,m_3) &= \pi^{4-2\varepsilon}\Gamma^2(1+\varepsilon)\,(1+3\varepsilon+7\varepsilon^2) \\ &\times\Big\{-\frac{1}{2\varepsilon^2}(m_1^2+m_2^2+m_3^2)+\frac{1}{\varepsilon}(m_1^2\ln m_1^2+m_2^2\ln m_2^2+m_3^2\ln m_3^2) \\ &-\frac{1}{2}\Big[m_1^2\ln^2 m_1^2+m_2^2\ln^2 m_2^2+m_3^2\ln^2 m_3^2 \\ &+(m_1^2+m_2^2-m_3^2)\ln m_1^2\ln m_2^2+(m_1^2-m_2^2+m_3^2)\ln m_1^2\ln m_3^2 \\ &+(-m_1^2+m_2^2+m_3^2)\ln m_2^2\ln m_3^2+F(m_1^2,m_2^2,m_3^2)\Big]\Big\}+\mathcal{O}(\varepsilon) \end{aligned} \tag{5B.5}$$

where the function F is symmetric with respect to m_1^2, m_2^2 and m_3^2, and has the following Feynman parameter representation:

$$\begin{aligned} F(m_1^2, m_2^2, m_3^2) &= \{m_1^4 + m_2^4 + m_3^4 - 2(m_1^2 m_2^2 + m_2^2 m_3^2 + m_3^2 m_1^2)\} \\ &\times \int_0^1 \mathrm{d}x_1 \int_0^1 \mathrm{d}x_2 \int_0^1 \mathrm{d}x_3 \frac{\delta(1 - x_1 - x_2 - x_3)}{x_1 x_2 m_3^2 + x_2 x_3 m_1^2 + x_3 x_1 m_2^2} . \end{aligned} \tag{5B.6}$$

In terms of the function Φ used in section (5.2), it can be written as

$$F(m_1^2, m_2^2, m_3^2) = m_3^2 \lambda^2 (x, y) \Phi (x, y) \tag{5B.7}$$

with

$$x \equiv \frac{m_1^2}{m_3^2} \quad , \quad y \equiv \frac{m_2^2}{m_3^2}, \tag{5B.8}$$

$$\lambda^2(x, y) = (1 - x - y)^2 - 4xy, \tag{5B.9}$$

$$\begin{aligned} \Phi(x, y) &= \frac{1}{\lambda} \left\{ 2 \ln \left(\frac{1 + x - y - \lambda}{2} \right) \ln \left(\frac{1 - x + y - \lambda}{2} \right) - \ln x \ln y \right. \\ &\left. -2 \operatorname{Li}_2 \left(\frac{1 + x - y - \lambda}{2} \right) - 2 \operatorname{Li}_2 \left(\frac{1 - x + y - \lambda}{2} \right) + \frac{\pi^2}{3} \right\} \end{aligned} \tag{5B.10}$$

If the largest mass is m_1 or m_2, we should choose this mass as the dimensionless-making parameter in (5B.7) and (5B.8) (instead of m_3). In the region where $\lambda^2 < 0$, the function (5B.7) can be represented in terms of Clausen's functions (see eq. 5.2.52). To obtain results for integrals (5B.2) with higher integer powers of denominators, we use the recursive procedure of section (5.2.4).

We also need to evaluate massive integrals with numerators. To do this, in the one-loop case we used the following explicit formula:

$$\begin{aligned} &\int \frac{\mathrm{d}^n p}{[p^2 - m^2]^\nu} [2(k_1 p)]^{N_1} [2(k_2 p)]^{N_2} \Bigg|_{N_1 + N_2 - \text{ even}} \\ &= \frac{N_1! \, N_2!}{(n/2)_{(N_1+N_2)/2}} \left\{ \sum_{\substack{2j_1 + j_3 = N_1 \\ 2j_2 + j_3 = N_2}} \frac{(k_1^2)^{j_1} (k_2^2)^{j_2} [2(k_1 k_2)]^{j_3}}{j_1! \, j_2! \, j_3!} \right\} \int \frac{\mathrm{d}^n p}{[p^2 - m^2]^\nu} (p^2)^{(N_1+N_2)/2} , \end{aligned} \tag{5B.11}$$

and the integral on the l.h.s. vanishes if $(N_1 + N_2)$ is odd. The sum in braces is over all non-negative integers j_1, j_2, j_3 obeying two conditions: $2j_1 + j_3 = N_1$ and $2j_2 + j_3 = N_2$, so it is a single finite sum. We also use the standard notation for the Pochhammer symbol (5.2.9).

When we have a two-loop integral with a numerator and two denominators (corresponding to a product of two one-loop tadpoles), the following formula can be derived:

$$\int\int \frac{\mathrm{d}^n p\, \mathrm{d}^n q}{[p^2-m_1^2]^{\nu_1}[q^2-m_2^2]^{\nu_2}}\, [2(kp)]^{N_1}\, [2(kq)]^{N_2}\, [2(pq)]^{N_3}\Bigg|_{\substack{N_1+N_3-\text{ even}\\ N_2+N_3-\text{ even}}}$$

$$= \frac{N_1!\, N_2!\, (k^2)^{(N_1+N_2)/2}}{(n/2)_{(N_1+N_2)/2}} \left\{ \sum_{\substack{2j_1+j_3=N_1\\ 2j_2+j_3=N_2}} \frac{(N_3+j_3)!}{j_1!\, j_2!\, j_3!\, ((N_3+j_3)/2)!\, (n/2)_{(N_3+j_3)/2}} \right\}$$

$$\times \int\int \frac{\mathrm{d}^n p\, \mathrm{d}^n q}{[p^2-m_1^2]^{\nu_1}[q^2-m_2^2]^{\nu_2}}\, (p^2)^{(N_1+N_3)/2}\, (q^2)^{(N_2+N_3)/2}\,, \tag{5B.12}$$

and the integral on the l.h.s. of (5B.12) is equal to zero if (N_1+N_3) or (N_2+N_3) is odd. The sum in braces is of the same structure as in (5B.11).

We also need an analogous formula for the two-loop integral with three denominators:

$$\int\int \frac{\mathrm{d}^n p\, \mathrm{d}^n q}{[p^2-m_1^2]^{\nu_1}[q^2-m_2^2]^{\nu_2}[(p-q)^2-m_3^2]^{\nu_3}}\, [2(kp)]^{N_1}\, [2(kq)]^{N_2}\Bigg|_{N_1+N_2-\text{ even}}$$

$$= \frac{N_1!\, N_2!\, (k^2)^{(N_1+N_2)/2}}{(n/2)_{(N_1+N_2)/2}} \sum_{\substack{2j_1+j_3=N_1\\ 2j_2+j_3=N_2}} \frac{1}{j_1!\, j_2!\, j_3!}$$

$$\times \int\int \frac{\mathrm{d}^n p\, \mathrm{d}^n q}{[p^2-m_1^2]^{\nu_1}[q^2-m_2^2]^{\nu_2}[(p-q)^2-m_3^2]^{\nu_3}}\, (p^2)^{j_1}(q^2)^{j_2}[2(pq)]^{j_3}\,, \tag{5B.13}$$

and this integral is also equal to zero if (N_1+N_2) is odd.

In all formulae (5B.11), (5B.12) and (5B.13), the remaining momenta in the numerators on the r.h.s. can be expressed in terms of denominators, and we arrive at the result expressed in terms of integrals (5B.1) and (5B.2) without numerators.

References

[1] G. 'tHooft and M. Veltman, *Nucl.Phys.* B44 (1972) 189.

[2] C.G. Bollini and J.J. Giambiagi, *Nuovo Cim.* 12B (1972) 20.

[3] K.G.Chetyrkin, V.A.Ilyin, V.A.Smirnov and A.Yu.Taranov, *Phys.Lett.* B225 (1989) 411.

[4] V.A. Smirnov, *Renormalization and asymptotic expansions* (Birkhäuser, Basel, 1991).

[5] E.E. Boos and A.I. Davydychev, *Teor.Mat.Fiz.* 89 (1991) 56 (*Theor.Math.Phys.* 89 (1991) 1052).

[6] A.I.Davydychev, *J.Math.Phys.* 32 (1991) 1052; 33 (1992) 358.

[7] A.Erdelyi, W.Magnus, F.Oberhettinger and F.G.Tricomi, *Higher transcendental functions* (Bateman manuscript project), Vol.1 (McGraw-Hill, New York, 1953).

[8] A.I.Davydychev and M.N.Dubinin, in: *Proc. XIV Workshop "Problems on High Energy Physics and Field Theory", Protvino, 1991* (Nauka, Moscow, 1992), p.294.

[9] L.Lewin, *Polylogarithms and associated functions* (North Holland, 1981).

[10] C. Ford and D.R.T. Jones, *Phys.Lett.* B274 (1992) 409; *errata:* B285 (1992) 399.

[11] D.J. Broadhurst, *Z.Phys.* C47 (1990) 115.

[12] J. van der Bij and M. Veltman, *Nucl.Phys.* B231 (1984) 205;

[13] L.Culumovic, D.G.C.McKeon and T.N.Sherry , *Ann.Phys.* 197 (1990) 94.

[14] W.N. Bailey, *Generalized hypergeometric series* (Cambridge University Press, Cambridge, 1935).

[15] A.P. Prudnikov, Yu.A.Brychkov and O.I.Marichev, *Integrals and series. Additional chapters* (Nauka, Moscow, 1986).

[16] R. Scharf, Diploma thesis, Würzburg, 1991.

[17] A.I. Davydychev, *J.Phys.* A25 (1992) 5587.

[18] C. Ford, I. Jack and D.R.T. Jones, *Nucl.Phys.* B387 (1992) 373.

[19] F.V. Tkachov, *Phys.Lett.* B100 (1981) 65;
K.G. Chetyrkin and F.V. Tkachov, *Nucl.Phys.* B192 (1981) 159.

[20] A.C. Hearn, *REDUCE user's manual*, RAND publication CP78 (Santa Monica, 1987).

[21] F. Hoogeveen, *Nucl.Phys.* B259 (1985) 19.

[22] D. Kreimer, *Phys.Lett.* B273 (1991) 277.

[23] F.V. Tkachov, Preprint INR P-358 (Moscow, 1984);
G.B. Pivovarov and F.V. Tkachov, Preprints INR P-0370, II-459 (Moscow, 1984).

[24] K.G. Chetyrkin and V.A. Smirnov, Preprint INR G-518 (Moscow, 1987);
K.G. Chetyrkin, *Teor.Mat.Fiz.* 75 (1988) 26; 76 (1988) 207.

[25] S.G. Gorishny, *Nucl.Phys.* B319 (1989) 633.

[26] K.G. Chetyrkin, Preprint MPI-PAE/PTh 13/91 (Munich, 1991).

[27] V.A. Smirnov, *Commun.Math.Phys.* 134 (1990) 109.

[28] K.G. Chetyrkin and F.V. Tkachov, *Phys.Lett.* B114 (1982) 340;
K.G. Chetyrkin and V.A. Smirnov, *Phys.Lett.* B144 (1984) 419;
Preprint NPI MSU 89-3/80 (Moscow, 1989).

[29] D.J. Broadhurst, J. Fleischer and O.V. Tarasov, Open University preprint OUT-4102-43 (Milton Keynes, 1993).

[30] D. Kreimer, *Phys.Lett.* B292 (1992) 341.

Chapter 6

Numerical integration of two-loop self-energy diagrams

6.1 Introduction

In order to compute two-loop radiative corrections in the theory of electroweak interactions, one will need to know the numerical values of scalar two-loop self-energy diagrams in the general mass case. It is not possible to express them in terms of polylogarithms. For small or large values of the external momentum p^2, the series expansions of chapter 5 can be used, but what is really needed is a method that works for arbitrary values of p^2.

For the convergent integral $T_{12345}(p^2; m_1^2, m_2^2, m_3^2, m_4^2, m_5^2)$, such a method was discovered by Kreimer [1], who calculates the integral directly in momentum space, doing the last two integrations numerically. Another way to calculate this diagram, using a numerical integration over Feynman parameters, is presented in ref. [2].

Throughout this chapter, we shall use the notation introduced in section 4.2. We shall extend Kreimer's algorithm to $T_{234}(p^2; m_2^2, m_3^2, m_4^2)$, $T_{1234}(p^2; m_1^2, m_2^2, m_3^2, m_4^2)$, and $T_{11234}(p^2; m_1^2, m_1^2, m_2^2, m_3^2, m_4^2)$, which are ultraviolet divergent. As is shown in ref. [3], all two-loop Feynman diagrams contributing to gauge boson self-energies in the standard model can be expressed in terms of these three functions, T_{12345}, products of one-loop integrals and two-loop vacuum integrals. The special case of T_{11234} with $m_1^2 = 0$, which is also infrared divergent, will not be considered here.

The extension of the algorithm is possible because we now have at our disposal a number of analytical expressions for special mass situations, which have the same ultraviolet divergences as the integrals we wish to calculate. By subtracting appropriate combinations of these special integrals, we can reduce our problem to the numerical evaluation of a convergent integral.

In section 6.2, we describe how we obtain these combinations and how the remaining numerical integration is performed. Then, in section 6.3, we discuss the results of this general numerical approach and compare them with some results found by other methods.

6.2 Kreimer's method

Each of the integrals T_{234}, T_{1234} and T_{11234} is ultraviolet divergent. In order to calculate them numerically, we shall decompose them into two terms:

$$T = T_N + T_A \,. \tag{6.2.1}$$

This decomposition must satisfy two conditions. Firstly, the numerical part T_N must be finite, so that it can be calculated by numerical integration. Secondly, the analytical part T_A must be a combination of integrals for which analytical expressions are known.

To find a suitable decomposition, we use the following identity:

$$\frac{1}{k^2 - m^2} = \frac{1}{k^2} + \frac{m^2}{k^2(k^2 - m^2)} \,. \tag{6.2.2}$$

Applying this to propagators 3 and 4 in T_{234}, we obtain

$$\begin{aligned} T_{234}(p^2; m_2^2, m_3^2, m_4^2) = & -T_{234}(p^2; m_2^2, 0, 0) + T_{234}(p^2; m_2^2, m_3^2, 0) + T_{234}(p^2; m_2^2, 0, m_4^2) \\ & + m_3^2 m_4^2 T_{23344}(p^2; m_2^2, m_3^2, 0, m_4^2, 0) \,. \end{aligned} \tag{6.2.3}$$

The first three terms on the right hand side of this equation are all known analytically. For the first term, where two masses are zero, we can use the result (4.6.21) obtained in chapter 4. The case when only one mass is zero can also be calculated analytically. The result, in the notation of section 4.6, is:

$$\begin{aligned} & T_{234}(p^2; m_1^2, m_2^2, 0) = \\ & \quad \frac{1}{2\delta^2}(m_1^2 + m_2^2) \\ & \quad \frac{1}{\delta}\left\{\frac{3}{2}(m_1^2 + m_2^2) - m_1^2 L_{m_1} - m_2^2 L_{m_2} - \frac{1}{4}p^2\right\} \\ & \quad + m_1^2(L_{m_1}^2 - 3L_{m_1}) + m_2^2(L_{m_2}^2 - 3L_{m_2}) + \frac{1}{2}p^2 L_p \\ & \quad + \frac{1}{4}p^2\left\{\ln\left(\frac{m_1^2}{-p^2}\right) + \ln\left(\frac{m_2^2}{-p^2}\right) - \frac{13}{2}\right\} \\ & \quad + (m_1^2 + m_2^2)\left\{3 + \frac{1}{2}\zeta(2) - \frac{1}{4}\ln^2\left(\frac{m_1^2}{m_2^2}\right)\right\} \\ & \quad + \frac{1}{2}\left(m_1^2 - m_2^2\right)\left\{\mathrm{Li}_2\left(\frac{m_1^2 - m_2^2}{m_1^2}\right) - \mathrm{Li}_2\left(\frac{m_2^2 - m_1^2}{m_2^2}\right)\right\} \\ & \quad + \frac{1}{4}p^2\left\{\left(\frac{m_1^2}{p^2}\right)^2 - \left(\frac{m_2^2}{p^2}\right)^2\right\}\ln\left(\frac{m_1^2}{m_2^2}\right) \\ & \quad + \frac{1}{4}\left(p^2 + m_1^2 + m_2^2\right)\frac{m_2^2}{p^2}(r_1 - r_2)\left\{-\ln(r_1) + \ln(r_2)\right\} \end{aligned}$$

$$+m_1^2\left(1-\frac{m_2^2}{p^2}\right)\left\{\mathrm{Li}_2\left(\frac{1-r_1}{-r_1}\right)+\mathrm{Li}_2\left(\frac{1-r_2}{-r_2}\right)-\mathrm{Li}_2\left(\frac{m_1^2-m_2^2}{m_1^2}\right)\right\}$$
$$+m_2^2\left(1-\frac{m_1^2}{p^2}\right)\left\{\mathrm{Li}_2\left(1-r_1\right)+\mathrm{Li}_2\left(1-r_2\right)-\mathrm{Li}_2\left(\frac{m_2^2-m_1^2}{m_2^2}\right)\right\}. \quad (6.2.4)$$

The last term on the right hand side of eq. (6.2.3) is finite, due to the extra propagators it contains. Therefore, both requirements mentioned above are satisfied if we define

$$T_{234A}(p^2;m_2^2,m_3^2,m_4^2) = -T_{234}(p^2;m_2^2,0,0)+T_{234}(p^2;m_2^2,m_3^2,0)+T_{234}(p^2;m_2^2,0,m_4^2), \quad (6.2.5)$$

$$T_{234N}(p^2;m_2^2,m_3^2,m_4^2) = m_3^2m_4^2T_{23344}(p^2;m_2^2,m_3^2,0,m_4^2,0). \quad (6.2.6)$$

In a similar way, the following identities for T_{1234} and T_{11234} can be derived:

$$\begin{aligned}T_{1234}(p^2;m_1^2,m_2^2,m_3^2,m_4^2) &= T_{1234}(p^2;m_1^2,m_2^2,0,0)\\ &+m_3^2T_{12334}(p^2;m_1^2,m_2^2,m_3^2,0,0)+m_4^2T_{12344}(p^2;m_1^2,m_2^2,0,m_4^2,0)\\ &+m_3^2m_4^2T_{123344}(p^2;m_1^2,m_2^2,m_3^2,0,m_4^2,0), \end{aligned} \quad (6.2.7)$$

and

$$\begin{aligned}T_{11234}(p^2;m_1^2,m_1^2,m_2^2,m_3^2,m_4^2) &= T_{11234}(p^2;m_1^2,m_1^2,m_2^2,0,0)\\ &+m_3^2T_{112334}(p^2;m_1^2,m_1^2,m_2^2,m_3^2,0,0)+m_4^2T_{112344}(p^2;m_1^2,m_1^2,m_2^2,0,m_4^2,0)\\ &+m_3^2m_4^2T_{1123344}(p^2;m_1^2,m_1^2,m_2^2,m_3^2,0,m_4^2,0). \end{aligned} \quad (6.2.8)$$

The first terms on the right hand sides of eqs. (6.2.7) and (6.2.8) are given by eqs. (4.6.25) and (4.6.31), respectively. All the other terms are convergent. This leads us to define

$$\begin{aligned}T_{1234A}(p^2;m_1^2,m_2^2,m_3^2,m_4^2) &= T_{1234}(p^2;m_1^2,m_2^2,0,0), && (6.2.9)\\ T_{1234N}(p^2;m_1^2,m_2^2,m_3^2,m_4^2) &= T_{1234}(p^2;m_1^2,m_2^2,m_3^2,m_4^2)\\ &\quad -T_{1234}(p^2;m_1^2,m_2^2,0,0), && (6.2.10)\\ T_{11234A}(p^2;m_1^2,m_1^2,m_2^2,m_3^2,m_4^2) &= T_{11234}(p^2;m_1^2,m_1^2,m_2^2,0,0), && (6.2.11)\\ T_{11234N}(p^2;m_1^2,m_1^2,m_2^2,m_3^2,m_4^2) &= T_{11234}(p^2;m_1^2,m_1^2,m_2^2,m_3^2,m_4^2)\\ &\quad -T_{11234}(p^2;m_1^2,m_1^2,m_2^2,0,0). && (6.2.12)\end{aligned}$$

Now, let us discuss Kreimer's method. For timelike external momenta p, he calculates the integral T_{12345} in the p-rest frame. Integrating over the space components of the loop momenta analytically, he is left with a two dimensional integral over the time components of the loop momenta, which can be written as

$$T_{12345}(p^2;m_1^2,m_2^2,m_3^2,m_4^2,m_5^2) =$$
$$-\frac{4}{p^2}\int_{-\infty}^{\infty}\mathrm{d}x\int_{-\infty}^{\infty}\mathrm{d}y\frac{1}{w_1^2-w_2^2}\frac{1}{w_4^2-w_5^2}\ln\left(\frac{(w_1+w_3+w_4)(w_2+w_3+w_5)}{(w_2+w_3+w_4)(w_1+w_3+w_5)}\right), \quad (6.2.13)$$

with

$$w_1 = \left[x^2 - \frac{m_1^2}{p^2} + i\varepsilon\right]^{1/2} \tag{6.2.14}$$

$$w_2 = \left[(x+1)^2 - \frac{m_2^2}{p^2} + i\varepsilon\right]^{1/2} \tag{6.2.15}$$

$$w_3 = \left[(x+y)^2 - \frac{m_3^2}{p^2} + i\varepsilon\right]^{1/2} \tag{6.2.16}$$

$$w_4 = \left[y^2 - \frac{m_4^2}{p^2} + i\varepsilon\right]^{1/2} \tag{6.2.17}$$

$$w_5 = \left[(y-1)^2 - \frac{m_5^2}{p^2} + i\varepsilon\right]^{1/2} . \tag{6.2.18}$$

The square roots $w_1, \ldots, w_5$ should all be chosen in the first quadrant. The result, (6.2.13), is also valid for spacelike external momenta. It turns out that the remaining x- and y-integrations can readily be performed numerically.

Following exactly the same arguments, analogous representations for the integrals T_N defined above can be derived:

$$T_{234N}(p^2; m_2^2, m_3^2, m_4^2) = -4p^2 \int_{-\infty}^{\infty} \mathrm{d}x \int_{-\infty}^{\infty} \mathrm{d}y \ln\left(\frac{(w_2+w_3+w_4)(w_2+\tilde{w}_3+\tilde{w}_4)}{(w_2+\tilde{w}_3+w_4)(w_2+w_3+\tilde{w}_4)}\right), \tag{6.2.19}$$

$$T_{1234N}(p^2; m_1^2, m_2^2, m_3^2, m_4^2) = 4\int_{-\infty}^{\infty} \mathrm{d}x \int_{-\infty}^{\infty} \mathrm{d}y \frac{1}{w_1^2 - w_2^2} \ln\left(\frac{(w_1+w_3+w_4)(w_2+\tilde{w}_3+\tilde{w}_4)}{(w_2+w_3+w_4)(w_1+\tilde{w}_3+\tilde{w}_4)}\right), \tag{6.2.20}$$

$$T_{11234N}(p^2; m_1^2, m_1^2, m_2^2, m_3^2, m_4^2) = \frac{4}{p^2}\int_{-\infty}^{\infty} \mathrm{d}x \int_{-\infty}^{\infty} \mathrm{d}y \frac{1}{(w_1^2-w_2^2)^2} \left\{\ln\left(\frac{(w_1+w_3+w_4)(w_2+\tilde{w}_3+\tilde{w}_4)}{(w_2+w_3+w_4)(w_1+\tilde{w}_3+\tilde{w}_4)}\right) - \frac{(w_1^2-w_2^2)(\tilde{w}_3+\tilde{w}_4-w_3-w_4)}{2w_1(w_1+w_3+w_4)(w_1+\tilde{w}_3+\tilde{w}_4)}\right\}, \tag{6.2.21}$$

where, in addition to $w_1, \ldots, w_5$, the variables

$$\tilde{w}_3 = \left[(x+y)^2 + i\varepsilon\right]^{1/2}, \tag{6.2.22}$$

$$\tilde{w}_4 = \left[y^2 + i\varepsilon\right]^{1/2}, \tag{6.2.23}$$

are used.

It is possible to take the limit $\varepsilon \to 0$ before performing the x- and y-integrations, provided one remembers that the square roots w_i should be positive when w_i^2 is positive, and on the positive imaginary axis when w_i^2 is negative. When p^2 is negative, the w_i are always positive, and the integrals T_N are real. However, when p^2 is positive, there are regions where some of the w_i are imaginary. This can give rise to imaginary parts in the integrals T_N.

At first sight, one might think that the integrands in eqs. (6.2.13) and (6.2.20) have singularities where the denominators $w_1^2 - w_2^2$ and $w_4^2 - w_5^2$ vanish. However, that is not the case, since the numerators also vanish at those points. This also happens in eq. (6.2.21), but there, the cancellation is more delicate because the factor $w_1^2 - w_2^2$ occurs to the second power.

In order to perform the numerical integrations, we map the integration region onto a unit square. We do this by first shifting the integration variables so that the zeros of the denominators $w_1^2 - w_2^2$ and $w_4^2 - w_5^2$ coincide with the axes. Then, we map the infinite plane onto one quadrant:

$$\int_{-\infty}^{\infty} \mathrm{d}x \int_{-\infty}^{\infty} \mathrm{d}y F(x,y) =$$
$$\int_0^{\infty} \mathrm{d}x \int_0^{\infty} \mathrm{d}y \left\{ F(x,y) + F(-x,y) + F(x,-y) + F(-x,-y) \right\} . \quad (6.2.24)$$

Finally, we map this quadrant onto a unit square using transformations of the form $x = x'/(1-x')$ and $y = y'/(1-y')$. The integrations are done with the Monte Carlo program VEGAS [4].

6.3 Results

To check the reliability of the method, we looked at a number of special cases where we could compare the results obtained by numerical integration with results obtained by other methods.

The first case we considered was T_{234}, where we put $m_2 = 0$. For several values of m_3, m_4 and p^2, we compared the numerical results, obtained using 140000 points for the Monte Carlo integration, with the analytical result (6.2.4) and found agreement to four digits.

Next, we studied the imaginary part of T_{234} for general values of the masses. It is finite in $D = 4$. According to Cutkosky's rules, it is equal to a three-particle phase space integral (see Fig. 4.5). Using the method of section 4.4, it can be written as a two dimensional integral. One of the integrations can easily be done analytically, yielding

$$\begin{aligned} &\operatorname{Im} T_{234}(p^2; m_2^2, m_3^2, m_4^2) \\ &= \frac{1}{2i} \Delta T_{234}(p^2; m_2^2, m_3^2, m_4^2) \\ &= -\frac{\pi}{p^2} \int_{(m_3+m_4)^2}^{\left(\sqrt{p^2}-m_2\right)^2} \mathrm{d}s \frac{1}{s} \sqrt{\lambda(p^2, s, m_2^2)\lambda(s, m_3^2, m_4^2)} . \end{aligned} \quad (6.3.1)$$

We calculated this one dimensional integral numerically and found agreement with the results of Kreimer's method to four digits.

As a check on T_{1234}, we looked at the special cases $T_{1234}(p^2;0,0,m^2,0)$ (4.6.23) and

$$\begin{aligned} T_{1234}(p^2;0,0,m^2,m^2) &= \frac{1}{2\delta^2}+\frac{1}{\delta}\left\{\frac{5}{2}-L_p\right\}+\frac{19}{2}-\frac{1}{2}\zeta(2)+L_p^2-5L_p \\ &\quad -\frac{1}{2}\ln^2(-x)+3\ln(-x)+3\,\frac{r_1-r_2}{x}\ln(r_1) \\ &\quad +\frac{1}{2}\left(1+\frac{2}{x}\right)\ln^2(r_1)\,. \end{aligned} \tag{6.3.2}$$

Once again, we found the results of the numerical integration agreed with the analytical results to four digits.

The numerical calculation of (6.2.21) seems to be more difficult. At the moment, the errors are still rather large, especially for timelike external momenta. This is probably due to the large cancellations that occur in the numerator when the denominator vanishes, but we expect this can be brought under control.

The great advantage of Kreimer's method is its generality. In special cases, it cannot compete in speed or precision with analytical formulae, but in the general mass case, it provides results where other methods fail. In principle, it is possible to derive one dimensional integral representations for these scalar integrals, but one would have to consider many different cases, depending on whether some masses are smaller or larger than others, separately. With Kreimer's method, all cases are treated at the same time.

References

[1] D. Kreimer, *Phys. Lett.* B273 (1991) 277.

[2] J. Fujimoto, Y. Shimizu, K. Kato and Y. Oyanagi, in "New Computing Techniques in Physics Research II" , ed. D. Perret-Gallix, World Scientific 1992, p. 625.

[3] G. Weiglein, R. Mertig, R. Scharf, and M. Böhm, in "New Computing Techniques in Physics Research II" , ed. D. Perret-Gallix, World Scientific 1992, p.617;
G. Weiglein, R. Scharf and M. Böhm, Reduction of general two-loop self-energies to standard scalar integrals, to be published.

[4] G.P. Lepage, *J. Comp. Phys.* 27 (1978) 192;
G.P. Lepage, Cornell preprint CLNS-80/447 (1980).

Samenvatting

De invloed van topquarks op de productie van meerdere jets en op electrozwakke parameters

Men stelt zich voor, dat alle materie opgebouwd is uit twee soorten deeltjes, leptonen en quarks. De theorie, die deze deeltjes beschrijft, wordt het standaardmodel genoemd. Naast leptonen en quarks komen in het model nog enkele andere deeltjes voor. Dat zijn de ijkbosonen: het foton, het gluon, het W-deeltje en het Z-deeltje, die zorgen voor de overdracht van krachten tussen de leptonen en de quarks, en verder het Higgs-deeltje. Op het ogenblik komen alle experimenteel bekende gegevens over het gedrag van deze deeltjes overeen met de voorspellingen van het standaardmodel. Twee voorspellingen zijn echter nog niet uitgekomen. Ten eerste zouden er volgens het model zes soorten quarks moeten zijn, maar is de zesde soort, het topquark, nog niet waargenomen. Ten tweede is ook het Higgs-deeltje nog niet gezien.

Er bestaat een goede kans, dat het topquark binnenkort gevonden zal worden in experimenten die uitgevoerd worden bij Fermilab in de Verenigde Staten. Daar worden protonen en antiprotonen versneld en vervolgens met elkaar in botsing gebracht. Bij die botsingen zullen topquarks en antitopquarks in paren ontstaan. Ze zullen echter niet zelf waargenomen worden, omdat ze een zeer korte levensduur hebben. In plaats daarvan zal men hun vervalsproducten waarnemen en daaruit het kortstondige bestaan van het topquark moeten opmaken. De moeilijkheid daarbij is, dat dezelfde vervalsproducten ook door andere reacties kunnen ontstaan, waar helemaal geen topquarks bij betrokken zijn. Het is daarom erg belangrijk om te weten hoe vaak die achtergrondreacties plaats vinden, in verhouding tot het aantal reacties waarin topquarks ontstaan.

Er zijn verschillende manieren waarop de topquarks en antitopquarks kunnen vervallen. In dit proefschrift wordt vooral veel aandacht besteed aan het verval waarbij er uiteindelijk een neutrino, een geladen lepton en vier *jets* van hadronen (uit quarks samengestelde deeltjes) ontstaan. De belangrijkste achtergond hierbij is de reactie waarin vier jets en een W-deeltje ontstaan, en het W-deeltje vervolgens in een neutrino en een geladen lepton vervalt. De werkzame doorsnede voor deze achtergrondreactie — een grootheid, die aangeeft hoe vaak de reactie op zal treden bij een gegeven aantal proton-antiproton botsingen — wordt berekend in hoofdstuk 2, en

blijkt van dezelfde orde van grootte als die van het topquarksignaal te zijn.

Het doel van de experimenten bij Fermilab is niet alleen het bestaan van topquarks aan te tonen, maar ook hun massa te bepalen. In beginsel kan dat eenvoudig door het aantal gevonden topquarks te tellen, en dan gebruik te maken van het, door de theorie gegeven, verband tussen de werkzame doorsnede en de topmassa. Omdat het echter heel moeilijk is om de werkzame doorsnede nauwkeurig uit te rekenen, kan men op deze wijze de topmassa niet erg nauwkeurig bepalen. Daarom wordt in hoofdstuk 3 een manier voorgesteld, waarop de topmassa bepaald zou kunnen worden door de energieën en impulsen van de vervalsproducten te meten, zonder het verband tussen de werkzame doorsnede en de topmassa te gebruiken.

Men kan ook uit andere experimenten iets over de topmassa te weten komen. Het topquark beïnvloedt namelijk de eigenschappen van de andere deeltjes in het standaardmodel door stralingscorrecties. Door die eigenschappen nauwkeurig te meten, vindt men, indirect, grenzen op de mogelijke waarden van de topmassa.

Stralingscorrecties kunnen overzichtelijk voorgesteld worden met behulp van Feynmandiagrammen. De bijdragen van diagrammen met één gesloten lus zijn al berekend, maar als in de toekomst de experimenten nog nauwkeuriger worden, dan zal men ook de bijdragen van diagrammen met twee lussen mee moeten nemen. De tweede helft van dit proefschrift gaat over de berekening van zulke twee lusdiagrammen. We beperken ons tot diagrammen met twee uitwendige lijnen.

In hoofdstuk 4 worden diagrammen uitgerekend, waarin sommige van de inwendige lijnen massaloze leptonen of quarks voorstellen. De uitkomsten kunnen ook worden gebruikt als een goede benadering voor diagrammen waarin leptonen of quarks voorkomen, waarvan de massa klein is vergeleken met de massa's van het W- en het Z-deeltje.

Er komen echter ook diagrammen voor, waarin geen enkele massa verwaarloosd kan worden. In die gevallen blijkt de aanpak van hoofdstuk 4 niet te werken. Wat wel kan, is zo'n diagram schrijven als een oneindige reeks. We laten dit zien in hoofdstuk 5. Aan de hand van enkele voorbeelden wordt de convergentie van de reeksen onderzocht. De reeksen convergeren alleen voor waarden van de uitwendige impuls binnen zekere gebieden, maar binnen die gebieden is de convergentie vrij snel, zodat men met slechts enkele termen goede benaderingen krijgt.

Tenslotte wordt in hoofdstuk 6 een nog algemenere manier om deze diagrammen te berekenen beschreven, die voor willekeurige waarden van de uitwendige impuls te gebruiken is. Hierbij worden de diagrammen eerst geschreven als tweedimensionale integralen, die vervolgens numeriek uitgerekend worden.

Curriculum vitae

Ik ben op 12 december 1965 in Keulen geboren. Nadat ik in 1984 aan het Haags Montessori Lyceum het eindexamen VWO behaald had, begon ik natuurkunde te studeren aan de Rijksuniversiteit te Leiden. Het propaedeutisch examen werd in augustus 1985 afgelegd. Na een experimentele stage in de groep Quantumvloeistoffen onder leiding van prof. dr. R. de Bruyn Ouboter ging ik naar de groep theoretische hoge-energiefysica, waar ik onder leiding van prof. dr. F.A. Berends een scriptie schreef over de renormalisatie van de Z-breedte. In juni 1989 volgde het doctoraal examen Natuurkunde.

Op 1 september 1989 trad ik als onderzoeker in opleiding in dienst van de Stichting voor Fundamenteel Onderzoek der Materie om bij prof. dr. F.A. Berends aan een promotieonderzoek te beginnen. Tijdens de promotieperiode bezocht ik in 1989 de "Herbstschule für Hochenergiephysik" te Maria Laach, Duitsland, in 1990 en 1991 de "AIO/OIO-School theoretische hoge-energiefysica" in Twente en in 1990 de zomerschool "Z^0 Physics: Cargèse 1990" te Cargèse, Corsica. Mijn bijdrage aan het onderwijs bestond uit het geven van werkcolleges bij het college Veldentheorie.

List of publications

1. On the Production of a W and Jets at Hadron Colliders,
   F.A. Berends, W.T. Giele, H. Kuijf and J.B. Tausk,
   Nucl. Phys. B357 (1991) 32.

2. Top-quark search in multijet signals, F.A. Berends, J.B. Tausk, W.T. Giele,
   Phys. Rev. D47 (1993) 2746.

3. Scalar two-loop integrals for gauge boson
   self-energy diagrams with a massless fermion loop,
   R. Scharf and J.B. Tausk, Leiden Preprint INLO-Pub-7/93.

4. Two-loop self-energy diagrams with different masses
   and the momentum expansion,
   A.I. Davydychev and J.B. Tausk,
   Nucl. Phys. B397 (1993) 123.

5. Momentum expansion of two-loop self-energy diagrams
   occurring in the standard model,
   A.I. Davydychev and J.B. Tausk,
   in Proc. VII Intern. Workshop (Sochi, Russia, October 1992),
   Yad. Fiz. 56 (1993) No. 11, 137.

6. Large momentum expansion of two-loop self-energy diagrams
   with arbitrary masses,
   A.I. Davydychev, V.A. Smirnov and J.B. Tausk,
   Leiden Preprint INLO-Pub-5/93.

Stellingen

1. De renormalisatieschema's van Böhm, Hollik en Spiesberger en van Sirlin geven tot op één-lusniveau dezelfde uitkomsten voor zowel het verval van het muon als van het Z-deeltje.

   M. Böhm, W. Hollik en H. Spiesberger, Fortschritte der Physik 34 (1986) 687; A. Sirlin, Physical Review D22 (1980) 971.

2. Het zou interessant zijn om na te gaan, hoe de theoretisch voorspelde vorm van de Z-resonantie veranderen zou door het meenemen van de exacte energie-afhankelijkheid van het imaginaire deel van de tweelus-Z-zelfenergie.

3. Om de constanten V_{max} en K_m te bepalen, die voorkomen in de Michaelis-Menten vergelijking,

$$\frac{\mathrm{d}[S]}{\mathrm{d}t} = \frac{-V_{max}[S]}{[S] + K_m},$$

   waarmee men de afbraak van een stof S onder invloed van een enzym beschrijft, is het nuttig om de geïntegreerde vorm van deze vergelijking te gebruiken.

   C.W. Wharton en R.J. Szawelski, Biochemical Journal 203 (1982) 351.

4. Omdat c-quarks soms voor b-quarks kunnen worden aangezien, is het van belang om te weten, hoe vaak er bij de reactie $p\bar{p} \to W + 4$ jets c-quarks in de eindtoestand voorkomen.

5. Bij het bepalen van de parton-dichtheidsfuncties uit diep-inelastische verstrooiingsexperimenten moet men rekening houden met de longitudinale structuurfunctie F_L.

6. Voor twee niet-negatieve gehele getallen N_1 en N_2 geldt de volgende vergelijking:

$$\left[(2k \cdot p)^{N_1}(2k \cdot q)^{N_2}\right]$$
$$= \frac{\Gamma(n/2)N_1!N_2!}{\Gamma((n+N_1+N_2)/2)} \Sigma \frac{1}{j_1!j_2!j_3!} \left[(k^2)^{(N_1+N_2)/2}(p^2)^{j_1}(q^2)^{j_2}(2p \cdot q)^{j_3}\right]$$

waarin de som loopt over alle niet-negatieve gehele getallen j_1, j_2, j_3 met de beperking dat $2j_1 + j_3 = N_1$, $2j_2 + j_3 = N_2$. Hierbij kan het symbool $[\ldots]$ op twee manieren worden gelezen: als een dimensioneel geregulariseerde één-lusintegraal,

$$[X] = \int \mathrm{d}^n k\, f(k^2)\, X\,,$$

of als een twee-lusintegraal,

$$[X] = \int \mathrm{d}^n p \int \mathrm{d}^n q\, g(p^2, q^2, p \cdot q)\, X\,.$$

7. De berekening van S-matrixelementen voor processen waarbij twee gluonen betrokken zijn met polarisatievectoren J_1 en J_2 kan soms verkort worden door de tensor

$$J_1^\mu J_2^\nu$$

te vervangen door

$$-\frac{(F_1 \cdot F_2)^{\mu\nu}}{K_1 \cdot K_2}\,.$$

In deze uitdrukking zijn K_1 en K_2 de impulsen van de gluonen, en worden de tensoren F_i gegeven door

$$F_i^{\mu\nu} = K_i^\mu J_i^\nu - J_i^\mu K_i^\nu \qquad (i = 1, 2).$$

8. Het zou nuttig zijn om naast het telefoonnummer ook de postcode in de telefoongids te vermelden.

9. Het huisvestingsbeleid van veel Nederlandse gemeenten remt de mobiliteit van de bevolking.

J.B. Tausk, Leiden, september 1993.